DEEP LEARNING BASED APPROACH
TO MAXIMIZE PV POWER PRODUCTION

A Thesis Submitted
In Partial Fulfillment of the Requirements
for the Degree of

DOCTOR OF PHILOSOPHY

by

RAHMA AMAN
(2K21/PhD/EE/08)

Under the Supervision of

Dr. M. Rizwan	**Dr. Astitva Kumar**
Professor	**Assistant Professor**
DTU, Delhi	**NSUT, Delhi**

Department of Electrical Engineering

DELHI TECHNOLOGICAL UNIVERSITY
(Formerly Delhi College of Engineering)
Shahbad Daulatpur, Main Bawana Road, Delhi-110042. India

June, 2025

CANDIDATE's DECLARATION

I Rahma Aman hereby certify that the work which is being presented in the thesis entitled "**Deep Learning Based Approach to Maximize PV Power Production"** in partial fulfillment of the requirements for the award of the Degree of Doctor of Philosophy, submitted in the Department of Electrical Engineering, Delhi Technological University is an authentic record of my own work carried out during the period from 1.08.2021 to 30.08.2025 under supervision of Prof. M. Rizwan and Dr. Astitva Kumar.

The matter presented in the thesis has not been submitted by me for the award of any other degree of this or any other Institute.

Place: Delhi   **(Rahma Aman**)

Date: 13.06.2025

This is to certify that the student has incorporated all the corrections suggested by the examiners in the thesis, and the statement made by the candidate is correct to the best of our knowledge.

Signature of Supervisor(s)

ABSTRACT

The performance and dependability of SPV systems are heavily impacted by environmental conditions such as solar irradiation, temperature, humidity, dust deposition, and shadowing etc. These circumstances create nonlinearity, intermittency, and soiling induces deterioration, which reduces SPV power production and increases maintenance requirements, and further complicates grid integration. This work proposes a complete AI-based framework that combines deep learning approaches, real-time soiling analytics, thermal imaging, and cleaning method assessment to improve the forecasting, fault detection, and maintenance efficiency of solar PV systems.

A hybrid deep learning model that combines CNN and LSTM was created to anticipate short-term solar power production using meteorological data such as UV index, humidity wind speed, temperature, cloud cover etc. The developed model outperformed classic MLP, standalone CNN, and LSTM models, particularly in bright and cold circumstances, with a R^2 value of up to 0.9898. In addition, the research addressed soiling effect using a real-time dust monitoring system, which allowed for precise modelling of power losses. A layered LSTM architecture was used to estimate dirty PV power production, resulting in an astounding 99.13% prediction accuracy and allowing for preventive maintenance planning.

Thermal imaging was used to mitigate performance deterioration caused by hotspots, together with powerful deep learning classifiers such as AlexNet, ResNet-18, and Inception-ResNet-v2. These models demonstrated excellent detection accuracies up to 99.3% for defects produced by dust and partial shadowing, allowing for accurate and timely fault diagnosis. To meet the increased need for efficient cleaning tactics, many procedures were tested, including manual, robotic, sprinkler-based, and nano-coating technologies. Manual cleaning is still commonly employed, although its inefficiency under changing soiling patterns and seasonal circumstances restricts its usefulness. To provide data-driven and balanced decision-making, a hybrid MICMAC-TOPSIS framework was used to evaluate and rank cleaning solutions using technical, environmental, safety, and economic factors. The study found that nano-coating and robotic cleaning systems are the most efficient alternatives for long-term performance and

sustainability, whereas manual approaches are the least effective. The MCDM technique allowed for objective prioritizing of possibilities, which aided the creation of a context-sensitive cleaning strategy.

This interdisciplinary architecture combines forecasting, diagnosis, and maintenance into a single intelligent system, laying the groundwork for completely autonomous, self-optimizing SPV operations. The findings lay a solid foundation for the future development of novel, AI integrated, condition-based cleaning solutions aided by multi-criteria analysis that can dynamically adapt to site-specific environmental conditions, ensuring consistent energy yield, lower operational costs, and long-term SPV system performance.

LIST OF PUBLICATION

• List of papers (s) published in Peer Reviewed Referred International Journals

1. R. Aman, M. Rizwan and A. Kumar, "A novel deep learning framework for PV module thermal condition monitoring". Electrical Engineering, 2024 1-17. Impact factor 1.6 (SCIE Journal).

2. R. Aman, M. Rizwan and A. Kumar, "Fault classification using deep learning- based model and impact of dust accumulation on solar photovoltaic modules." Energy Sources, Part A: Recovery, Utilization, and Environmental Effects, Vol. 45, Issue 2, pp. 4633-4651, 2023, ISSN: 4633-4651. Impact factor 2.3 (SCIE Journal).

3. R. Aman, M. Rizwan and A. Kumar, "A novel hybrid intelligent approach for solar photovoltaic power prediction considering UV index and cloud cover". Electrical Engineering 107, 1203–1224, 2025, Impact factor 1.6 (SCIE Journal).

4. R. Aman, M. Rizwan and A. Kumar, "Novel Deep Learning Assisted Framework for the Assessment of Real Time Dust Accumulation Data on Solar PV Modules, AJSE, Impact factor: 2.5 (SCIE Journal)

• List of Paper(s) Published in Peer Reviewed International Conference

1. R. Aman, M. Rizwan and A. Kumar, "Comparative Analysis of Transfer Learning Techniques for Enhanced Fault Detection in Solar Photovoltaic Modules." 2024 IEEE 4th International Conference on Sustainable Energy and Future Electric Transportation (SEFET), 31st July – 3rd August, 2024, Hyderabad, India. [Scopus Indexed Conference].

2. R. Aman, A. Abdul, D. Kumar, A. Kumar, and M. Rizwan, "An IoT integrated novel self-cleaning strategy for enhancing efficiency of solar photovoltaic modules," IEEE Trans. Ind. Inform., [Under Review].

3. M. Rizwan, R. Aman, and A. Kumar, "An optimized deep learning framework for solar PV power forecasting using advanced hyperparameter tuning technique," in Proc. 2nd Int. Conf. Sustainable Power and Energy Research (ICSPER 2025), [Accepted].

4. R. Aman, M. Rizwan and A. Kumar, "Investigating the Effect of Dust on the Performance of Rooftop Solar Photovoltaic System," 2023 International Conference

on Modeling, Simulation & Intelligent Computing (MoSICom), Dubai, United Arab Emirates, 2023, pp. 99-104, [Scopus Indexed Conference].

5. R. Aman and M. Rizwan, "Power Enhancement and Hotspot Reduction of a Rooftop Solar PV Array Using MOSFETs", 2022 International Conference on Electrical, Computer, Communications and Mechatronics Engineering (ICECCME 2022), Maldives, pp. 1-6, [Scopus Indexed Conference]

6. R. Aman and M. Rizwan, "A Modified Shade Dispersion Technique to Enhance the Performance of Photovoltaic System Under Various Shading Conditions," 2022 IEEE Delhi Section Conference (DELCON), New Delhi, India, 2022, pp. 1-7, doi: 10.1109/DELCON54057.2022.9753011. [Scopus Indexed Conference].

- **List of other publications**

1. R. Aman, M. Aminovich, Z. Ulmas, A. Kumar, and M. Rizwan, "A Novel Hybrid GWO-Bi-LSTM Based Metaheuristic Framework for Short Term Solar Photovoltaic Power Forecasting", JRSE [Revision].

2. R. Aman, A. Abdul, D. Kumar, A. Kumar, and M. Rizwan, "An IoT integrated novel self-cleaning strategy for enhancing efficiency of solar photovoltaic modules," IEEE Trans. Ind. Inform., [Under Review].

3. M. Rizwan, R. Aman, and A. Kumar, "An optimized deep learning framework for solar PV power forecasting using advanced hyperparameter tuning technique," in Proc. 2nd Int. Conf. Sustainable Power and Energy Research (ICSPER 2025), [Accepted].

4. R. Aman, M. Rizwan and A. Kumar "Novel Hybrid MICMAC-TOPSIS based Framework for Solar Photovoltaic Module Cleaning", 5th IEEE International Conference on Sustainable Energy and Future Electric Transportation (IEEE SeFet 2025) (Accepted)

5. A. Gupta, A. Jangra, A. Goyal, M. Rizwan, R. Aman, and A. Azeem "Novel Autonomous SPV Module Cleaning Using Shape Memory Alloy and Internet of Things for Enhanced Energy Efficiency", 5th IEEE International Conference on Sustainable Energy and Future Electric Transportation (IEEE SeFet 2025) (Accepted)

ACKNOWLEDGEMENTS

This acknowledgment would not be complete without mentioning my husband. He has been the steady wind under my wings. He is my core support system and words cannot articulate my admiration for him. He gave me unconditional support and continues to be a source of inspiration during my research.

I am wholly indebted to ALMIGHTY who is omnipotent and superpower of the universe.

Place: Delhi   **(Rahma Aman)**

Date: 13.06.2025

Table of Contents

LIST OF TABLES

List of Figures

LIST OF SYMBOLS AND ABBREVIATION

List of Symbols

Symbol	Description
i_t	Input gate
f_t	Forget gate
o_t	Output gate
g	Activation function
b	Bias parameters
Z	Propagation rule
j	neuron
T_{amb}	Ambient temperature
Tm	Module temperature
T_{min}	Minimum Temperature
T_{max}	Maximum Temperature
V	Voltage
I	Current
G, S_m	Solar irradiance (W/m²)
H_o	Global solar radiation on any horizontal surface under clear sky
H	hourly global solar radiation
C	Monthly average proportion of daylight sky covered by clouds
$E_{gl}(\lambda)$	UV global irradiation at the surface
$E(\lambda)$	Erythemal photobiological global radiation at the surface
SR	Soiling Ratio
η	Efficiency
t_{loss}	Transmission loss
ρ_D	Dust depostion

β	Tilt angle
R_b	Inclination to horizontal radiation
ΔT	Temperature difference
d_{pv}	Distance of PV from ground
d_a	Distance of anemometer from ground
u	Wind speed
E	Evaporation
R^2	Coefficient of determination
P_s	Soiled power output
P_c	Cleaned power output
$T^\circ\,C$	Temperature
Wp	Watt Peak (Maximum rated power of PV module)

List of Abbreviations

AC	Alternating Current
AI	Artificial Intelligence
ANN	Artificial Neural Network
ARIMA	Autoregressive Integrated Moving Average
ARMA	Auto regression moving average
Bi-LSTM	Bidirectional Long Short-Term Memory
CNN	Convolutional Neural Network
DC	Direct Current
DBNs	Deep Belief Networks
DCNN	Deep Convolution Neural Network
DRNN	Deep Recurrent Neural Network
DL	Deep Learning
DIM	Direct Influence Matrix
DNI	Direct Normal Irradiance
FFNN	Feed Forward Neural Network
FLIR	Forward Looking Infrared (Camera)

GHI	Global Horizontal Irradiance
GW	Gigawatts
GRU	Gated Recurrent Unit
IoT	Internet of Things
IR	Infrared
LSTM	Long Short-Term Memory
MA	Moving average
MAE	Mean Absolute Error
MAPE	Mean Absolute Percentage Error
MCDM	Multi-Criteria Decision Making
MDI	Matrix of Direct Impact
MII	Matrix of Indirect Impact
MICMAC	Matrice d'Impacts Croisés Multiplication Appliquée à un Classement
ML	Machine Learning
MLP	Multi-Layer Perceptron
MNRE	Ministry of New and Renewable Energy
MSE	Mean Squared Error
MWIR	Mid-Wave Infrared
NN	Neural Networks
PVPG	PV Power Generation
RBN	Restricted Boltzmann Machine
RBFNN	Radial Base Function Neural Network
RMSE	Root Mean Square Error
RM	Regression Model
RNN	Recurrent Neural Network
SAE	Sparse Autoencoder
SPV	Solar Photovoltaic / Solar Photovoltaic System
SVM	Support Vector Machine
SR	Soiling Ratio
S2S	Sequence to Sequence

TL	Transfer Learning
TOPSIS	Technique for Order Preference by Similarity to Ideal Solution
TW	Terawatts
UV	Ultraviolet
UVE	Ultraviolet Erythemal Energy
UVI	Ultraviolet Index
V-I	Voltage-Current
W-SVM	Wavelet Support Vector Machine
WHO	World Health Organization

CHAPTER 1

INTRODUCTION

1.1 GENERAL

1.1.1 Renewable Energy Scenario Worldwide

The global energy scenario is undergoing a rapid transformation toward sustainability, with renewable energy becoming increasingly significant. The world installed a record 510 GW of renewable energy capacity in 2024, which represents a 50% year-on-year increase the fastest in two decades. Fig.1.1 illustrates that SPV technology was the driving force behind this expansion, with over 75% of the new installations attributable to it. The total installed capacity of SPV systems worldwide has exceeded 1.6 TW as of early 2025, rendering it the fastest-growing renewable energy source. This development is primarily driven by lower installation costs, strong government incentives, increased environmental awareness, and advancements in energy storage and forecasting. However, this expansion is not without its challenges. Grid integration, storage, and the intermittent nature of solar energy demand intelligence forecasting and system optimization techniques are necessary to ensure efficiency and stability in a variety of climatic zones and energy markets [1].

1.1.2 Renewable Energy Scenario in India

India has become a worldwide leader in the implementation of renewable energy, especially in the solar energy domain. Despite the significant expansion in capacity, operational limitations especially dust deposition on modules and forecasting inaccuracies persist in hindering the optimum performance of solar systems. Recent improvements have concentrated on using intelligent cleaning technologies and AI-driven forecasting systems to tackle these difficulties. Numerous experimental projects have used robotic cleaning systems, real-time dust sensors, and computational dust modelling to mitigate soiling losses and decrease human maintenance. Concurrently, deep learning architectures are being engineered for short-term photovoltaic power forecasting using dynamic meteorological data inputs. These AI-driven systems seek to facilitate predictive

maintenance, optimize grid integration, and augment the operational efficiency of solar power facilities.
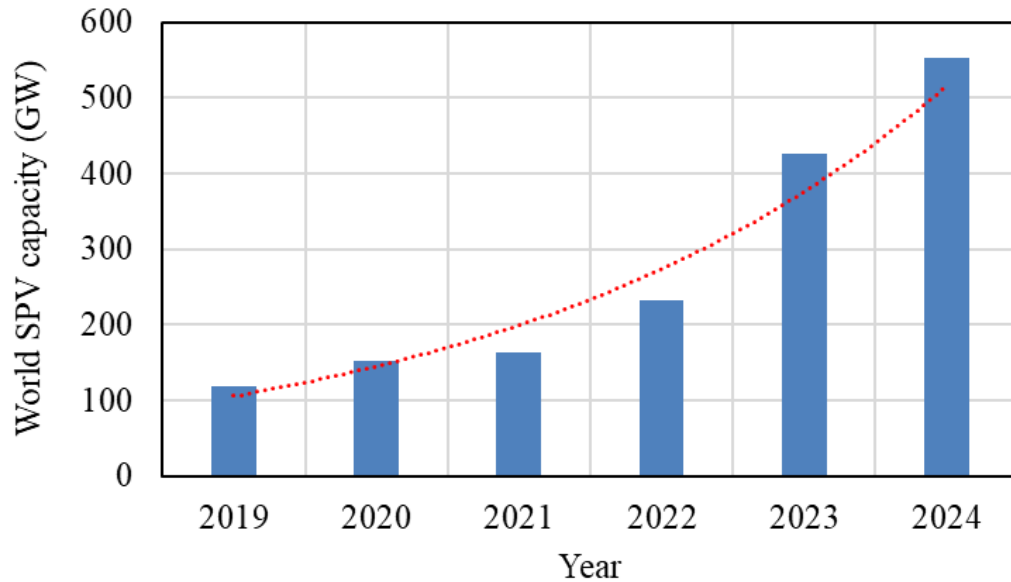
Fig. 1. 1 World SPV Capacity for 5 Years

As of early 2025, India's total installed power generation capacity is approximately 470,448 MW (470.448 GW), as depicted in the Fig. 1.2. Driven by aggressive renewable energy integration and infrastructure modernization, India's power sector remains one of the largest and fastest-growing in the world.

Thermal power (coal, gas, diesel) comprises 247,590 MW which is 52.6% of the base-load supply. Solar, wind, biomass, minor hydro, and waste-to-energy are among the RES that have grown significantly to 167,710 MW which is 35.65%. This growth has contributed to India's progress toward its 500 GW non-fossil commitment by 2030. Nuclear energy accounts for 8,180 MW which is 1.77%, while large hydropower contributes 46,968 MW which is about 9.98%. Notwithstanding these technical breakthroughs, structural challenges such land acquisition impediments, transmission congestion, and supply chain interruptions remain. The MNRE has extended the project commissioning date for affected plants to December 2025, recognizing the difficulties encountered by developers.
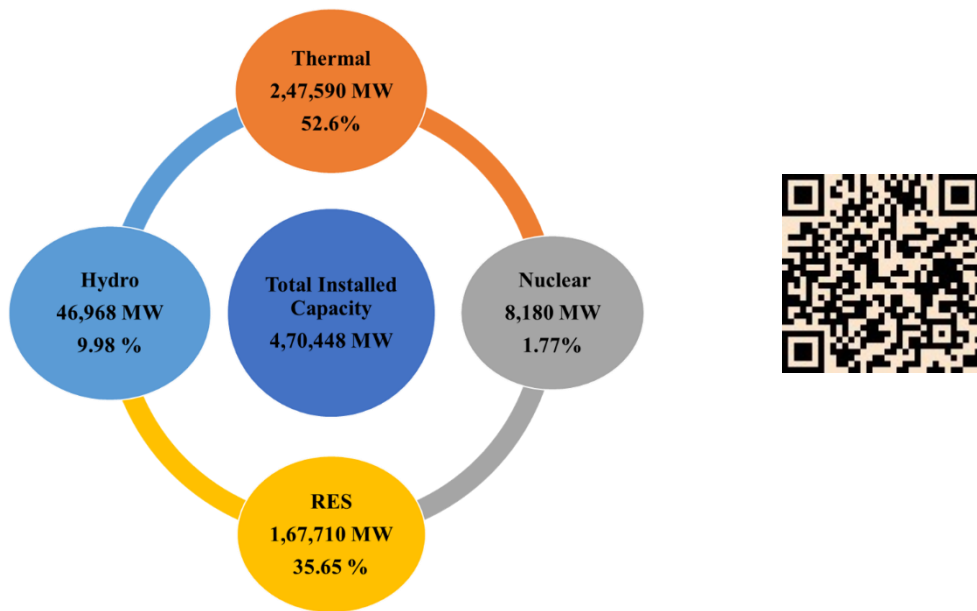
Fig. 1. 2 Total Installed Capacity and its Dynamic QR Code.
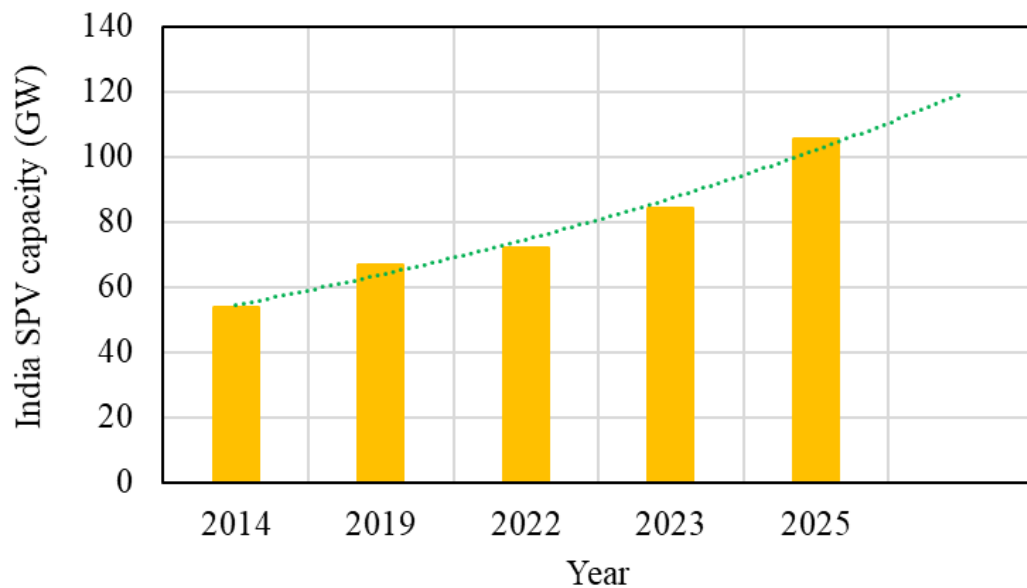
Fig. 1. 3 India SPV Capacity during 2014-2025

These developments collectively indicate a strategic transition in Indias solar sector, moving from simple capacity expansion to the incorporation of intelligent, adaptive, and self-optimizing solar infrastructure.

1.1.3 Enhancing Solar Power Production: Challenges and Future Directions

Enhancing SPV power production is essential for attaining long-term energy security, achieving climate objectives, and facilitating the sustainable growth of contemporary electrical systems. Notwithstanding significant advancements in SPV implementation, certain operational and environmental issues persist, hindering system performance and dependability. One of the most urgent concerns is contamination resulting from dust collection, especially common in arid and semi-arid areas like northern and western India. Research indicates that energy production may decrease by 10% to 30% as a result of soiled module surfaces, significantly affecting performance if not adequately remedied. Conventional cleaning techniques such as hand washing and water spraying are labour-intensive, time-consuming, and increasingly unsustainable in areas experiencing severe water constraint. Furthermore, hotspot development, caused by partial shade, cell discrepancies, or localized dust, leads to irreversible module deterioration, power losses, and, in severe instances, fire hazards.

A notable issue is the sporadic and erratic character of solar irradiation, which impedes stable energy production and complicates load balancing and grid integration. Traditional statistical and rule-based forecasting models often prove insufficient, since they do not adequately account for the complex nonlinear and dynamic interactions inherent in real-time meteorological data. Moreover, the lack of predictive maintenance protocols, real-time system monitoring, and proactive fault detection mechanisms elevates operational costs and leads to unanticipated downtimes.

Recent advancements aim to address these constraints by using AI-based forecasting models, including LSTM, Bi-LSTM, and CNN. These DL frameworks can accurately handle time-series data and environmental elements, enabling short-term photovoltaic power estimates that adjust to real-world unpredictability. The development of autonomous cleaning technologies, such as robotic dust sweepers, electrostatic repulsion devices, and superhydrophobic or photocatalytic surface coatings, is concurrently gaining momentum. These devices are designed to reduce losses caused by soiling without necessitating physical intervention.

The future of SPV optimization will be defined by the integration of physics-informed machine learning, edge computing, and IoT-enabled smart diagnostics. These integrated

solutions provide real-time defect identification, adaptive maintenance planning, and intelligent cleaning management. They together represent a transition from traditional photovoltaic systems to self-healing, adaptive, and resilient solar infrastructures. This advanced ecosystem—driven by deep learning, computer vision, and autonomous technology embodies the next frontier in optimizing solar energy production while maintaining operational sustainability across various climatic and geographic environments.

1.2 FUNDAMENTALS OF SPV SYSTEMS

SPV systems are designed to transform solar energy into electricity using the photovoltaic effect shown in semiconducting materials. A conventional SPV system consists of many essential components: SPV modules, inverters, mounting frames, balance of system parts, and optional energy storage devices.

The fundamental component of the system, SPV modules, comprises linked solar cells usually constructed from crystalline silicon that produce DC energy upon exposure to sunlight. The DC output is then transformed into AC by inverters to ensure compatibility with the utility grid or local load specifications. Mounting structures provide perfect module alignment and stability, and monitoring and control units enable real-time performance assessment, fault identification, and energy flow management. The efficacy of SPV systems is affected by several environmental parameters like solar irradiation, ambient temperature, angle of incidence, dust accumulation, and shadowing. Internal losses, such as mismatch losses, thermal impacts, and deterioration due to age, adversely affect the net energy output. Precise modelling, consistent maintenance, and astute optimization strategies are crucial for maximizing output efficiency and prolonging the operational lifespan of photovoltaic systems.

1.3 INTEGRATION OF AI IN SPV SYSTEMS

The implementation of AI in SPV systems represents a notable progression towards the development of intelligent, autonomous, and highly efficient solar energy infrastructures. AI techniques, including ML and DL, are used to improve several operational areas, such as power forecasting, defect detection, performance optimization, and autonomous maintenance.

AI-driven forecasting models, including LSTM, GRU, CNN-LSTM, and ensemble learning architectures, can learn intricate temporal patterns in real-time meteorological data, facilitating precise short- and medium-term forecasts of photovoltaic power generation. This forecasting capacity is essential for aligning power supply with grid demand, especially in areas with variable weather patterns. In fault management, computer vision techniques integrated with thermal imaging and DCNNs are used to identify and categorize abnormalities such as hotspots, cell fractures, and shading defects. These solutions provide real-time issue diagnostics, minimizing operating downtime and enhancing the safety and dependability of solar infrastructure. Moreover, AI is crucial in mitigating performance decline due to soiling by intelligently evaluating dust collection and implementing automatic cleaning systems. This encompasses robotic systems, electrostatic repellents, and hydrophobic coatings, all governed by AI-driven decision algorithms that enhance cleaning frequencies and resource efficiency.

The integration of AI, edge computing, and IoT technologies is facilitating the development of advanced SPV systems that are predictive, self-correcting, and responsive to fluctuating environmental circumstances.

1.4   RESEARCH MOTIVATION AND PROBLEM FORMULATION

Despite the fast growth and extensive deployment of SPV systems across the world, their actual field performance often falls short of theoretical predictions. This disparity is caused by a number of ongoing operational and environmental issues, including as dust collection, hotspot development, intermittent irradiation, and a lack of adaptive, intelligent control systems. In large-scale SPV systems, traditional maintenance procedures, such as manual inspection and cleaning, are not only labour-intensive and time-consuming, but also reactive, resulting in delayed problem identification, poor energy production, and higher operating expenses. Furthermore, standard statistical or rule-based models for SPV power forecasting lack the complexity to deal with complicated, non-linear climatic patterns, especially when the atmospheric conditions change dynamically. This leads to erroneous power projections, which impairs grid stability, energy trading accuracy, and effective load balancing particularly in high-penetration renewable energy conditions.

Motivated by these constraints, the current study provides a complete AI-driven framework for greatly improving the performance, reliability, and efficiency of SPV systems. The work is structured around the following key research objectives:

DL based forecasting models, such as LSTM and Bi-LSTM networks, have been developed to provide accurate, real-time predictions of SPV power production while combining several meteorological factors.

The use of thermal imaging and sophisticated image processing methods to identify, classify, and mitigate performance-degrading events such as hotspots, shading, and partial faults.

Design and mathematical modelling of dust buildup processes, as well as experimental validation under various climatic conditions, are required to precisely assess the influence of soiling on module efficiency.

Development of intelligent and resource-efficient cleaning solutions, integrating robotic platforms, surface modification (e.g., hydrophobic or photocatalytic coatings), and AI-based decision algorithms to minimize energy losses and operational overhead.

The ultimate goal of this study is to close the gap between the physical limits of SPV systems and computational advances in AI and sensor technologies. The suggested strategy, which combines predictive analytics, real-time diagnostics, and intelligent maintenance techniques, aims to increase energy production, decrease maintenance load, and prolong the operational lifetime of SPV systems. Finally, this research adds to the development of autonomous, adaptable, and high-performance SPV energy systems, allowing for a more sustainable and scalable solar future.

1.5   THESIS ORGANIZATION

This thesis is divided into seven chapters: an introduction, a literature review, an exploration of deep learning techniques for SPV power forecasting, mathematical modelling of dust accumulation, hotspot detection and mitigation using image processing, design and development of mitigation technologies, and a conclusion with future research directions.

Chapter 1 covers renewable energy, with an emphasis on SPV systems. It examines the worldwide and Indian renewable energy realities, as well as the obstacles associated with

increasing SPV power generation. Furthermore, the use of artificial intelligence in SPV systems is investigated. The chapter concludes with the research motivation and problem formulation, followed by a summary of the thesis framework.

Chapter 2 provides a literature review of SPV power forecasting strategies. It investigates the influence of dust collection on SPV modules and mitigation tactics, as well as the establishment of hotspots and how to reduce their consequences. The chapter ends with an appraisal of research gaps and contributions.

Chapter 3 focuses on the deep learning method to SPV power forecasting. It emphasizes the importance of meteorological characteristics and weather conditions in forecasting, delves into several deep learning models, and describes data collecting and preparation techniques. The design and implementation of models, as well as performance evaluation and results, are discussed in detail.

Chapter 4 discusses the mathematical modelling of dust collection on SPV modules. The effect of dust on module efficiency is investigated, and mathematical models for dust buildup are created. The models are evaluated using simulations and case studies, and the findings are described in detail.

Chapter 5 covers hotspot generation in SPV modules as well as image processing-based mitigating approaches. It studies the causes and consequences of hotspots and presents image processing techniques for hotspot identification. The chapter also goes over the creation of mitigation approaches, experimental settings, and data collecting, followed by a discussion of the findings.

Chapter 6 examines the design and development of dust-mitigation solutions for SPV modules. It examines existing technologies, suggests novel mitigation strategies, and describes the design and development process. The success of these strategies is assessed using outcomes and analysis.

Chapter 7 concludes the thesis by investigating the research's contributions and emphasizing their limitations. Future research paths are indicated for improving SPV power forecasting and system efficiency.

CHAPTER 2

LITERATURE REVIEW

2.1 INTRODUCTION

This chapter presents a detailed review of the major study issues in SPV systems, such as power forecasting, dust buildup impacts, soiling mitigation, and hotspot identification. Both traditional and advanced AI-based techniques are explored, with a focus on deep learning, image processing, and automated maintenance technologies. The analysis highlights key research needs in real-time forecasting, intelligent cleaning, and AI-powered problem diagnosis. These discoveries serve as the cornerstone for the issue formulation and AI-based optimization approach presented in this thesis.

2.2 SPV POWER FORECASTING TECHNIQUES

Solar energy is generally regarded as a prominent renewable energy source owing to its minimal environmental effect and ability to supply global energy demand. Although the COVID-19 epidemic temporarily impacted the market in early 2020, the SPV industry swiftly recovered, topping 800 GW of installed capacity. However, the intrinsic fluctuation and nonlinear behaviour of solar irradiance, especially under overcast situations, provide considerable hurdles to reliable power forecasting and grid stability[2] [3].

On cloudy days, the solar irradiation received by SPV modules experiences considerable changes due to cloud movement, which significantly impacts SPV production. Due to its non-stationary and non-linear characteristics, it is necessary to predict solar irradiance to provide more reliable solar photovoltaic plants and manage supply and demand. Numerous methods exist for forecasting solar irradiance [4]. The increasing frequency [4]. The increasing frequency of SPV systems in constructed areas makes accurate forecasting both more critical and increasingly difficult to do. Forecasting methodologies have been extensively classified into statistical methods, artificial intelligence models, and hybrid framework [5] [6] [7]. Some statistical methods used for SPV prediction in many works but this model can only learn from linear data since they lack the ability to process complicated information. For this reason, ST-based approaches are not suggested for

solving issues that need nonlinear predictions, such as those linked with SPV power. It has become clear that AI-based models perform far better than their physical and statistical counterparts. It has been shown that AI-based models are more effective than physical and statistical ones [8],[9]. In [10] a wavelet-coupled support W-SVM model was used to predict worldwide incident sun radiation using a constrained meteorological dataset. The predictor variables for this model were sunlight hours (S_t), lowest temperature (T_{min}), maximum temperature (T_{max}), wind speed (U), evaporation (E), and precipitation (P). [11] use wavelet transforms (WT) and artificial intelligence to predict the one-hour power output of a photovoltaic (PV) system based on solar radiation and temperature data. The proposed method employs wavelet transform to enhance SPV power time-series data and AI to more effectively capture nonlinear photovoltaic variability. Contemporary machine learning techniques are used to enhance the reliability and stability of photovoltaic systems. Time-series LSTM network, ConvLSTM, CNN, RF, SVM, and XGBoost regression models forecasted solar irradiance in Johannesburg, RF, SVM, and XGBoost regression models predicted Johannesburg's sun irradiance In [12] AI-driven methodologies surpass conventional techniques. AI-driven methodologies may manage flawed inputs, facilitate straightforward updates and maintenance, and engage in reasoning. In [13] proposes a random forest that integrates current and past SPV power forecasts from many models together with meteorological data to improve day-ahead SPV power estimations. The annual performance of the integrated model is evaluated against various combination techniques. Smart persistence, artificial neural networks, and random forests are evaluated for predicting global horizontal, beam normal, and diffuse horizontal solar irradiance in Odeillo, France, a region characterized by considerable weather fluctuation [14]. In [15] offers a five-layer CNN-LSTM model for solar photovoltaic power forecasts using data from Temixco, Morelos, Mexico. In the hybrid model, convolutional layer filters analyze local data properties, while the long short-term memory network captures temporal aspects. The five-layer hybrid model is ultimately contrasted with a single LSTM, a two-layer CNN-LSTM hybrid model, and two notable benchmarks.LSTM and CNNs are perhaps the most popular DL approaches. The primary concept behind employing such models on time-series data is that LSTM networks are capable of capturing sequence pattern information, whereas CNN models are beneficial for extracting valuable features and may filter out

noise in the input data. However, although LSTM networks are designed to work with temporal correlations, they only use the attributes provided in the training set, whereas CNNs are not typically adapted for long temporal dependencies despite being used to extract patterns of local trend and the same pattern that appears in different regions of time-series data. Thus, a hybrid model that combines the strengths of both deep learning approaches might enhance the accuracy of predictions. Hybrid model forecasting is one of the most appropriate models for forecasting power. The authors in [16] Proposed a CNN-LSTM model to forecast anomalies in photovoltaic power generation (PVPG) that existing machine learning models struggled to comprehend well. The hybrid model can precisely forecast the amount of photovoltaic electricity generated by including factors that influence its production. Subsequently, to demonstrate the model's utility, they contrasted it with other machine learning techniques. The model extracts patterns from multivariate time series data on the PVPG and temporal variations. The findings indicate that the 5D CNN-LSTM model effectively predicts PVPG, outperforming both the standalone LSTM model and the 2D CNN-LSTM model. Some algorithms improve performance further by categorizing input days based on weather conditions or integrating results from various predictors [17]. Comparative studies consistently indicate that CNN-based and hybrid deep learning frameworks outperform standalone models in predicting solar radiation and electricity production based on irradiance, temperature, cloud cover [18][19]. These improvements highlight the need of AI and hybrid deep learning for accurate, robust, and real-time SPV power forecasts.

Forecasting power production is critical from an economic standpoint. Furthermore, SPV power generation forecasting allows the systematic planning of electricity production to effectively address difficulties such as system stability and balance in power generation. In spite of this, it is difficult to get hourly solar energy data, even from stations that have previously taken measurements. Because of this, it is essential to estimate solar energy in order to fulfil the requirements for renewable energy. Researchers employ models such as fuzzy logic to anticipate SPV production for smart grids in order to estimate the amount of solar energy that is produced globally [20][21]. As solar energy continues to expand, it is becoming increasingly vital to make accurate predictions regarding radiation, the author in [22] a study conducted in Spain utilized a combination of models such as Support Vector

Regression (SVR) and Random Forest Regression (RFR) in order to enhance short-term observations of radiation. Accurate estimates of SPV assist reduce the need for additional backup energy, which in turn drives down costs and improves the efficiency of power dispatch, which in turn helps to maintain grid stability.

In recent years, different models have arisen to forecast SPV power over a long period. The SPV power forecasting models are based on CNN and LSTM neural networks [23]. Various complex models based on machine learning have been suggested to enhance the accuracy of solar power forecasting by utilizing a variety of meteorological inputs and datasets. In [24], a hybrid LSTM-CNN model was trained on one year of data, accounting for parameters including relative humidity, temperature, pressure, global horizontal irradiance, wind speed, and cloud type. It outperformed conventional models across a variety of seasons and atmospheric conditions, achieving a Mean Absolute Error (MAE) that ranged from 27.38 W/m² to –37.02 W/m². [25] A comparative study between LSTM and ANN, which utilized inputs such as temperature, humidity, cloudiness, radiation, and seasonal features (month and day) over a year, demonstrated that LSTM outperformed ANN. The RMSE values for LSTM were 1.23–1.82%, while those for ANN were 1.67–8.02%. Another method, LSTM-PVPF, was introduced in [26] . It was tested over a three-year period and utilized six input parameters, including wind speed, ambient temperature, and daily rainfall. It reported MAPE values ranging from 6 to 9%, which is suitable for large-scale datasets and provides high prediction accuracy at a reduced computational cost. In [27] author proposed a CLSTM model that was exclusively derived from solar irradiance data over a 12-year period. This model achieved an RMSE of approximately 1.515%, an MAE of approximately 4.672%, and an APB of approximately 1.233%. It also exhibited superior performance compared to isolated models such as CNN, LSTM, and DNN.

2.3 ANALYSIS OF DUST ACCUMULATION AND ITS EFFECT ON SPV MODULES

Dust significantly impacts the performance and productivity of SPV modules. The characteristics of dust (such as kind, size, shape, meteorology, etc.) vary according on the geographical location [28].

Environmental variables directly affect PV cell performance and efficiency, making them important in mathematical modeling of SPV systems. By including these parameters, models may better anticipate SPV system behavior under different situations. To achieve the optimal design of SPV systems with great dependability, mathematical models are used, and the impacts of weather conditions and solar irradiation are included in these models. Researchers wanted to provide models and methods to determine SPV system variables. Literature studies have modeled transmittance ratio [29], reduction in solar energy gain [30], degradation rate [31] solar cell power, efficiency, and I-V characteristics [32].

The sophistication of models is enhanced by the inclusion of additional factors that influence the system's performance. However, there is always a trade-off between the accuracy, complexity, and number of factors in the derived model.

More than 100 parameters have been examined in [33] to predict the soiling losses in PV systems at 20 stations in the United States. Particulate matter (PM), particularly PM10 and PM2.5, as well as certain precipitation parameters and the average number of days between consecutive rainfalls, were identified as the most effective soiling predictors. In [34], a NN model was proposed that predicts SPV power output by considering the physical, chemical, and spectral characteristics of soil. The model utilizes a hybrid data clustering algorithm to provide efficient data preprocessing and a new data division technique to ensure that the training data set contains an adequate amount of data. In comparison to other networks, the neural network hybrid models demonstrated superior performance for both known and unknown soil samples. A RM and neural network NN were devised in another study [35] to forecast the loss of SPV power as a result of artificial soiling. The NN model was found to be more effective at certain irradiance levels and soil types, while the RM model was more effective at other levels and types. Both models were experimentally validated at a diversity of irradiance levels and five types of soils. In order to determine the power loss resulting from soiling in 1 MWp plants in Southern Italy, four Bayesian neural network (BNN) models were created to be used both before and after cleansing [36]. In [37] author seeks to create a dust-solar cell model. The single-diode model models PV cell performance based on current-voltage relationships. Soiled SPV modules affect installation production. The module's angle of inclination and climatic conditions such as aerosols, relative humidity, ambient temperature, pressure, etc. cause this effect. In [38] authors setup an experimental SPV plant

to analyses soiling losses and anticipate SPV plant production in one to three hours. The author in [39] develops a computational model to research the impacts of residue and encompassing temperature on the presentation of a SPV framework. The models assess change productivity using improved counterfeit brain organization ANN models' multi-input multi-output. The model-building approach is displayed and confirmed for accuracy using several measures. Daily cleaning boosts SPV system performance, and an artificial neural network boosts accuracy to 99.8%. The author in [40] uses artificial neural networks to assess and anticipate the power production of a grid-connected 20-kWp SPV power plant in Tiruchirappalli, India, a reputable manufacturing industry. A multilayer perceptron-based ANN model is suggested for power generation day-ahead prediction. A monocrystalline silicon SPV module's power was predicted by an artificial neural network. PV module soiling refers to the deposition of dust, soil, and microfibers from the environment, as well as the growth of minute particles such as moss and fungi. It is a lesser-known factor that substantially reduces the power output by operating as a barrier for photons of effective light used by a module. The anticipated loss in irradiance and power can be calculated using a soiling ratio (SR) parameter [41]. Author in [42] presents methodologies to quantify SR and soiling rate (S_{rate}) for two representative commercial technologies, polycrystalline or multi crystalline silicon (mc-Si) and thin-film cadmium telluride (CdTe) modules, through soiling monitoring stations deployed in the selected climate regions. These methodologies can be applied to polycrystalline or multi crystalline silicon (mc-Si) and thin-film cadmium telluride (CdTe) modules. Data used to compute SR and S_{rate} in accordance with the international standard IEC 61724-1/2017 was used. Since SPV module cleaning is essential, constant monitoring and evaluation are required to optimize these processes [43].

2.4 HOTSPOT FORMATION AND ITS MITIGATION TECHNIQUES IN SPV MODULES

Solar energy has emerged as one of the most promising and commonly used renewable energy sources owing to its availability, sustainability, and little environmental effect [44]. However, various operational and environmental parameters, including as dust deposition, shade, temperature, humidity, and module aging, have a significant impact on SPV system

efficiency [45] [46] [47]. Dust collection is especially harmful since it limits the quantity of incoming solar energy while also causing heat hotspots and permanent module degradation. The type and content of dust particles, such as red soil, limestone, and fly ash, have been proven to drastically affect the optical characteristics of the SPV surface, resulting in decreased performance. Theoretical models have been created to forecast the effect of regional air pollution on PV production, and they have been confirmed using experimental data from contaminated metropolitan areas [48]. Furthermore, the interactions between dust, humidity, and air velocity are complicated and interconnected, requiring a comprehensive approach to solar cell design and performance improvement [49].

Empirical investigations in Kathmandu found that natural dust deposition caused a 29.76% decline in efficiency over a five-month period, emphasizing the importance of cleaning frequency and dust density (measured at 9.67 g/m²) [50]. Similar studies in Eastern Saudi Arabia have shown that SPV modules left uncleaned for more than six months might lose up to 50% of their power, stressing dust as a major driver of long-term deterioration [51] [52]. Author in [53] conducted a thorough examination of the kinds of defects induced by environmental variables and established baseline procedures for defect analysis and monitoring.

To offset these performance losses and improve problem detection capabilities, researchers have increasingly relied on AI solutions. Recent research has used signal processing, feature extraction, and machine learning methods like SVMs and NNs to predict fault location and severity with greater accuracy [54][55]. Thermographic imaging has emerged as a promising technique in this context, allowing for non-invasive and quick assessment of PV modules by identifying thermal anomalies associated with dust-related hotspots [56][57]. IR thermography, together with fuzzy logic, has been utilized to automatically detect defect types by comparing IR pictures of problematic and healthy panels [58].

Deep learning technologies have improved fault diagnoses. The author in [59] created a deep learning system for detecting and classifying hotspot defects and hot substring faults in terrestrial and aerial thermal pictures, with an outstanding 98% accuracy In addition, a DRNN was presented to estimate regional dust concentration and investigate dust dispersion patterns using unique pre-processing and segmentation approaches. The model

accurately predicted with a R² of 78.7% and MAE of 3.67, tested under three real-world scenarios [60].

Building on these advances, a transfer-learning-based multi-scale CNN was presented for detecting PV faults using thermographic pictures. The model corrected class imbalance by oversampling and obtained 97.32% accuracy in identifying 11 distinct defect types, including diode failure, hot spots, and fractures [61]. Other research has shown that drone-based picture classification is useful for assessing PV deterioration, making this the first time such datasets have been used for automated diagnostics.These deep CNNs outperformed expectations in terms of accuracy, recall, and F1-score, demonstrating their suitability for large-scale monitoring [62].

In addition, multispectral deep CNNs have been used for visual defect identification, while anisotropic diffusion filters and sophisticated segmentation algorithms have improved picture clarity for diagnostic tasks [63] [64]. A Naive Bayes-CNN hybrid architecture has been proposed to fuse temporal video frame data for more robust crack identification, demonstrating unique data fusion approaches [65]. Furthermore, two-dimensional CNNs trained on scalogram features extracted from SPV system time-series data have successfully classified a broad variety of abnormalities [66].
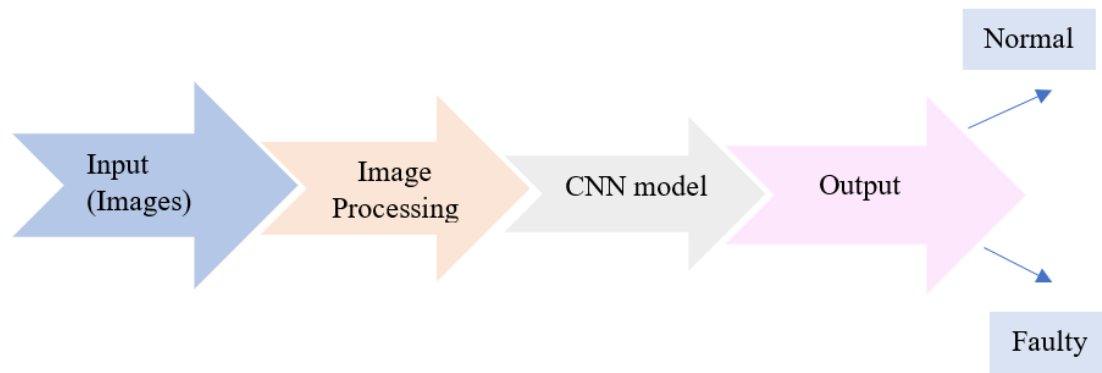
Fig. 2. 1 Schematic Representation of a CNN Algorithm

Finally, when combined with transfer learning, convolutional neural networks such as Alex-Net have shown high generalization capabilities across domains, allowing for accurate classification of SPV modules flaws even under complicated environmental settings [67]. These developments highlight the importance of sophisticated inspection systems in improving SPV module dependability, lowering maintenance costs, and facilitating the worldwide transition to sustainable energy. Despite algorithm-based SPV

failure detection research, best classifier performance remains an issue. Their performance depends on the type of problem, input signals or images, number of inputs, number of layers, and network settings. In Fig. 2.1. complete CNN algorithm is given.

In [68] a deep learning-based SPV module defect detection method using electroluminescence images. It addresses two technical challenges: generating high-quality EL images for limited samples, and creating an efficient model for automatic defect classification using the generated EL image. A deep joint learning model discussed in [69] identifies the kind and location of hot areas. Categories of experiments are done on the acquired dataset to benchmark the suggested framework. It has limited fault detection capability, is expensive and time-consuming, and is incapable of quickly identifying the actual site of the defect [70]. This research in [71] describes a novel method for identifying modules that detect hot areas and locating them. To provide a robust detection framework, two new region-based convolutional neural networks are combined. The key contribution is the use of thermography and telemetry data to offer a module condition monitoring response. CNN model automatically classifies thermographic pictures into hotspot and operational classes. Various pre-processing approaches were assessed to decrease picture noise. Using a dataset with various acquisition procedures, the model achieved 99% accuracy [72]. The suggested technique beats benchmarked alternatives in effectiveness and efficiency [73] proposes an end-to-end deep learning pipeline that uses EL pictures to identify, localise, and segment cell-level irregularities in solar PV modules. The modular pipeline uses modified Faster-RNN for object recognition, Efficient Net for image classification, and autoencoder for weakly supervised segmentation. The modular pipeline enables upgrading deep learning models to state-of-the-art upgrades and adding new functions. A new automated solar cell fault detection and classification system is provided in [74]. Support vector machine is used for classification in different applications [75].Further the proposed Deep Feature-Based (DFB) technique classifies deep neural network-extracted image features using support vector machines, K-Nearest Neighborhood, Decision Tree, Random Forest, and Naive Bayes. The suggested method in [76] automatically classifies thermographic pictures from the system's CNN with 98% accuracy in two-minute testing. This method is faster than others in literature, with lower expenses, diagnostic time, and power production losses. This study develops a computer

vision method to semi-automatically extract PV modules from thermographic UAV footage. Deep 2-dimensional CNN are utilized in a novel approach to extract features from 2-D scalograms of PV system data, thereby facilitating the detection and classification of faults. An exhaustive quantitative evaluation of the proposed method is juxtaposed with previous approaches to PV array failure classification, such as traditional machine learning and deep learning [77]. [78] presents two improved RF classifiers for FDD: the Euclidean distance-based reduced kernel RF (RK-RFED) and the K-means clustering-based reduced kernel RF. [79] uses two sophisticated convolutional neural network models to categories the panel's defect type and identify its area of interest. The proposed method compares classification models using F1 score, with ResNet-50 transfer learning model scoring 85.37 %.

2.5 MITIGATION TECHNIQUES OF DUST ACCUMULATION ON SPV MODULES

Dust is generated by desert storms, volcanic eruptions, industrial emissions, building debris, traffic, automobile emissions, microorganisms, pollen, plant matter, dander, and other sources. Dust-related energy losses from SPV modules are a huge problem that cannot be ignored [80]. However, dust is among the critical factors influencing the economics, output, and performance of SPV modules. The geographical places specify the dust properties, such as types, sizes, shapes, and meteorology. Researchers have recently focused on developing effective methods to reduce and remove dust accumulation on SPV modules, as dust significantly reduces their efficiency. Various approaches, including mechanical cleaning systems, hydrophobic and self-cleaning coatings, and even electrostatic and robotic cleaning solutions, have been explored to maintain the best energy output and reduce maintenance costs [81]. A study of 186 US SPV sites found that cleaning an SPV plant halfway through dry summer without rainfall can boost energy harvesting by 0.81% to 4.7% yearly and up to 9.8% using an automated cleaning system [82].

Two types of cleaning methods, passive and active, are used to improve SPV module power. Passive SPV module cleaning options include rain, tilting modules for natural shedding, hydrophobic coatings, and smooth surfaces. Manual, automatic, and self-cleaning SPV modules using robotic arms with water jets are active techniques. Passive

methods are cheap but inefficient to work in all situations. The active methods clean better but cost more. SPV modules are being cleaned using one of three techniques: mechanical, coating, and electrostatic. The four mechanical methods, air-blowing, robotic, water-blowing, and ultrasonic vibration, are studied to clean the surface of SPV modules. These techniques require much energy to operate and have moving parts. While consuming much water is a significant limit of this method, especially in dry areas. Electrostatic cleaning has been the subject of a new design and implementation. Considering the electrode designs, the cleaning performance of this device has been evaluated [83]. The electrostatic dust removal action of transparent conductive films made of carbon nanotubes is the basis for a novel electrostatic adsorption dust removal technique for SPV modules investigated in this work [84]. This study investigates the optimal counteracting force required to eliminate dust particles stuck to SPV modules. A self-cleaning system that utilizes fluid velocities to lift dust particles stuck to a SPV modules surface while minimizing the generated static charge has been developed [85]. This work offers the design and experimental analysis of a revolutionary self-powered SPV module cleaning mechanism system to clean the SPV module. This cleaning method does not require electricity from the SPV module, which must be cleaned because it is powered by two little SPV modules with rechargeable batteries [86]. The author in [87] presents an SPV module cleaning robot that autonomously cleans SPV modules regularly. The robot cleans the surface of the modules by using air blowing, liquid spraying, wiping with a wiper, and drying any moisture on the modules using a cylindrical brush. The suggested robot is operated by the IoT from a remote location, thereby minimizing human labour at the solar facility and enabling remote monitoring SPV modules to generate electricity from solar irradiation directly. How much light SPV modules use impacts their efficiency. SPV modules use 30%–40% of incident solar irradiation. Due to ambient dust and module glass reflection, a lot of incident irradiation remained unutilized. To overcome these technological challenges, self-cleaning/superhydrophobic antireflection coatings are popular [88]. Solar superhydrophobic coatings are a difficult area of study due to the necessity to attain both transparency and high-water repellent qualities, a combination that is frequently discussed in detail in the existing literature. While many of the research focus on superhydrophobic coatings broad uses, such as water and oil separation, ice formation resistance, biofouling

avoidance, and self-cleaning characteristics, few focus specifically at their development for solar energy systems. The necessity for optical transparency severely restricts the materials and production processes available, making the development of coatings appropriate for SPV modules extremely challenging. The authors in [89] tries to reduce that gap by determining the influence of dust accumulation on SPV module performance, and the function of transparent, self-cleaning superhydrophobic surfaces in minimizing associated optical, thermal, and economic losses. Dust-related power loss in SPV systems must be mitigated to deploy solar in arid places economically. High aerosol concentrations and frequent sandstorms cause solar array dust to accumulate. Dust remains due to occasional light showers. An automated robotic cleaning system was used to test the effectiveness of dry-cleaning SPV modules [90]. Existing cleaning methods have drawbacks like high cost, energy use, and limited efficiency. There is a requirement for a cleaning system that offers a low-power, efficient solution that works well on any module orientation.

2.6   SUMMARY OF GAPS AND RESEARCH CONTRIBUTIONS

➢ Most current models use restricted meteorological inputs, neglecting critical parameters such as module temperature, wind speed, and humidity that affect photovoltaic output. Deep learning methodologies provide enhanced precision; nevertheless, hybrid models that include these characteristics remain underexplored.

➢ Thermal imaging is extensively used for defect detection; however, it has not yet been incorporated into real-time, AI-driven performance improvement.

➢ The impacts of dust deposition, taking into account particle type, humidity, and geographical fluctuation, are not well modelled.

➢ Present cleaning techniques mostly rely on physical labour or predetermined schedules, with limited advancements in intelligent, adaptive cleaning systems that adjust to seasonal and environmental variations.

These deficiencies underscore the need for a cohesive, intelligent system to improve forecasting, problem detection, and maintenance in SPV operations.

2.7   PROBLEM FORMULATION

The main objectives of the proposed research work based on the above-mentioned research gap is formulated as follows:

1. SPV power forecasting using deep learning approach considering meteorological parameters and weather conditions

2. Study analysis for hotspot formation and its mitigation technique using image processing.

3. Mathematical and analysis of dust accumulation on SPV modules.

4. Design and development of new technologies for mitigation of dust accumulation on SPV modules.

CHAPTER 3

DEEP LEARNING APPROCH FOR SPV POWER FORECASTING

3.1 INTRODUCTION

SPV power generation has emerged as a critical component in the global transition to renewable energy. However, the inherent variability and intermittency of solar electricity present considerable hurdles to its integration into the electrical grid. Accurate forecasting of PV power generation is critical for effective grid management, load balancing, and energy trading. Deep learning approaches have grown in prominence in time series forecasting in recent years due to their capacity to understand complicated, nonlinear relationships in data. This chapter investigates the use of deep learning models in forecasting SPV power generation, showing both the benefits and drawbacks of such approaches.

3.2 FORECASTING METHODS

Based on these time horizons various forecasting models have been studied and implemented various models are short term forecasting models are statistical model, intelligent techniques, hybrid models and long and medium-term forecasting models are econometric models, end use models and statistical models. Accurate prediction is a main challenging area for the SPV system when integrated with grid. For keeping the SPV modules working at its maximum efficiency with a maximize output following research problems are proposed and formulated. Statistical models are categorized as AR, MA, ARMA, and ARIMA, while intelligent models include fuzzy logic, genetic algorithm, and expert system. Machine learning models are linear regression, SVR, FFNN, RBFNN, MLP, Beysian Algorithm, Decision Tree, Reinforcement and deep learning includes DRNN, LSTM, GRU, DCNN, DBN, RBN, SAE, S2S as shown in Fig. 3.1.
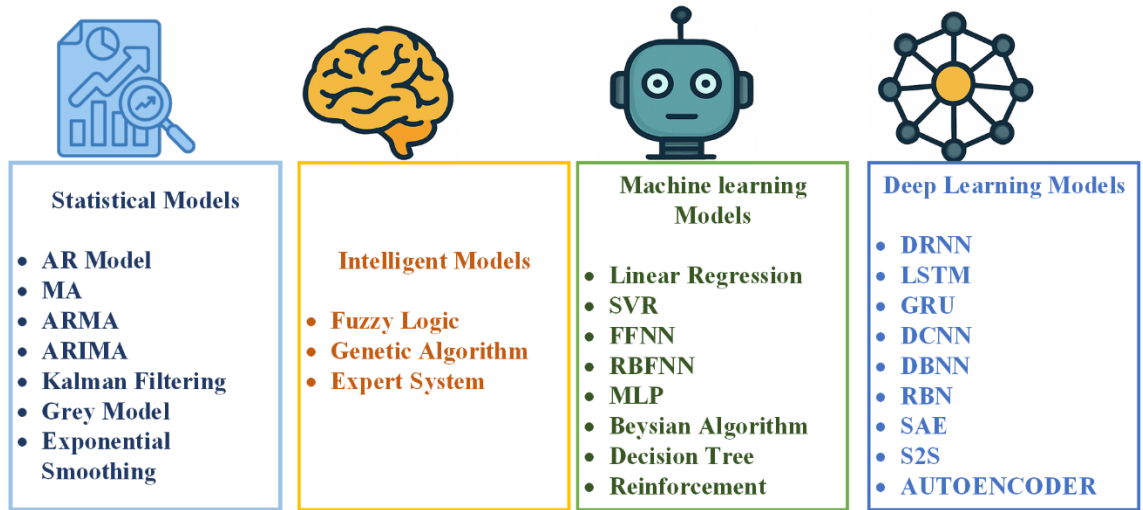
Fig. 3. 1 Forecasting Models for Medium and Long-Term Forecasts

3.3 PROPOSED TECHNIQUE

3.3.1 CNN for Feature Extraction

The efficacy of models depends on by the quantity of stacked layers and the kind and dimensions of the kernel. Convolutional and pooling layers are used to extract profound characteristics from the input layer data.
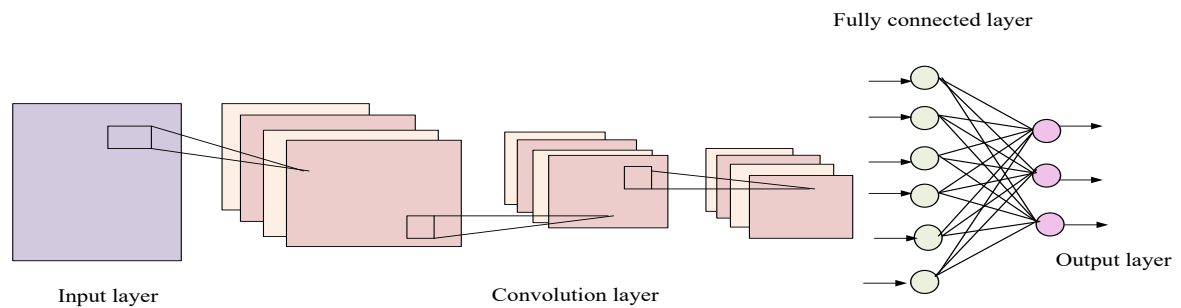
Fig. 3. 2 Schematic Architecture of CNN

The characteristics are then sent to the fully connected layer, which classifies the resultant values. A CNN is used to extract hierarchical image features. Consequently, a CNN may extract pertinent information from sequential and two-dimensional input data [91]. A CNN fundamentally seeks to construct many filters that may extract latent features by sequential

convolution and data pooling, as seen in Fig. 3.2. Ultimately, the fully connected layer integrates these abstract characteristics, and an activation function is used to address the classification or regression task. In the convolution layer, the feature maps from the preceding layer are convolved with a convolution kernel, resulting in the generation of output feature maps via an activation function [92]. The convolution layer applies a convolution kernel to the feature maps from the preceding layer, resulting in the generation of output feature maps.1D-CNNs are often used to analyze natural language or time series due to their capability to manage sequential data. 1D-CNNs vary from 2D-CNNs since both the convolution kernel and the data sequence possess a one-dimensional configuration. As seen in Fig. 3.3, the kernel of a 1D-CNN traverses a singular dimension.

Kernal

Time series data

X- axis

Seconds
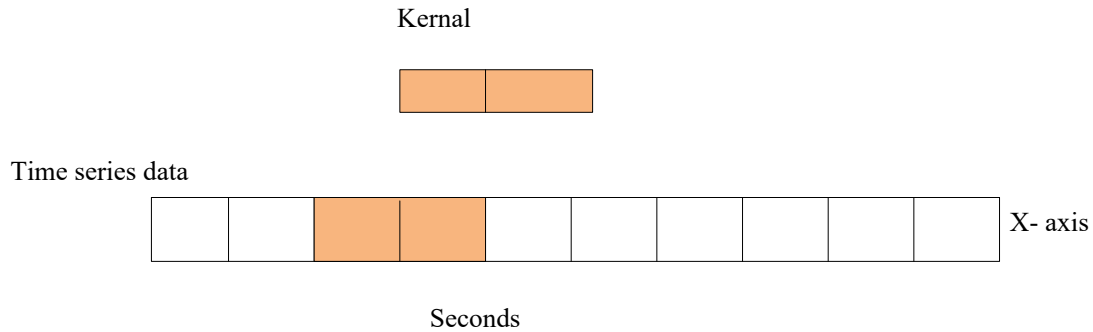
Fig. 3. 3 1D-CNN Computation Method

3.3.2 LSTM Model

The LSTM network is a kind of recurrent neural networks. In contrast to conventional MLPs, RNNs use the temporal context of the incoming data. The LSTM network has layers that facilitate the modelling of long-term relationships in sequential data. The network has been trained to identify patterns and trends in SPV power, including temporal connections that allow precise projections. The LSTM output elucidates the temporal dynamics of SPV power generation. This is feasible with an RNN because to the recurrent interconnections among the neurons. An LSTM may retain and retrieve information due to the configuration of neurons inside a memory cell. These memory cells may retain information indefinitely. Figure 3.4 illustrates that the memory unit has three gates designated as "Input gate (i_t)," "Forget gate (f_t)," and "Output gate (o_t)," together with a recurrent connection. It regulates the ingress and egress of information inside the cell. Every gate in the LSTM receives information from the input neuron. Each gate is equipped

with a mechanism for activation and deactivation. It has a single input, x_t, and two feedbacks from the preceding state, s_{t-1} and c_{t-1}. The sigmoid activation function (g) is used by gates, whilst the tanh function is utilized by states. The memory unit of the LSTM may be elucidated by a series of equations, wherein w represents the weight parameter and b denotes the bias. An LSTM has a fundamental architecture of three layers: forget, input, and output. Initially, x_t and s_{t-1} are included into the LSTM design. A decision is made about the retention of the information. All tasks are executed by the forget layer f_t [93].

$$f_t = g\left(w_{xf}x_t + w_{hf}s_{t-1} + b_f\right) \tag{3.1}$$

where activation function (g). Also, the input layer it is given by equation 3.2.

$$i_t = g(w_{xi}x_t + w_{hi}s_{t-1} + b_i) \tag{3.2}$$

$$c_t = f_t c_{t-1} + i_t it_t \tag{3.3}$$

The last step is to use the following expressions in the output layer to get the output data.

$$it_t = tanh(w_{xc}x_t + w_{hc}s_{t-1} + b_i t_i) \tag{3.4}$$

$$o_t = g(w_{xo}x_t + w_{ho}s_{t-1} + b_0) \tag{3.5}$$

$$s_t = o_t \, tanh(c_t) \tag{3.6}$$

The process described above keeps going back and forth. This model learns weight parameters (w) and bias parameters (b) to minimize the difference between actual training values and LSTM output values
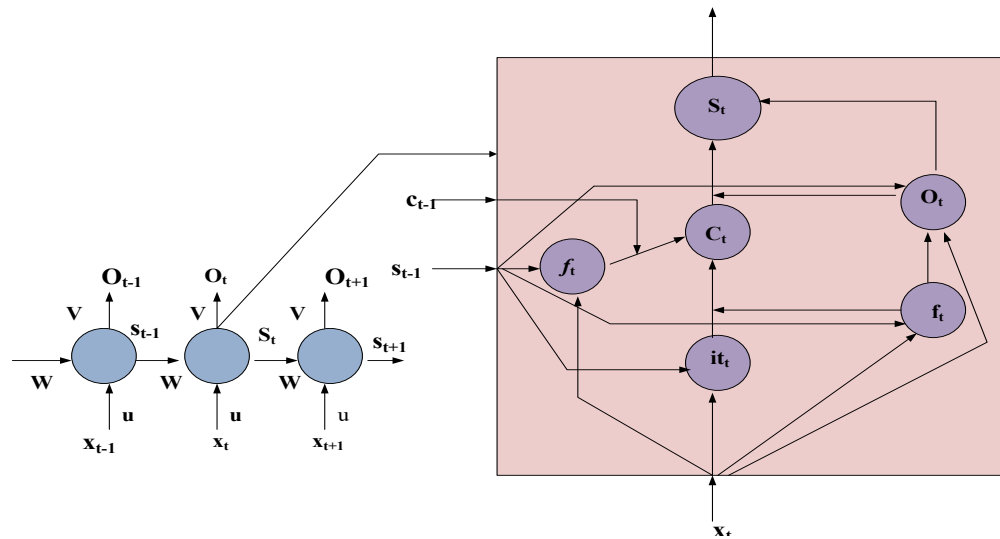
Fig. 3. 4 An Internal Architecture of a LSTM Cell

3.3.3 CNN-LSTM MODEL

In this method CNN and LSTM layers are combined as shown in Fig. 3.5 here, the selected inputs are sent to the CNN layer first for feature extraction, then to the flatten layer, and finally to the LSTM layer for prediction. After pre-processing, the CNN layer uses time series to find local features. The one-dimensional CNN works well for time series applications because the convolution kernel moves in a clear direction. This allows it to automatically pull out the unobserved data characteristics in the time direction. The retrieved features from the encoder CNN are fed into the LSTM architecture. The training data, as well as the various gates of the LSTM network, are constantly changed so that the LSTM model may find the relationships between the input and output sequence [94]. The proposed model parameters considered are shown in Table 3.1 and the proposed work is shown in Fig. 3.6. Following are the steps for proposed work.

Stage 1- Input dimension reconstruction

1. Inputs are selected that are correlated with the SPV power six inputs are considered for training the models.

2. The reconstruction of inputs such as cloud cover, UV index, Wind Speed, Irradiance, temperature, humidity are done to extract spatial features while historical SPV power to obtain temporal features.

3. These inputs are given in proposed model CNN-LSTM and LSTM and CNN deep learning model

Stage 2- Model development

The Deep learning models are developed with the help of Jupyter notebook platform.

The 3 deep learning models are trained individually by giving the inputs\Fine tuning of parameters is done in this stage to make the model more accurate to predict SPV power

Step 3 – Evaluation and assessment

The 3 deep learning model are employed for evaluating the performance in terms of three weather conditions sunny, partially cloudy and extremely cloudy and four different seasons (winter, summer, rainy and post monsoon)

Stage 4- Interpret Results

The best SPV power prediction among the 3 deep learning models is analysed based on the performance metrices such as RMSE, MSE, MAE and R^2.

Table 3. 1 Hybrid CNN- LSTM Model Parameters

Model layers		Values
Inputs	Size	3,7
Conv1D	Kernal Size	2
Max pooling	Pooling size	2
Conv1D	Kernal size	2
Max pooling	Pooling size	2
Flatten	-	-
LSTM layers	Hidden Neurons/Activation	64/ Relu
LSTM layers	Hidden Neurons/Activation	64/ Relu
Learning rate	-	0.0001
No. of epochs	-	500
Optimiser	-	Adam
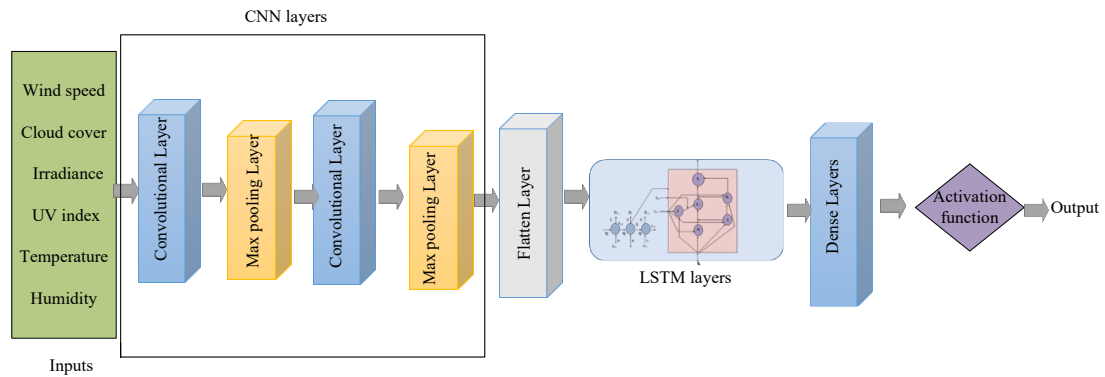
Fig. 3. 5 Structure of CNN-LSTM Hybrid Model
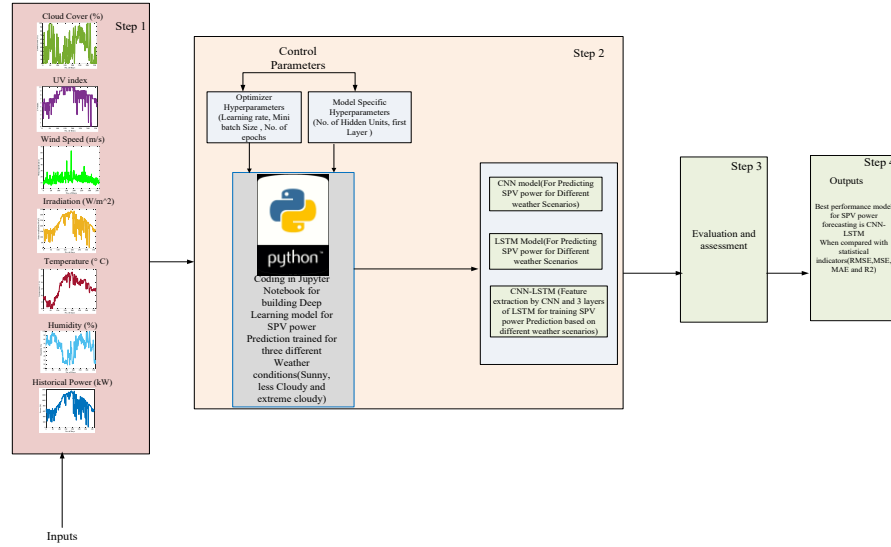
Fig. 3. 6 Flowchart of Proposed CNN-LSTM Model

3.3.4 Multilayer Perceptron (MLP)

MLP is one of the frequent artificial neural network architectures to resolve scientific issues. It can approximate non-linear connections. Complex function modelling ANNs. They can easily modify their weights and disregard noise and irrelevant data. They're user-friendly. MLP has two phases: the entry of data through the MLP's inputs and the error corrections through Backpropagation. This cycle is run numerous times to reduce error using Bayesian Regularization, a standard approach [17]. MLP consist of three layers i.e., input, output and hidden. For most problems, however, a single hidden layer is enough [18]. Fig. 3.7 shows a neuron (j), xi represents the inputs, wij represents the weights that connect each input I to the neuron j, and yj is the output of the neural network. Neurons conduct the propagation rule and activation function. Inputs and synaptic weights define the propagation rule (Z). The sum of inputs xi by neuron j weights wij is the most common. This function travels through the origin. Adding threshold bj removes this constraint. This is another fixed-value input whose weight bj must be modified. The rule for propagation is calculated.

In this equation, Z_j represents the result of applying the propagation rule to neuron j, x_i represents the input vector I, w_{ij} represents the weight that links input I to neuron j, and b_j represents the threshold that is linked with neuron j. The output of neuron j is determined by the activation function (A), which takes into account the neuron's activation. This is

28

dependent on the rules of propagation, such as A_j is the neuron's activation, and f is its activation function. Each layer of a neural network is interconnected with the ones below it, besides forming a neural network. In the context of neural networks, a layer refers to a collection of neurons that share a common z-index, the simultaneous information processing of the network. The neural network's behaviour is determined by each neuron activation function and the topology and training used to determine the weights.
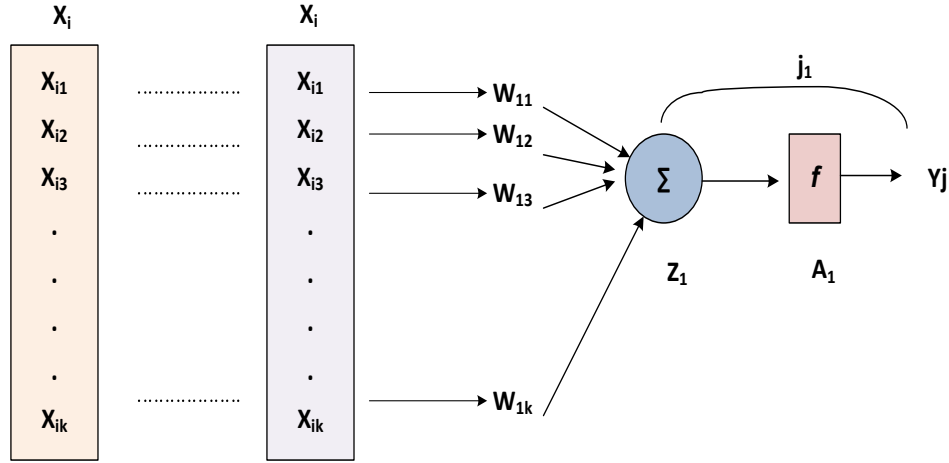
Fig. 3. 7 Schematic Representation of Neurons.

3.4   DATA PREPARATION

This chapter uses dataset which is dived into two cases

   Case 1: Irradiance, Temperature which are obtained from solar analyzer 9018T and humidity, windspeed are obtained from the solcast site and cloud cover, UV index and SPV power is mathematically modelled for obtaining higher accuracy results. Solcast has access high-resolution historical Time Series and TMY data with minimal uncertainty for energy simulations and reliable solar resource assessments. Prepared for integration through API and the solar analyzer is a portable instrument utilized for troubleshooting, monitoring, measuring, and analyzing a variety of SPV system parameters. The data used is for one year from 24 November, 2021 to 24 November, 2022 containing 52560 data i.e., 365 x 24 x 6, the data collected is at 10 minutes interval, the dataset comprises of inputs having irradiance, humidity, wind speed, Cloud cover, Temperatures, SPV power, UV index as shown in Fig. 3.8. The Fig. 3.9 is a correlation matrix from here the correlation of several meteorological parameters with power is been shown, in this proposed deep learning model

from the correlation matrix the inputs which are having highest correlation with SPV power is considered as an input for prediction of SPV power. The multi-input chosen in this work are Humidity, Temperature, UV index, Irradiance, Wind speed, Cloud cover, SPV power which are provided to the CNN, LSTM, CNN-LSTM model for prediction of SPV power.

Case 2. The data used for training was recorded at every 30 minutes and there are 17614 sample data. The data recorded at every 30 minutes. The meteorological data for New Delhi is collected and analyzed by the solcast site during one year. In this data the parameters that were included are direct normal irradiance, global horizontal irradiance (GHI), diffused horizontal irradiance, wind speed, air temperature, and relative humidity were all included in this data. The collected real-time data has a time step of 30 minutes.

3.4.1 Selection of Inputs based co-relation matrix

This section explains the inputs used to construct the SPV power prediction model. The choice of input variables and location is critical to the operation of the SPV system.

Despite the flat terrain, the movement of clouds and the kind of clearness index in the sky have an influence on the power output of the PV system. SPV power is affected by changes in ambient temperature, humidity, wind speed, cloud cover, UV index, and irradiance shown in Fig. 3.10. Mathematical computation of cloud cover and UV index is done in this section. The modelling of cloud cover and UV index with the help of meteorological parameters such as wind speed, irradiance, humidity, and temperature these data is recorded on intra hourly basis so as to get the cloud cover and UV index at 10 min of intervals. The usage of proper sorts of input parameters results in better performing prediction models. The inputs considered for prediction are shown in the Fig. 3.8. This figure is plotted considering one year of data

If the inputs used are redundant, have a low correlation factor, or essential parameters are missing, the prediction results will be complicated [95].

A) Modelling of SPV power.

To forecast SPV power, the real irradiance incident on the SPV , the exact wind speed on the SPV module, and the modules temperature must be estimated. The SPV power equation is as follows [16]:

$$P_c = P_r S_m(1 + K_1 \log(S_m) + K_2 \log(S_m)^2 + K_3 T_a + K_4 T_a \log(S_m) \tag{3.7}$$
$$+ K_5 T_a \log(S_m)^2 + K_6 T_a{}^2)$$

$$T_a = \frac{S_m}{26.9 + 6.2 * w_{in}} \tag{3.8}$$

$$S_m = \frac{S_{m1}}{1000} \tag{3.9}$$

$$T_a = T_{a1} - 25^o C \tag{3.10}$$

$$W_{in} = \frac{D_m{}^{0.2}}{D_a} * w_s \tag{3.11}$$

where P_c is the real time module estimated power, win is the speed of wind on the module, T_a is the change in temperature caused by wind speed, and K_1 - K_6 are PV module constants. Da is the distance between the PV module and the ground surface, and Dm is the distance between the anemometer and the ground surface. Table 3.2 shows the values of the constants used to calculate SPV power. The power received for one year is displayed in Fig. 3.8 g) when P_r is set to 5 kW.

Table 3. 1 Parameters for Calculating SPV Power

Parameters	Values
K_1	-0.046689
K_2	-0.072844
K_3	-0.002262
K_4	0.000276
K_5	0.000159
K_6	-0.000006
D_m	10 meters
D_a	7.2 meters

B) Modelling of Cloud Cover

Cloud cover is the percentage of the sky that is obscured by clouds at a given place and time. It is frequently stated as a percentage or fraction range from 0 to 1, with 0 representing clear sky with no clouds and 1 representing totally overcast sky with clouds covering the whole sky.

Authors in [96] included Cloud cover, temperature, relative humidity, and wind speed to develop a model for estimating global solar irradiance. The correlation can be expressed as

$$H = \frac{\left[H_o \sin \alpha_s \left(a_0 + a_1 \frac{N}{10} + a_2 \left(\frac{N}{10}\right)^2 + a_3(T_a) + a_4.RH + a_5 w_s + d \right) \right]}{k} \tag{3.12}$$

There is an inverse relation between cloud cover and Irradiance which means more the cloud less will be the Irradiance

where a_0, a_1, a_2, a_3, a_4, a_5, d, and k are regression coefficients; N is the cloud cover in tenths; T_a is the ambient temperature (°C). Here H is hourly global solar radiation (GSR) and H_o is GSR on any horizontal surface under clear sky [97]

There is an inverse relation between cloud cover and Irradiance which means more the percentage of cloud cover less will be the Irradiance

$$H = H_o[1 - (1 - k)\,C] \tag{3.13}$$

where H_0 represents the expected daily global radiation for a clear sky, C represents the monthly average proportion of the daylight sky covered by clouds, and k represents a constant defining solar radiation transmission inside clouds. This formula has a structure similar to the Anstrom-Prescott (A-P) formula, which describes the relationship between sunlight duration (S) and global solar radiation (H) as: Calculate H from equation (12) Relation between H and S is as below.

$$H = H_o \left[a + b \left(\frac{S}{S_o} \right) \right] \tag{3.14}$$

a and b are regression coefficients to be found If the estimate is exact and devoid of aesthetic flaws, the total cloud amount should follow the relationship as[98]:

$$C = \left[1 - \left(\frac{S}{S_o} \right) \right] \tag{3.15}$$

Nonlinearity was discovered in the connection between C and $(1 - \frac{H}{H_o})$, where H_o represents extraterrestrial solar radiation.

In this work, a relationship between cloud cover and sunlight every 10 minutes for a one-year New Delhi location data is considered having latitude is 28.75 longitude is 77.12. For more accurate cloud cover estimation sunshine hour data is required.

We can estimate S/S_0 using the correlations reported in (3.13). Then, multiplying this amount by S_0 gives us the value of S. cloud cover is calculated from (3.14).

C) Modelling of UV index

The UV Index is scaled from 0 to 11, with 0 being the lowest and 11 being the most intense. These figures are organised as follows:

In UV index 2 or less means low, 3 to 5 means Moderate, 6 to 7 means High, 8 to 10 means very high and 11 or higher means extreme as in Table 3.3, ultra violet (UV) radiation this effect the SPV power as the correlation with power is 0.8574.

UV relation with SPV power is linear as the UV is more power production will be high, UV index is related to Irradiance as in equation (3.16)

$$\text{UVI} = \frac{1}{25} \, \text{mW/m}^2 UVE \tag{3.16}$$

$$UVE = 40 \int_{0.28}^{0.40} E_{gl}(\lambda)\varepsilon(\lambda)d\lambda \tag{3.17}$$

where $E_{gl}(\lambda)$ and $\varepsilon(\lambda)$ are UV global irradiation at the surface and erythemal photobiological global radiation at the surface and the erythemal photobiological reaction action spectrum for human skin at the wavelength (λ). Micrometres (μm) are used to talk about the boundaries of the integral. Each UVI measure is equal to 25 milliwatts per square metre of broadband UVE.

Table 3. 2 UV Index Scale Range

UV Index	Rating
11 or higher	Extreme
8 to 10	Very high
6 to 7	High
3 to 5	Moderate
2 or less	Low

The cloud cover and UV index from the Fig. 3.8 above shows that when the cloud cover is 1 UV index is minimum and vice versa the cloud cover and UV index is modelled with the help of the meteorological inputs and the data obtained is at every 30 minutes. The correlation of the inputs with SPV power is shown in Fig.3. 11 where the Irradiance is the best factor which effects the SPV power as in Table 3.4.
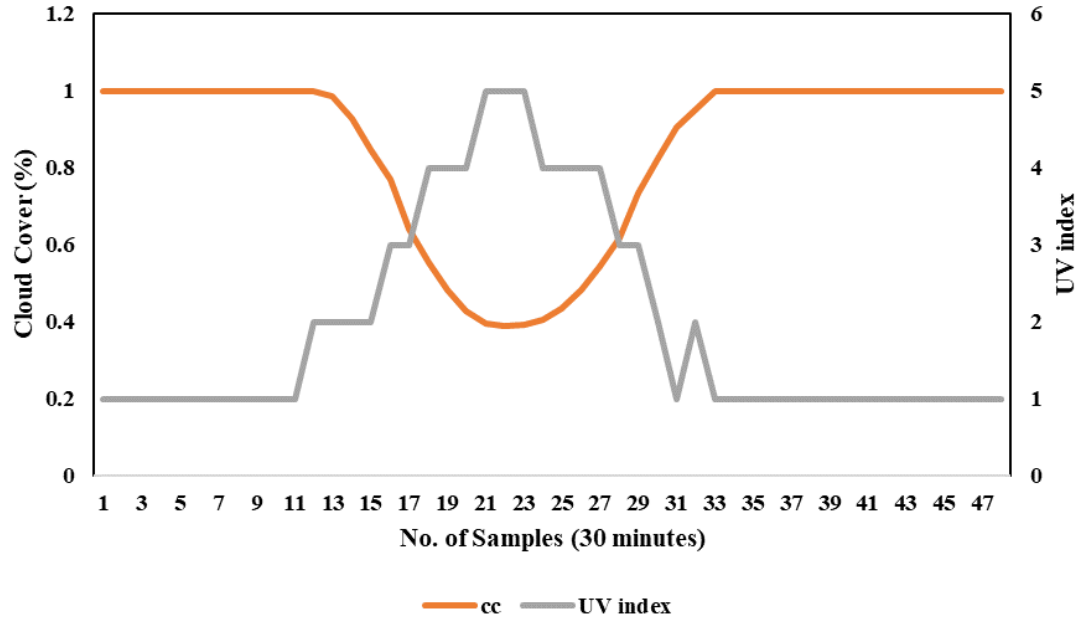
Fig. 3. 8 Cloud Cover and UV Index Relation for 24 Hours.

The power output of the SPV system is considerably influenced by a variety of meteorological parameters, as illustrated by a comprehensive correlation analysis of the dataset obtained from the Solcast platform. In Fig 3.10, the correlation matrix is shown, which clearly demonstrates the nature and strength of these relationships.

The UV index exhibits the greatest positive correlation with SPV power output among the observed parameters, with a correlation coefficient of 0.8574. This robust correlation suggests that the fundamental operating principle of photovoltaic cells is the direct correlation between increased photovoltaic generation and higher UV radiation levels. This is consistent with the fact that SPV cells convert ultraviolet and visible light into electricity.

Additionally, SPV power exhibits a moderate positive correlation of 0.6315 with temperature. Although moderate temperature increases can initially enhance the semiconductor properties of PV cells, excessive heating typically results in a decrease in efficiency. However, the overall impact is still positive to a significant extent under the normal operating conditions depicted in the dataset.

On the other hand, SPV power exhibits a very low positive correlation of 0.08937 with wind speed. While wind can indirectly improve SPV performance by cooling the modules and thereby reducing temperature-induced efficiency losses, its direct impact on solar

irradiance capture is negligible. Consequently, its influence on SPV output is negligible when examined with other variables.

SPV power output exhibits a moderate positive correlation of 0.3591 with sea level pressure. This implies that, although atmospheric pressure fluctuations can have a minor impact on solar irradiance penetration and, consequently, PV generation, they are not the determining factors.

Conversely, the output of SPV systems is negatively correlated with both humidity and cloud cover. The amount of sunlight that reaches SPV modules is reduced as a result of the scattering and absorption of solar radiation by the increased water vapor in the air, which is indicative of high humidity levels. In the same way, increased cloud cover prevents direct sunlight from reaching the surface and reduces GHI, which leads to a reduction in photovoltaic generation. The negative correlations underscore the fact that both humidity and cloud cover are critical adverse factors and must be meticulously incorporated into SPV power prediction models to enhance the reliability of the forecast.

A comprehensive set of meteorological parameters is included in the dataset obtained from Solcast, which serves as a solid foundation for predictive modelling. The direct relationships between the six specified input features (UV index, temperature, wind speed, sea level pressure, humidity, and cloud cover) and SPV power generation are numerically depicted in Table 3.4, while the feature correlation matrix in Fig. 3.10 visually summarizes these interrelationships.

Table 3. 3 Correlation Coefficient Between the Six Selected Inputs to the SPV Power

Inputs	Correlation Coefficient (R^2)
Irradiance	1
Temperature	0.6315
Humidity	-0.6509
Wind Speed	0.3937
Cloud cover	-0.2931
UV index	0.8574
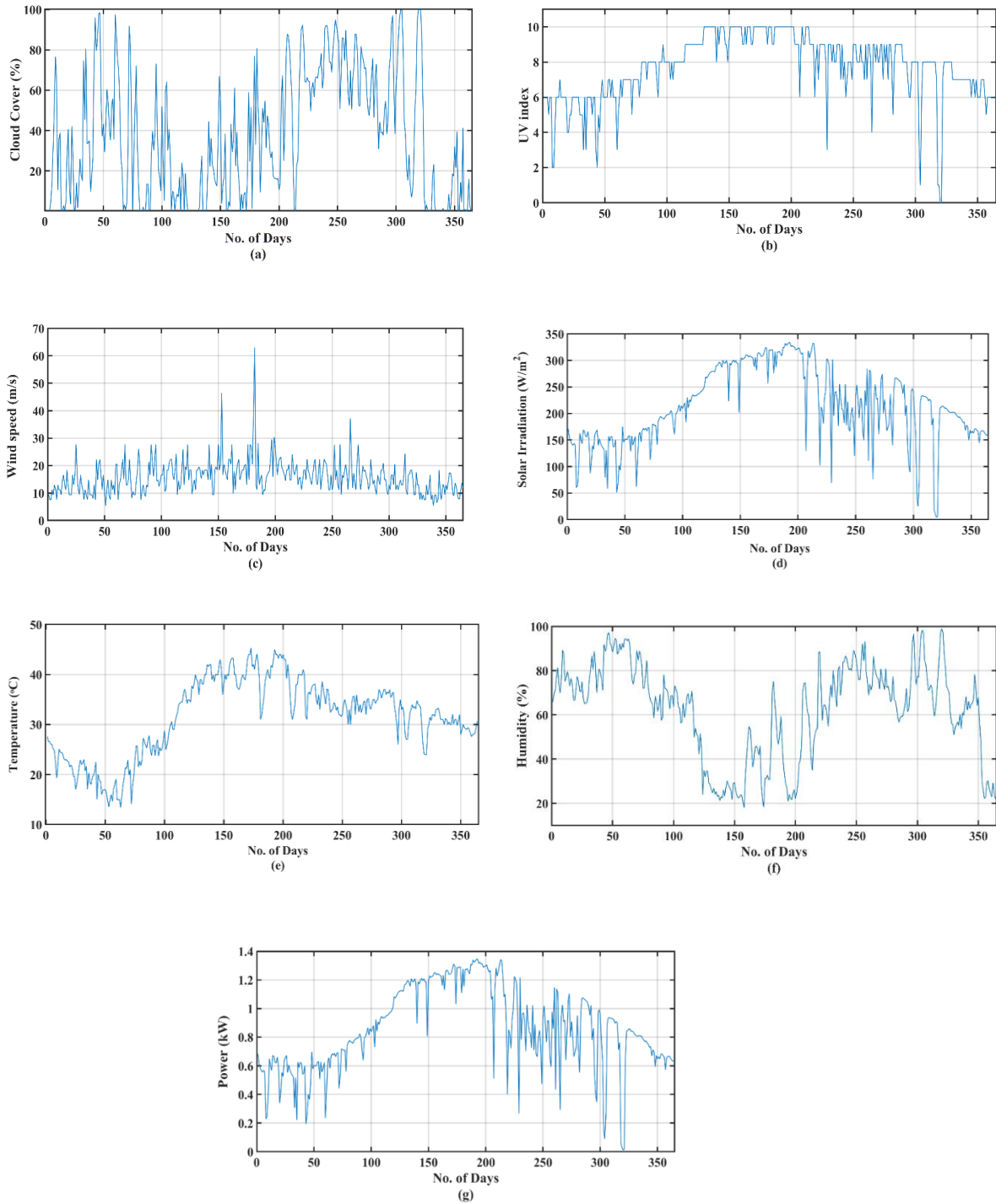
Fig. 3. 9 Daily plots of 1 year for (a) cloud cover (%) (b) UV index (c) wind speed (m/s) (d)

Irradiance (W/m2) (e) Temperature ° C (f) Humidity (%) and (g) power (kW)
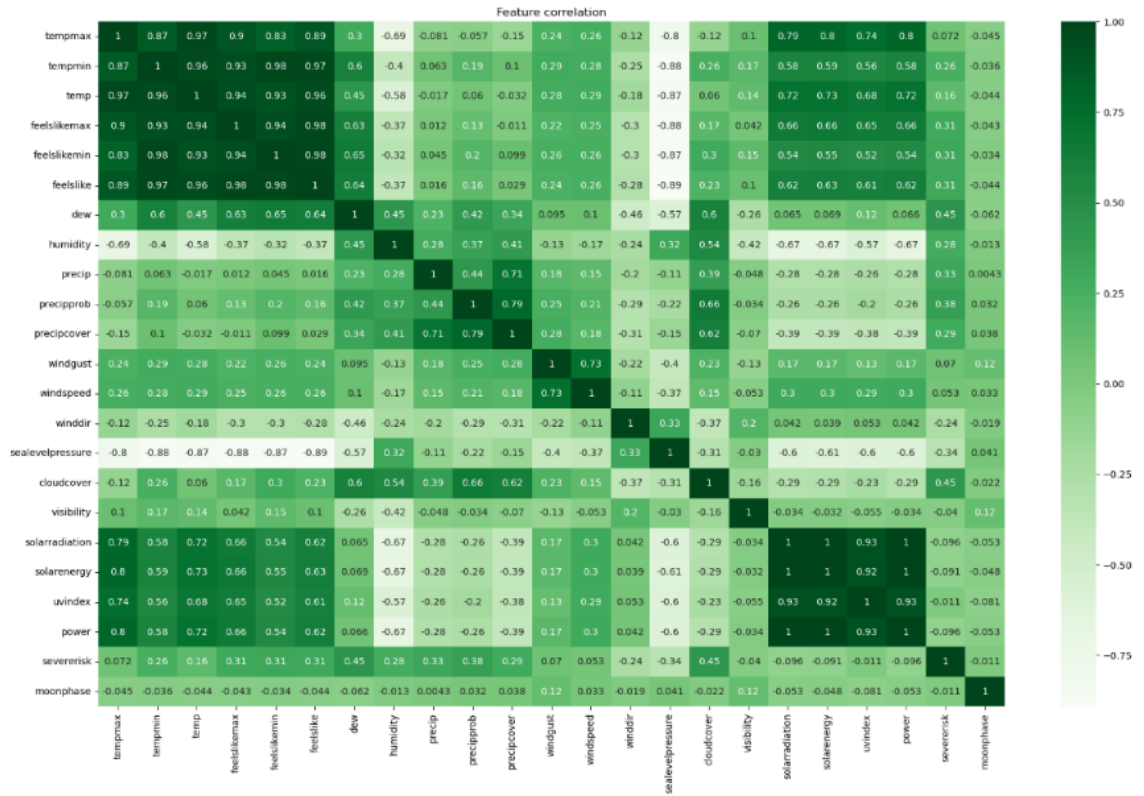
Fig. 3. 10 Feature Correlation Matrix

In conclusion, this correlation analysis emphasizes that humidity and cloud cover are the significant negative predictors of SPV power output, while UV index and temperature are the dominant positive predictors. Consequently, in order to improve the reliability of SPV energy yield predictions, forecasting models must strategically evaluate these parameters. Correlation plot of different inputs with SPV power is shown in Fig. 3.11 were Fig 3.11(a) illustrates a negative correlation between cloud cover and power, suggesting that solar generation is diminished in overcast conditions. Fig. 3.11(b) illustrates a robust positive correlation between the UV index and power output, with greater UV levels resulting in increased power output. Power generation is also mildly positively influenced by wind speed in Fig. 3.11(c), which may facilitate panel cooling. Solar radiation is the most critical factor, as evidenced by Fig. 3.11(d), which indicates a direct linear increase in power. Fig. 3.11(e) indicates that power output increases as temperature increases, although this may be contingent upon the efficacy of the panel at elevated temperatures. Finally, Fig. 3.11(f) suggests that solar power output is generally reduced as a result of increased humidity, which is likely due to atmospheric scattering and absorption.
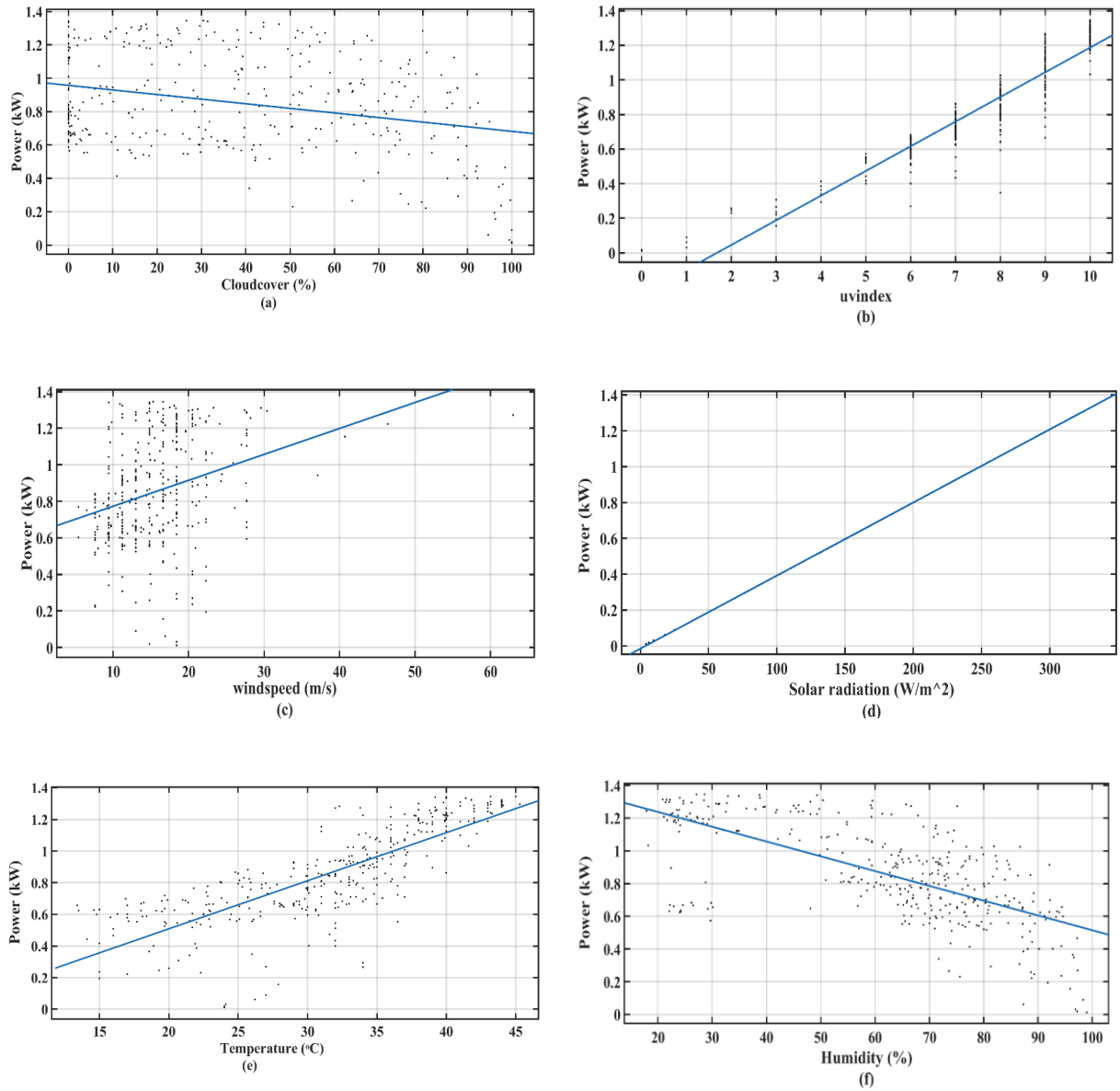
Fig. 3. 11 Correlation Plot of SPV Power with (a) Cloud Cover b) UV Index (c) Wind Speed (d) Irradiance (e) Temperature (f) Humidity

3.5 RESULT AND DISCUSSION

3.5.1 Result and Discussion for Dataset 1

Deep learning models and proposed hybrid models are employed for the prediction of SPV power using multivariate time series data. The selection of the inputs that are utilised in the

models that are run through deep learning is covered in Section 4. In the first place, a hybrid model that consists of CNN and LSTM features is presented. The dataset that was used for this analysis spanned one year containing 52560 (365*24*6), and additional LSTM layers were connected in order to learn the pattern of SPV power prediction based on weather scenarios i.e sunny, partially cloudy and extremely cloudy. The CNN model assisted in the extraction of features from the dataset. The outcomes that were predicted are then compared with the LSTM and CNN models. In this section. The dataset was divided into four seasons: winter, summer (pre monsoon), rainy and post monsoon. Deep learning models such as CNN, LSTM, CNN-LSTM, and ARIMA are trained to predict SPV power based on the seasonally divided dataset. To further improve the accuracy of SPV power predictions, the models were trained on data divided by different weather patterns. This section is divided into 2 parts first part discusses the prediction based on seasonal patterns i.e (winter, summer, rainy and post monsoon) and then in the second shows the prediction based on 3 weather conditions and third parts discusses the performance metrices.

Data is collected throughout a year and used to train deep learning models such as CNN-LSTM, CNN, and LSTM. In addition, the ARIMA model is trained to predict SPV power. The dataset contains 365 data points for a year. Fig. 3.12 (a) depicts a comparison prediction plot of deep learning models. The error plots are shown in Fig.3.12 (b). Based on the data shown in Fig. 3.12 a), it can be concluded that the CNN-LSTM model is a better approach for predicting SPV output, with less mistakes than other proposed methods.

(a)   (b)
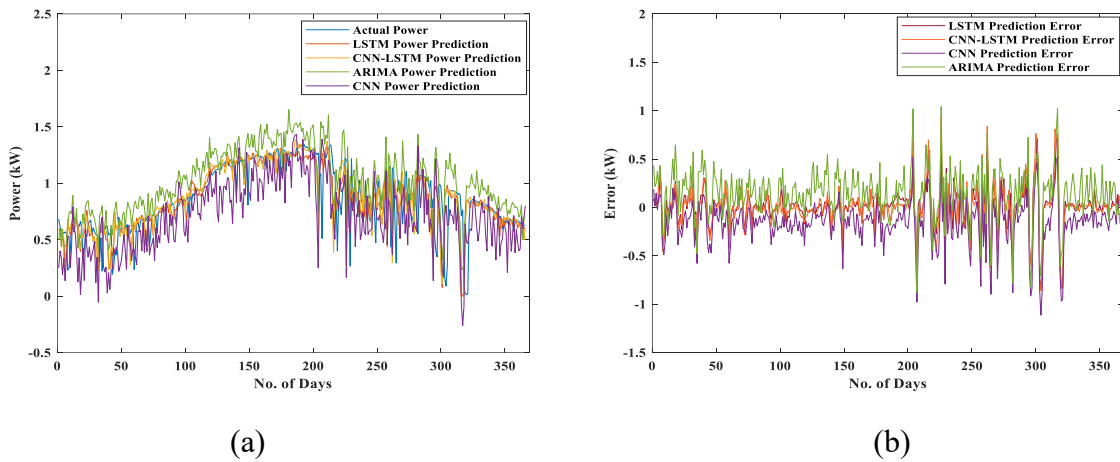
Fig. 3. 12 Comparison of CNN-LSTM, LSTM, CNN and ARIMA models for one year data a) solar PV power prediction plot with actual power   b) error plots

3.5.1.1   SPV Power Prediction Based on Different Seasons

The complete dataset is divided in four different seasons—winter, summer (pre monsoon), rainy (monsoon) and post monsoon—

The winter season encompasses the months of December to March.

The summer (pre monsoon) season spans from April to June.

The monsoon season, known as the rainy season, spans from June to September.

And the post monsoon season spans from October to December

These different seasonal pattern datasets are used to train the deep learning models for different seasons. The deep learning models are trained based on different seasonal pattern and SPV power prediction is made according to different seasons. From Fig. 3.13 it can be observed that maximum power is obtained in months of summer the variations are also less as compared to rainy, post monsoon and winter conditions. Fig. 3.13 below shows the SPV power prediction comparison plot and error plot of various deep learning models with the traditional model i.e. ARIMA.

Winter Season
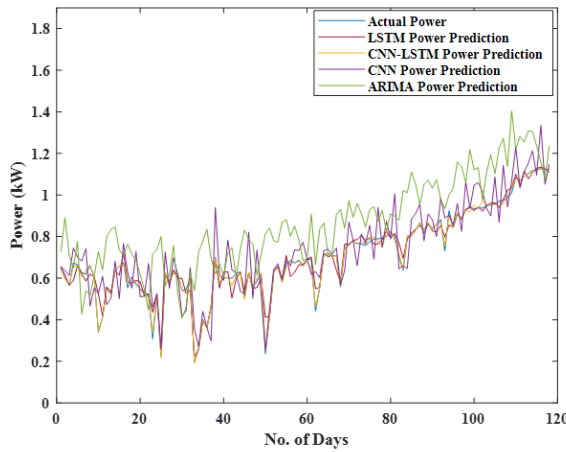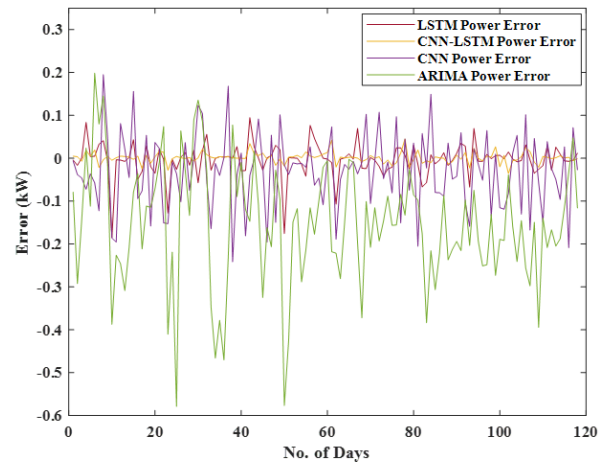
(a) Power plot   (b) Error Plot

Summer Season
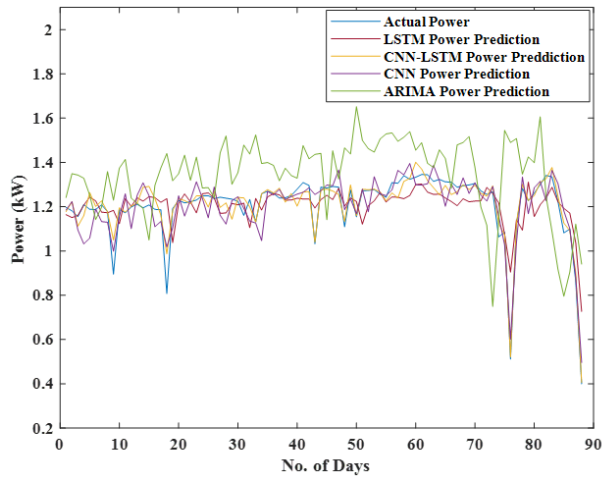
(c) Power plot
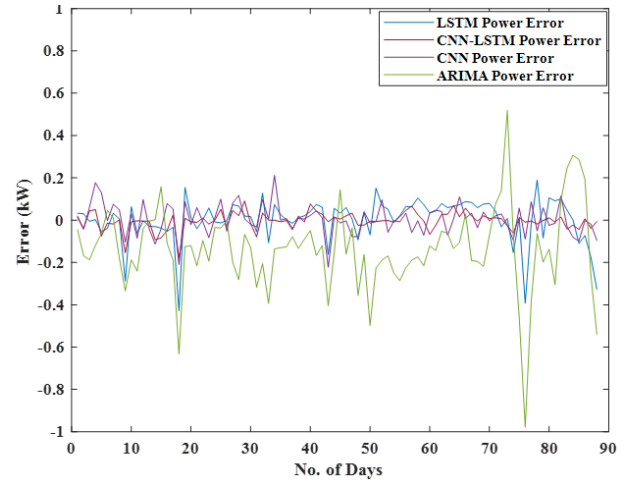
(d) Error Plot

Rainy Season

(e) Power plot

(f) Error Plot

41
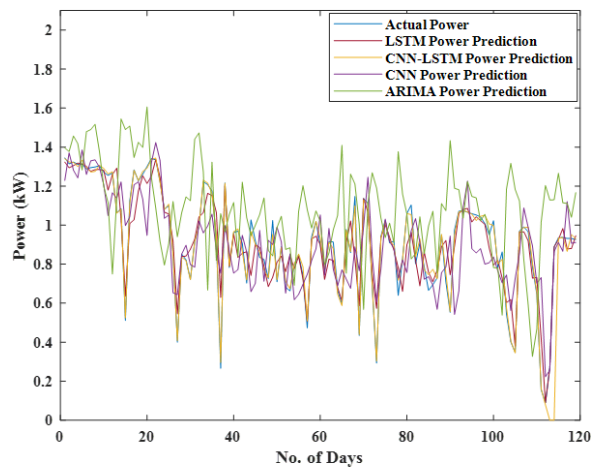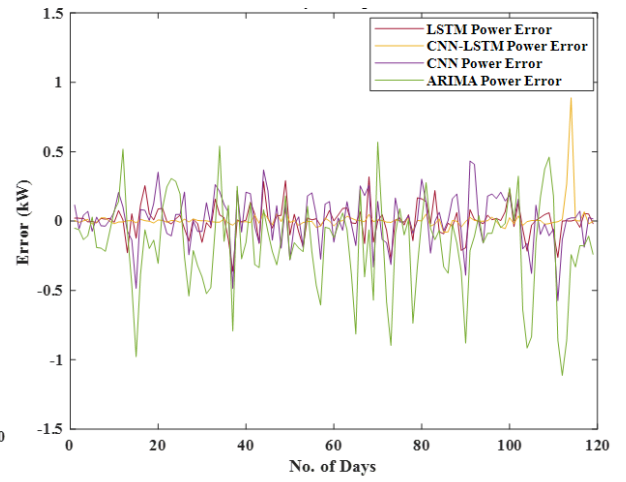
Post Monsoon   Season

(g) Power plot   (h) Error Plot
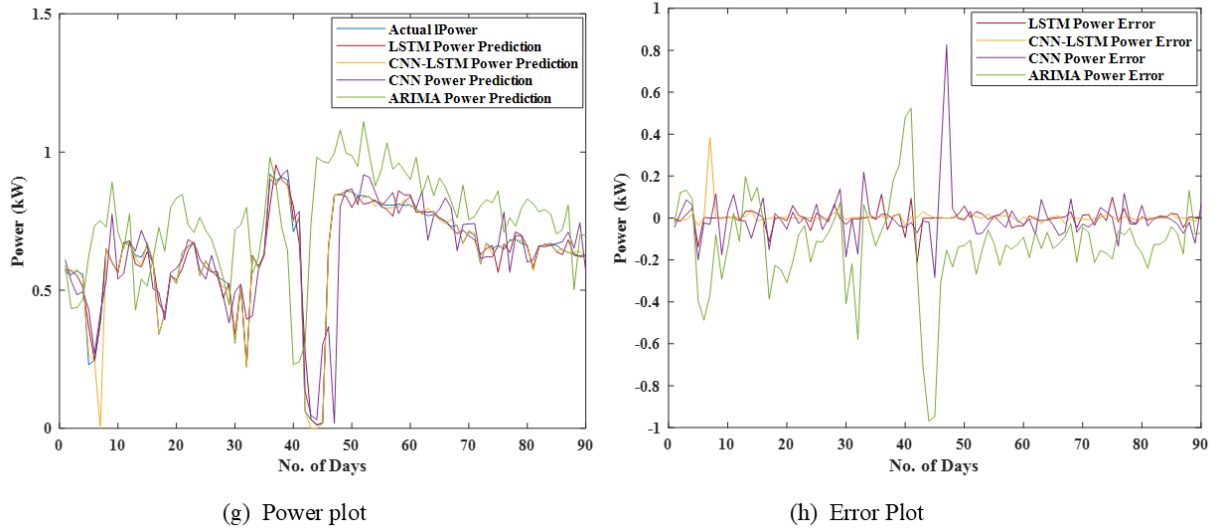
Fig. 3. 13 Comparison of Different Deep Learning Models With ARIMA Model in Four

Different Seasons

3.5.1.2   SPV power prediction based on weather conditions

One year of SPV power data is analyzed based on three different weather conditions these

weather conditions are obtained based on the Table 3.5.

Table 3. 4 Distributions of Different Weather Conditions

UV index	Type of weather conditions
0% to 20%	Clear day (sunny)
21% to 60 %	Partially Cloudy
61% to 100 %	Extremely Cloudy

Based on the above-mentioned Table 3.5 the dataset is divided into 3 different weather

scenarios. The sunny dataset has 144 data points, the partially cloudy dataset has 141 days,

and the Extremely cloudy dataset has 81 days

3.5.1.2.1.   SPV Power Prediction for Sunny Day

The data collected from sol cast site for one year where sunny condition data were used to

train the three models i.e CNN, LSTM and the proposed hybrid CNN-LSTM. The Sunny

data is 144 these data is used to train the deep learning models for SPV power prediction.

From Fig.3.14 (a) it can be observed when there is sun in sky power increases or decrease gradually in the sky. Seven inputs were given to all the three model for analysing they were Humidity, temperature, wind speed, Solar radiation, UV Index cloud cover, SPV power and the predicted output is SPV power the forecasted results for all the three models is shown in Fig. 3.14 (a) it is observed that CNN-LSTM predicted more accurately than CNN model and LSTM model. The error between all the three models is been compared which shows CNN-LSTM have less errors than the other two model the error plot is shown in Fig. 3.14 b) and it is observed that CNN -LSTM have less error than other CNN and LSTM model. Traditional methods of prediction are compared for sunny conditions in order to show that the proposed deep learning model performs much better than Traditional model the traditional model considered is ARIMA (Auto regressive integrated average).

(a)   (b)
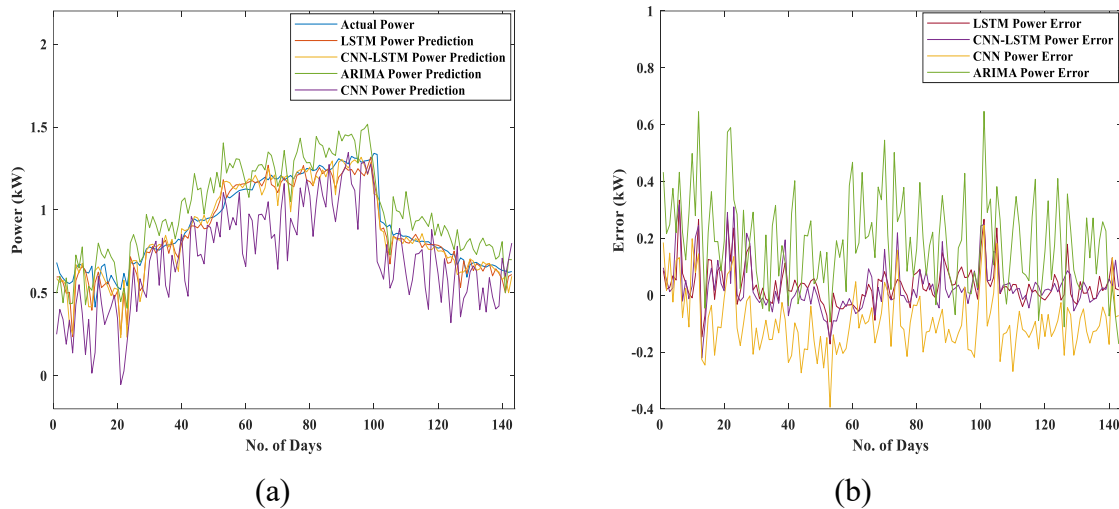
Fig. 3. 14 Comparison of CNN-LSTM, LSTM, CNN and ARIMA Models in Sunny

Conditions a) SPV Power Prediction Plot with Actual Power b) Error Plots

For comparison MSE is calculated for ARIMA model it comes out to be 0.00220 and MSE for proposed CNN-LSTM model comes out to be 0.000645 comparison is shown in Fig.3.13 (a). Additionally, the models are compared using Root Mean Square Error, Mean Absolute Error, Mean Square Error, and R^2 for the goal of conducting more accurate analyses.

3.5.1.2.2. SPV Power Prediction with Partially Cloudy Conditions

The data collected from sol cast site for one years where extremely cloudy condition data were used to train the three models i.e. CNN, LSTM and the proposed hybrid CNN-LSTM. The extremely cloudy data is 81 these data is used to train the deep learning models for SPV power prediction. In extremely cloudy condition frequent fluctuation of SPV power is observed. And the SPV power generated is less in extremely cloudy conditions. From Fig. 3.15 a) it can be observed when there are clouds in the sky, there is an immediate shift in the amount of fluctuation in the power generation. Seven inputs were

(a)   (b)
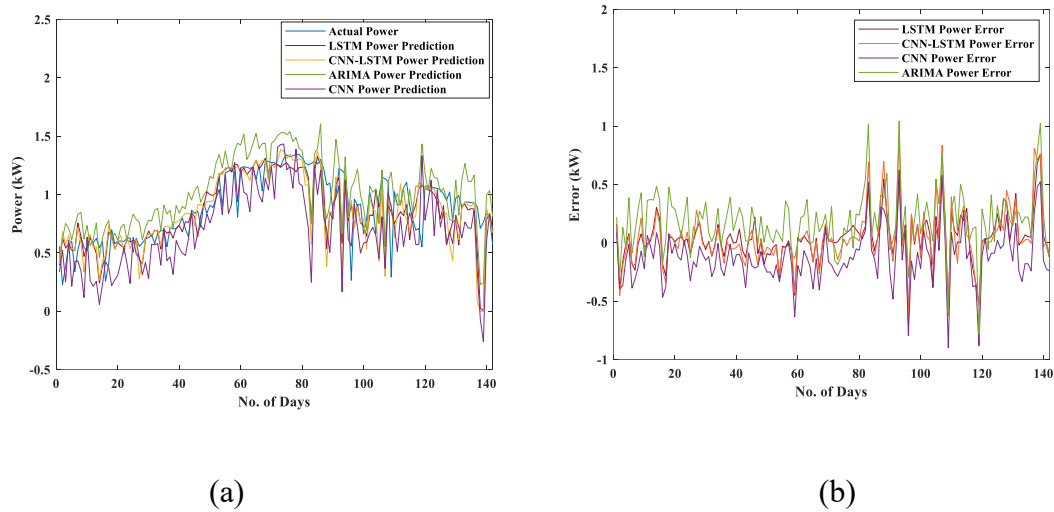
Fig. 3.15 Comparison of CNN-LSTM, LSTM, CNN and ARIMA Models in Partially Cloudy Conditions a) SPV Power Prediction Plot with Actual Power b) Error Plots

given to all the three model for analysing they were Humidity, temperature, wind speed, Solar radiation, UV Index cloud cover, SPV power and the predicted output is SPV power. The forecasted results for all the three models is shown in Fig. 3.15 it is observed that CNN-LSTM predicted more accurately than CNN model and LSTM model. The error between all the three models is been compared which shows CNN-LSTM have less errors than the other two model the error plot is shown in Fig. 3.15 (b). It can be observed that CNN-LSTM error is very less compared to CNN and LSTM model. Traditional methods of prediction are compared for extremely cloudy conditions in order to show that the proposed deep learning model performs much better than Traditional model, the traditional model considered is ARIMA. For comparison MSE is calculated for ARIMA model it

comes out to be 0.00820 and MSE for proposed CNN-LSTM model comes out to be 0.0012 the comparison is shown in Fig. 3.15.

3.5.1.2.3.   SPV Power Prediction with Extremely Cloudy Conditions

The data collected from sol cast site for one years where extremely cloudy condition data were used to train the three models i.e. CNN, LSTM and the proposed hybrid CNN-LSTM. The extremely cloudy data is 81 these data is used to train the deep learning models for SPV power prediction. In extremely cloudy condition frequent fluctuation of solar PV power is observed. And the SPV power generated is less in extremely cloudy conditions. From Fig. 3.16 (a) it can be observed when there are clouds in the sky, there is an immediate shift in the amount of fluctuation in the power generation. Seven inputs were given to all the three model for analysing they were Humidity, temperature, wind speed, Solar radiation, UV Index cloud cover, SPV power and the predicted output is SPV power. The forecasted results for all the three models is shown in Fig. 3.16 it is observed that CNN-LSTM predicted more accurately than CNN model and LSTM model. The error between all the three models is been compared which shows CNN-LSTM have less errors than the other two model the error plot is shown in Fig. 3.16 (b). It can be observed that CNN-LSTM error is very less compared to CNN and LSTM model.

(a)   (b)
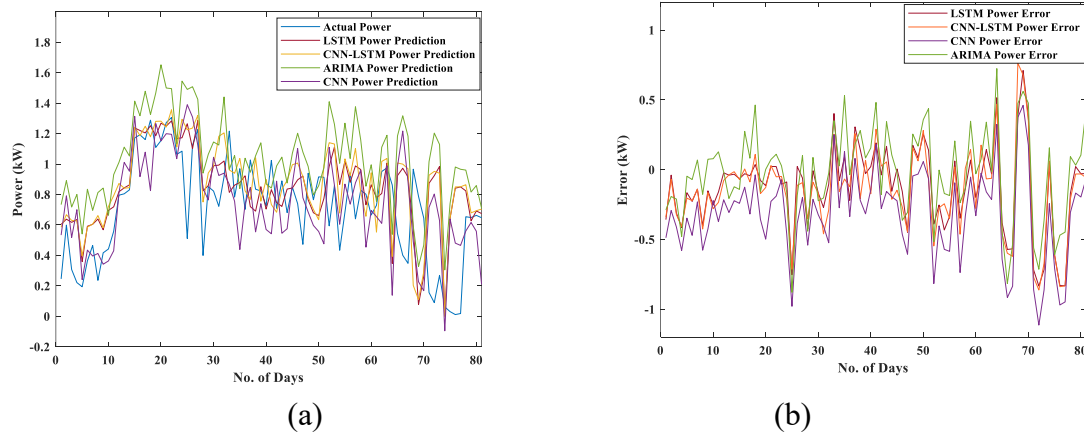
Fig. 3.16 Comparison of CNN-LSTM, LSTM, CNN and ARIMA Models in Extremely Cloudy Conditions a) SPV Power Prediction Plot with Actual Power b) Error Plots

Traditional methods of prediction are compared for extremely cloudy conditions in order to show that the proposed deep learning model performs much better than Traditional model, the traditional model considered is ARIMA. For comparison MSE is calculated for ARIMA model it comes out to be 0.00820 and MSE for proposed CNN-LSTM model comes out to be 0.0012 the comparison is shown in Fig. 3.16.

3.5.1.3 Performance Evaluation

Performance estimation is an essential factor for determining a model's prediction accuracy. RMSE, MAE, MSE and R^2 are variables used for comparison analysis. MAE aids in analysing the prediction model's constant prediction errors, RMSE assesses the model's overall accuracy, and R^2 represents the relationship strength between the predicted and actual values of the models. Table 3.7 for partially cloudy, extremely cloudy and sunny prediction error is shown.

$$MAE = \frac{1}{N}\sum_{i=1}^{N}|A_i - P_i| \tag{3.18}$$

$$NMAE = \frac{MAE}{Range(A_i)} \tag{3.19}$$

$$MSE = \frac{1}{N}\sum_{i=1}^{N}(A_i - P_i)^2 \tag{3.20}$$

$$NMSE = \frac{MSE}{Range(A_i)} \tag{3.21}$$

$$RMSE = \sqrt{\frac{1}{N}\sum_{i=1}^{N}(A_i - Pi)^2} \tag{3.22}$$

$$NRMSE = \frac{RMSE}{Range(A_i)} \tag{3.23}$$

$$R^2 = 1 - \frac{\sum_k (A_i - P_i)^2}{\sum_k (A_i - \bar{A})^2} \tag{3.24}$$

Where "N" number of windows, "A_i" actual value, and P_i does the Predicted value. The arithmetic mean of the actual value is $\bar{A}$.

Table 3.6 and 3.7 analyse the performance of proposed methodology for varying weather conditions and seasons, respectively. According to the Table 3.6, the CNN-LSTM

algorithm's performance is superior than that of both CNN and LSTM. performs better than LSTM in the majority of deep learning applications; nevertheless, when compared with the CNN-LSTM model, its performance is less accurate in terms of performance evaluation. It is possible to draw the conclusion from Table 3. 6 that the deep learning model is superior to cloudy weather circumstances in terms of its ability to forecast.

Table 3. 5 Estimation Errors of Various Prediction Model with Weather Conditions such as Sunny, Partially Cloudy and Extremely Cloudy

Model (Sunny)	MAE	NMAE	RMSE	NRMSE	MSE	NMSE	R^2
LSTM	0.0286	0.0308	0.04800	0.05175	0.00230	0.00248	0.9636
CNN	0.0271	0.0292	0.04406	0.04750	0.00194	0.00209	0.9643
CNN- LSTM	0.0163	0.0176	0.02541	0.02739	0.00064	0.00069	0.9898
ARIMA	0.435	0.469	0.05400	0.05821	0.00220	0.00237	0.9239
Model (Partially Cloudy)	MAE	NMAE	RMSE	NRMSE	MSE	NMSE	R^2
LSTM	0.9951	0.7420	0.14622	0.1090	0.02138	0.01594	0.7734
CNN	0.0919	0.0685	0.1237	0.0922	0.1529	0.1140	0.8378
CNN- LSTM	0.0236	0.0175	0.0346	0.0258	0.00120	0.00089	0.9872
ARIMA	0.1234	0.0920	0.19622	0.1463	0.00820	0.00611	0.7234
Model (Extremely Cloudy)	MAE	NMAE	RMSE	NRMSE	MSE	NMSE	R^2
LSTM	0.0719	0.0555	0.1046	0.0808	0.0109	0.0084	0.8967
CNN	0.0535	0.0413	0.1246	0.0962	0.03186	0.02461	0.7045
CNN- LSTM	0.2521	0.1947	0.0824	0.06366	0.00679	0.00524	0.9358
ARIMA	0.1576	0.1218	0.2146	0.1658	0.0423	0.0327	0.6045

Furthermore, it is possible to deduce from Table 3.7 that the models have a high level of accuracy when applied to the winter and post-monsoon datasets. In both Table 3.6 and Table 3.7, deep learning models perform better than the ARIMA.

CNN-LSTM is the deep learning model that performs the best across all of the weather patterns and seasons that were taken into consideration. In Table 3.8, the work of previous author is compared with the proposed, and the results show that the proposed model is more effective.

Table 3. 6 Estimation Errors for Various Prediction Model Trained Based on Different Seasons

Model (Winter)	MAE	NMAE	RMSE	NRMSE	MSE	NMSE	R^2
LSTM	0.02424	0.02601	0.0395	0.04237	0.00155	0.00166	0.9628
CNN	0.06323	0.06783	0.08511	0.09131	0.00724	0.00776	0.8271
CNN- LSTM	0.00862	0.00924	0.0126	0.0135	0.000158	0.000169	0.9962
ARIMA	0.0525	0.05632	0.08900	0.09548	0.00780	0.008368	0.9239
Model (Summer)	MAE	NMAE	RMSE	NRMSE	MSE	NMSE	R^2
LSTM	0.06974	0.07376	0.1037	0.10968	0.01075	0.01137	0.7225
CNN	0.05405	0.05716	0.0723	0.0765	0.00524	0.00554	0.7674
CNN- LSTM	0.02869	0.03034	0.0425	0.0449	0.00181	0.00191	0.9197
ARIMA	0.23363	0.24710	0.2789	0.2949	0.0123	0.01301	0.5674
Model (Rainy)	MAE	NMAE	RMSE	NRMSE	MSE	NMSE	R^2
LSTM	0.07394	0.05893	0.1094	0.08719	0.01196	0.00953	0.8396
CNN	0.14043	0.11193	0.18216	0.14519	0.03318	0.02645	0.6554
CNN- LSTM	0.02592	0.02066	0.08858	0.07060	0.00784	0.00625	0.8947
ARIMA	0.15578	0.1242	0.2345	0.1869	0.004323	0.00344	0.5556
Model (Post Monsoon)	MAE	NMAE	RMSE	NRMSE	MSE	NMSE	R^2
LSTM	0.02599	0.03228	0.0429	0.05298	0.0018	0.002236	0.95078
CNN	0.06499	0.08074	0.1195	0.1484	0.01429	0.01775	0.71822
CNN- LSTM	0.01203	0.0149	0.04225	0.0525	0.00178	0.00221	0.9523
ARIMA	0.07157	0.0889	0.24146	0.2998	0.01523	0.0189	0.6238

Table 3. 7 Comparison of the Proposed CNN -LSTM Method with Previous Work

Ref.	Method Proposed	Input Parameters	Dataset	Performance Metric	Observation
[99]	CNN-LSTM with a Semi Asynchronous Personalized Federated Learning Framework	Not given	990 days	0.689 (RMSE)	The suggested system improved the PV power production performance projection.
[100]	CNN-LSTM	Time sampling	1 month	0.03105 (RMSE)	CNN LSTM outperforms LSTM method
[101]	Deep ESN and CNN-Dee ESN	Wind speed, humidity, SPV power, radiation, diffuse radiation, average phase current, and temperature	11 months	0.04101(RMSE) 0.0381(MAE) 3.3313 (MAPE)	In SPV power generation prediction, the suggested hybrid model beat other single models
[15]	CNN-LSTM	SPV power	1 year	0.485 and 0.2775 RMSE for sunny and cloudy respectively	CNN-LSTM Outperforms in sunny Weather conditions
[102]	CNN-LSTM	Humidity Wind speed, output power, diffuse radiation	-	O.623 (RMSE)	The suggested hybrid prediction model outperforms the single model LSTM, CNN
[103]	MODWT-LSTM	Wind speed, wind direction, Active power, temperature, humidity, global horizontal radiation,	1 year	0.1231 (RMSE)	As compared to 1 day and 10 days, the suggested technique is found to be more dependable
	Proposed model	**Temperature, humidity, wind speed, cloud cover, UV index, solar irradiance, SPV power**	**12 Months**	**0.025407 RMSE (sunny) 0.03465 RMSE (partially cloudy) 0.0824 RMSE (Extremely cloudy)**	

3.5.2 Result and Discussion for Dataset 2

17614 records were taken with a 30-minute time span, from November 30, 2021, to December 1, 2022, available at the solcast site. These data set are the time series data, a historical record of solar radiation data and other weather parameters for the location of New Delhi. For the implementation of the suggested model, data was recorded. SPV power has been computed with the assistance of these recorded data taking into consideration the meteorological parameters. The data set is divided into training and testing sets to do forecasting. For the training set, 16500 data were used, while for the testing set, 614 data were used and remaining 1000 for validation. This was done in order to train the model. LSTM and MLP are the models that are being employed. Python is the environment in which these models are developed. In this case study 16500 data are used for training and for prediction here a window size is kept 5 so that while training process it uses 5 sample data as input for learning and predicting the power output. Table 3. 9 shows the parameters considered for building the model.

Table 3. 8 List of Parameters

Models	LSTM	MLP
Input size	5,1	5,1
Optimizer	Adam	Adam
Activation function	Relu	Relu
Epochs	10	10
Learning rate	0.001	0.001
No. of layers Hidden layer/neurons	1/64	1/100

In LSTM model first process is dividing the dataset into training and testing data set and then it is passed through the LSTM model and MLP model, then plotting the forecasted outputs i.e power, the plot for training is shown in   Fig. 3.17 here 16500 training samples, are used for forecasting using LSTM and MLP and its comparative plot is shown. Further the forecasted results of LSTM and MLP compared with the actual power plot considered for 109 data samples for test. for test are shown in Fig 3.18.

<center>(a)　　　　　　　　　　　　　　　　　　　　(b)</center>
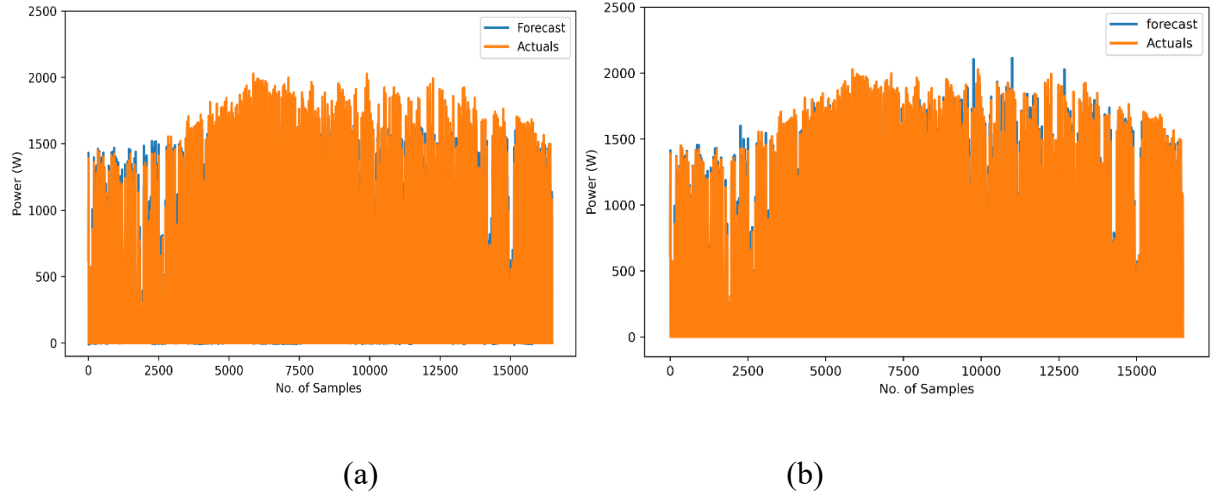
Fig. 3. 17 Train Data Forecasting using (a) LSTM (b) MLP

When MLP and LSTM forecasting models are compared LSTM performance is better than MLP as the performance evaluation i.e. RMSE, MSE, R^2, MAE for LSTM is better than MLP. Performance table is shown. Fig. 3.19. shows the comparison plot of LSTM and MLP with the actual data set, for the 1st 30 samples because the data set is very large so in order to see the comparison clearly only 30 samples are considered and plotted in Fig. 3.19. Table 3.10 shoes the comparison of statistical indicators for the Two considered model that is LSTM and MLP

<center>(a)　　　　　　　　　　　　　　　　　　　　(b)</center>
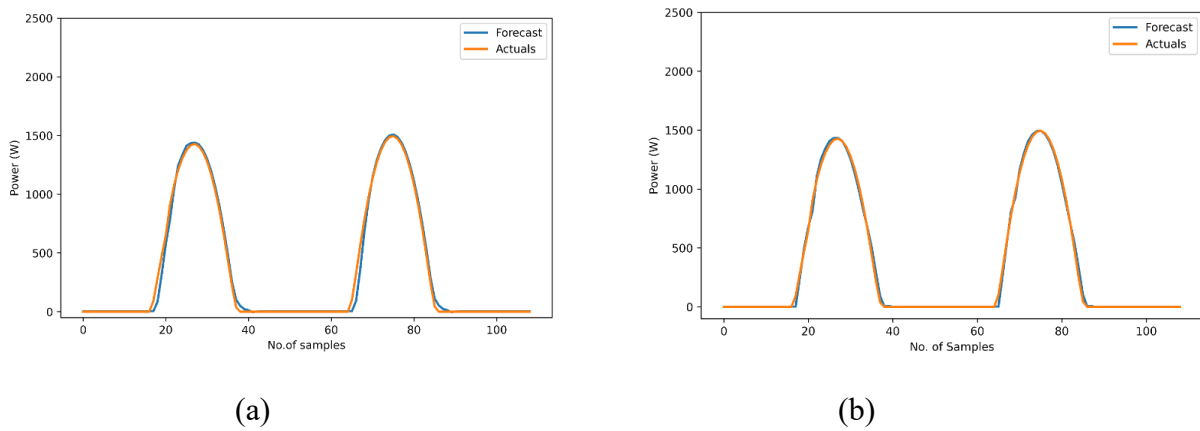
Fig. 3. 18 Test Data Forecasting using (a) LSTM (b) MLP
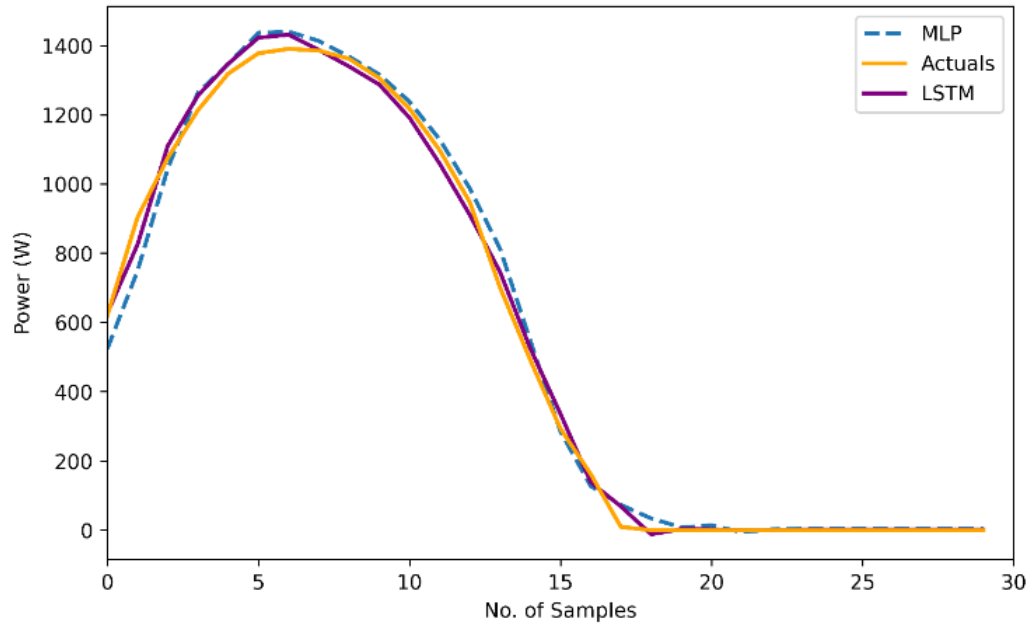
Fig. 3. 19 Forecasted SPV Power with Actual Power for both LSTM and MLP Techniques

Table 3. 9 Comparison of LSTM And MLP Estimation Errors

Models	MAE	MSE	RMSE	R^2
LSTM	**49.907**	**7989.66627**	**89.3849**	**0.97827**
MLP	43.7589	8781.0951	93.70749	0.97612

3.6   CONCLUSION

A prediction model for PV power generation can enhance the design, operation, and stability of PV power plants by making more accurate forecasts based on meteorological data. But because the weather changes all the time, it is difficult to know how much PV power is produced. To make a good prediction model that only uses past data and leaves out data on solar radiation that is highly correlated with PV power production, you need a statistical method for figuring out how past and short-term data depend on each other. In this chapter, a CNN-LSTM hybrid model is proposed for estimating how much PV power is produced. The suggested model addresses the shortcomings of the previous models while retaining their benefits. The proposed model has been compared to other deep learning models in which only LSTM and CNN models are given multiple inputs in dataset 1. However, their performance is less accurate than the hybrid model because in the proposed hybrid model, the CNN model first learns the pattern of different weather conditions, and then separate LSTMs for prediction SPV power help the model make more accurate

prediction of PV power. A quantitative evaluation also showed that the proposed model has RMSE of 0.0254, 0.03465 and 0.0824, MAE of 0.0163, 0.0236 and 0.2521, MSE of 0.000645, 0.00120 and 0.00679 and R^2 of 0.9898, 0.9872 and 0.9358 for sunny, partially cloudy and extremely cloudy-day data, respectively. The normalised RMSE, MAE and MSE comes out to be 0.0176, 0.02739, 0.00069 for sunny conditions. For partially cloudy conditions the normalised RMSE, MAE and MSE comes out to be 0.0175, 0.0258, 0.00089 and for extremely cloudy conditions the normalized RMSE, MAE and MSE comes out to be 0.1947, 0.06366 and 0.00524. This model works better when the weather is sunny. When different season datasets is considered the proposed CNN-LSTM models performs better in winter seasons and worst in rainy season. is It is seen that PV power is increased in sunny conditions and decreased in non-ideal conditions i.e partially cloudy and extremely cloudy. The amount of power a PV power plant can make depends on the size of the installation and the weather, so the model needs to be changed. In a future study, the power-generating capacity of PV power plants should be changed to predict SPV power. To make forecasts more accurate, optimisation methods automatically change models based on data from the system. Solar radiation and the properties of SPV modules must also be analysed. For dataset 2 Evaluation of the SPV power data was predicted and calculated from the meteorological parameters obtained from the solcast site for one year from November 30, 2021, to December 01, 2022. This information was divided into two categories: training and test sets for SPV power forecasting. The challenge of estimating photovoltaic power for the next 30 minutes was explored. The proposed model's findings were compared using the most widely used technique, i.e., MLP. MLP was used to estimate and examine its correctness and performance. In comparison to the MLP technique, the proposed LSTM model provided higher practical values in all performance metrics. It can be observed that deep learning models works better than MLP.

CHAPTER 4

MATHEMATICAL MODELLING OF DUST ACCUMULATION ON SPV MODULES

4.1 INTRODUCTION

SPV technology is widely acknowledged as a crucial element in the worldwide shift towards sustainable energy. Nonetheless, environmental variables, especially dust deposition on SPV modules, present considerable barriers to their effectiveness. Dust accumulation on SPV modules diminishes solar penetration, hindering energy production and possibly resulting in significant power output losses. This problem is particularly common in areas with dry or semi-arid climates, when dust deposition rates are elevated. As a result, comprehending and alleviating the impact of dust on SPV systems has emerged as a primary study focus in recent years.

Recent studies have aimed to quantify the effects of dust accumulation on SPV efficiency, emphasizing the correlation between environmental variables—such as wind speed, temperature, humidity, and particle concentration—and dust deposition rates. Researchers have created empirical models to evaluate the influence of dust layer thickness on SPV output and have investigated the contribution of climatic elements on dust accumulation dynamics. Machine learning and data-driven methodologies have gained prominence in the industry, with research using extensive datasets to forecast dust-related losses and enhance cleaning schedules. Nevertheless, while these models have enhanced comprehension, they often fail to include the intricate and changeable characteristics of dust buildup across many meteorological and geographical situations.

This work seeks to provide a comprehensive mathematical model for forecasting dust collection on SPV modules in light of these restrictions. Through the analysis of historical data about environmental conditions and module features, the model will elucidate the dynamic interactions that affect dust accumulation rates and retention. Recent breakthroughs in computer modelling and predictive analytics will be used to augment the model's precision, using approaches such as machine learning to refine parameter estimate and generalization across varied settings.

This study enhances the existing literature on SPV efficiency optimization by offering a thorough, flexible model for dust buildup. The findings are anticipated to enhance maintenance procedures and promote cost-efficient operation of SPV systems, particularly in arid, dust-prone areas. This model may effectively inform decision-making for solar plant operators, save operating expenses, and improve the long-term dependability of SPV installations, thereby promoting the wider use of solar energy.

4.2 METHODOLOGY OF WORK

4.2.1 Collection of Data

For the study analyses of soiling loss from the Dust IQ soil monitoring system installed on the rooftop of Utilization lab, New Delhi, the SPV module is first clean Fig. 4.1 represent the 5kW SPV system and the data is been collected from the Dust Explorer software in which the soiling loss and transmission losses are recorded for 6 months from March, 2023 to August 2023 i.e. 180*24= 4320 data points.

Data is collected at log interval of 60 minutes by the Dust IQ soil monitoring system. This monitoring system is installed on 5 kW PV system a total of 20 modules are arranged in a layout of 10 x 2, with 2 arrays of 10 modules in each array having SPV modules of 250 Wp rating. The location of the monitoring system is in center of the 5 kW PV system as shown in Fig. 4.1. It should be aligned with the SPV modules in terms of both azimuth and tilt angle. This guarantees that the soiling conditions assessed by Dust IQ accurately reflect the circumstances that impact the modules. The weather inputs considered are considered from solcast site [104] which is at every 60 minutes for 6 months.

4.2.2 Dust IQ Soil Monitoring System

To determine the quantity of dust and dirt that is present on SPV modules, Dust IQ uses an optical sensor technology. This technique involves evaluating the light that is transmitted and reflected from the surface of the module. It provides useful data that can be utilized to improve maintenance schedules and boost the overall performance of SPV power systems. This is accomplished by continually measuring the amounts of soiling that are present.
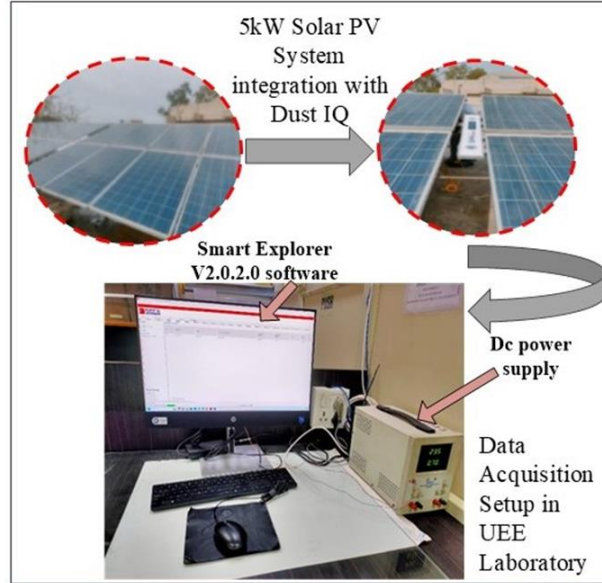
Fig. 4. 1 Dust IQ Setup on a 5 kW SPV System.

The unique, high-quality soil monitoring system device measures module soiling-induced light loss. The soiling of nearby PV modules causes light loss. Dust IQ soil monitoring system device has industrial data collecting and control system-optimized digital signal processing and interfaces. An intuitive interface with RS-485 Modbus® data transfer from Kipp & Zonen connects PLCs, inverters, digital control devices, and digital data recorders. Measurement of reflected light and local dust calibration are needed to determine light loss with the requisite accuracy. Table I lists Dust IQ soil monitoring system specifications for data recording on a 5-kW SPV module.

Table 4. 1 Specification of Dust IQ Soil Monitoring System

Range of Transmission loss (TL)	0 – 50 %
Range of Soiling Ratio (SR)	100 – 50 % (SR = 100 –TL)
Transmission loss measurement accuracy	± 1 % and ± 1/10 of reading
Ambient working temperature	-20 to +60 ˚C
Storage temperature	-20 to +80 ˚C
Power (DC)	12 to 30 VDC, 200 to 70 mA

Following are the steps of proposed work.

Step 1: Soiling Ratio data collection:

Use the soil monitoring device to collect reliable measurements of the degree of soiling on PV modules. The Dust IQ system uses advance sensing technology to analyses the build-up of dust, dirt, microfibers, and other particulate matter on module surfaces. Maintain frequent monitoring and data collecting to establish a comprehensive understanding of the soiling ratio over time.

Step 2: Soiled SPV power calculation:

Calculate the power output produced by the PV system considering climatic characteristics such as irradiance, temperature, windspeed, which is obtained from solcast these variables affect SPV power. And further SR is obtained from Dust IQ.

Step 3: Comparing soiled and cleaned power output:

Analyze the calculated power output without taking into account cleaning activities (Soiled power). Compare the uncleaned power output to the power output produced after the SPV modules consisting no dust accumulation. Calculate the difference between two power values further used to assess the impact of cleaning on power generating efficiency.

Step 4. Forecasting of soiled SPV power:

In order to further verify the generalizability of the model, k-fold cross-validation was implemented. The dataset was partitioned into k equal subsets (folds) in this method, and the model was iteratively trained on k-1 folds while being validated on the remaining fold. This procedure guaranteed that the model's performance was not excessively reliant on a specific data partition and that it maintained consistency across a variety of data distributions.

 Furthermore, data augmentation methodologies were implemented during the training phase. This incorporated controlled randomness and variability into the training set, thereby improving the model's resistance to unobserved variations and decreasing overfitting. The deep learning models exhibited enhanced adaptability to new, previously unencountered input conditions by synthetically expanding the diversity of training samples, such as through noise addition, temporal distortion, or synthetic soiling patterns.

 In general, the development of highly accurate, robust, and adaptive predictive models for estimating the performance degradation of soiled SPV modules under varying

environmental and operational conditions was facilitated by the combination of optimized hyperparameters, advanced deep learning architectures, rigorous cross-validation, and strategic data augmentation
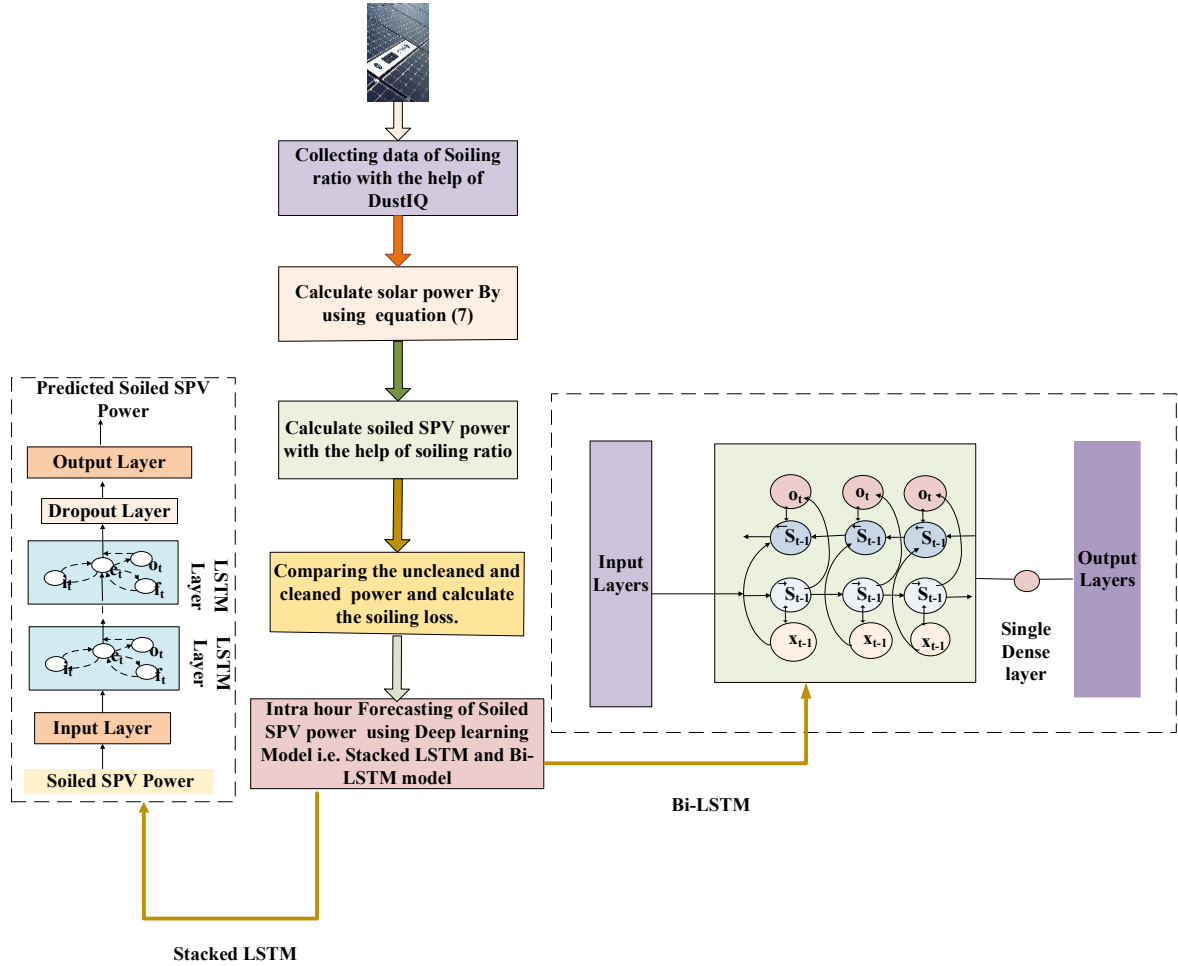
Fig. 4. 2 Architecture of the Proposed Work

4.2.3 Stacked LSTM Model

A stacked LSTM architecture is described as an LSTM model with numerous LSTM layers Fig. 4.2. In [105] author developed a stacked LSTM, sometimes known as deep LSTM. The stacked LSTM model, like the DRNN model, employs numerous LSTM layers that are stacked before being sent to a dropout layer and output layer at the final output. In a stacked LSTM, the first LSTM layer generates sequence vectors that are utilized as input to the succeeding LSTM layer. Furthermore, the LSTM layer gets input from its preceding timestep, enabling for the capture of data patterns. To minimize overfitting, the dropout layer additionally excludes 10% of the neurons. The fundamental structure of LSTM, as

shown in the LSTM layer in Fig. 4.2 consists of an input gate i_t, output gate o_t, forget gate f_t, and memory cell c_t. A single LSTM layer features a second-order RNN architecture that excels in storing consecutive short-term memories and retrieving them at a later time.

$$f_t = \sigma\left(W_f.x_t + U_f.h_{t-1} + b_f\right) \tag{4.1}$$

$$i_t = \sigma\left(W_f.x_t + U_i.h_{t-1} + b_i\right) \tag{4.2}$$

$$o_t = \sigma(W_o.x_t + U_o.h_{t-1} + b_o) \tag{4.3}$$

$$c_t = f_t.c_{t-1} + i_t.\sigma(W_c.x_t + U_c.h_{t-1} + b_c) \tag{4.4}$$

4.2.4 Bi-LSTM Model

The bidirectional LSTM model detects temporal relationships inherent in data in both directions. This means that, given a vector of inputs, the model can understand the link between past and future samples moving in both the past-to-future and future-to-past directions. Such models have been used in research [106], and the architecture of the bidirectional LSTM layer is shown in Fig. 4.2 of the of the proposed work. This design uses the same input, output, and one dense layer as the normal model. As previously stated, the bi-directional LSTM layer looks for temporal relationships in the data in two directions, while the traditional LSTM layer only scans in one direction. In the above two discussed Deep learning models are trained with soiled SPV power further performance optimized hyperparameters are used for training the models as discussed in Table 4.2.

Table 4. 2 Hyperparameter Configuration for Model Training

Hyperparameter	Stacked LSTM	Bi-LSTM
Number of LSTM Layers	2	2
Number of Units per Layer	64, 32	64, 32
Activation Function	ReLU	ReLU
Optimizer	Adam	Adam
Learning Rate	0.001	0.001
Batch Size	32	32
Dropout Rate	0.1	0.1
Number of Epochs	50	50

4.3 Mathematical Modelling for Proposed Work

This section develops a mathematical relation between dust and SPV power and helps in calculating soiled power with the help of soiling ratio.

4.3.1 Soiling Ratio

The SR is the ratio of the irradiance used by a module that has been soiled to the irradiance used by a module that has been cleaned in order to create the corresponding short-circuit current or power [107]. The SR is obtained from soil monitoring system

$$SR = \frac{Actual\ Power\ Output\ (Ps)}{Expected\ clean\ power\ (Pc)} \tag{4.5}$$

$$t_{loss} = 1 - SR \tag{4.6}$$

4.3.2 Transmission Loss

The transmission loss t_{loss} is represented in (4.6), refers to the transmission loss that occurs as a result of soiling. There are many different mathematical models that may be used to predict the performance of PV modules as a function of the amount of irradiance and the temperature.

4.3.3 Modelling of Dust

In this work an empirical correlation for dust deposition density ρ_D based on an optimal tilt angle β is developed. The study team included this association, power equation to compute dust in non-tracking tilting SPV modules (4.7). They also used math to examine the dust shield's effect on transmittance during tilt angle changes as in (4.11). Thus, they provided a second planned correlation (4.8-4.14).

$$\rho_D = 680.96 * e^{-0.0469*SR} \tag{4.7}$$

$$T_m = T_{amb} + \frac{S_m}{26.9+6.2*w_{in}} \tag{4.8}$$

$$T_a = T_m - 25^oC \tag{4.9}$$

$$W_{in} = \frac{D_m^{0.2}}{D_a} * w_s \tag{4.10}$$

$$T = T_{amb}\left\{1 - 34.37erf\left[0.17(-8.5 \times 10^{-3}\rho_{D_0}\beta + 0.82\rho_D)^{0.8473}\right]\right\} \tag{4.11}$$

$$S_{mt} = S_{tilted} . T \tag{4.12}$$

$$S_{tilted} = S_B R_b + S_D(1 - A_i)\left(\frac{1+cos\beta}{2}\right)\left[1 + f sin^3\left(\frac{\beta}{2}\right)\right] + S_D\left(\frac{1-cos\beta}{2}\right) \qquad (4.13)$$

$$S_m = \frac{S_{mt}}{S_{stc}} \qquad (4.14)$$

SB is direct radiation, SD diffuse radiation, The ratio of direct radiation on an inclination to horizontal radiation is R_b. Ai is the anisotropic index, and f is the correction coefficient, using S_{mt} from (4.12) calculate accurate solar irradiation considering tilt angle and effect of transmittance T. Density of dust on horizontal surface ρ_{D_0} (β= 0).

4.3.4 Effect of Soiling on Power

To model PV power, the irradiance is incident on the SPV module, the exact wind speed on the SPV module, and the SPV module temperature must be estimated. The SPV power equation is as follows

$$P_1 = P_r S_m(1 + K_1 log\,(S_m) + K_2 log(S_m)^2 + K_3 T_a + K_4 T_a log\,(S_m) + K_5 T_a log(S_m)^2$$
$$+ K_6 T_a{}^2) \qquad (4.15)$$

$$P_2 = P_1/SR \qquad (4.16)$$

P_r is the rated power, W_{in} is wind speed on SPV modules, T_a is wind-induced temperature change, T_m is module Temperature, T_{amb} is the ambient temperature, and $K_1 - K_6$ are SPV module constants. D_a is the distance between the PV module and the ground surface, and D_m is the distance between the anemometer and the ground surface [108]. S_{mt} here is calculated by (4.12) and then the S_m is calculated from (4.14). From which Ps is calculated from (4.15).

The (4.16) gives the cleaned power and (4.15) gives soiled power which is used for further soiled power forecasting. (4.18) shows the effect of soiling on power the old power equations discussed in [109] don't have soiling parameters Use the new S_{mt} calculated from (4.15).

The mathematical relation between soiling ratio and module temperature (T_m) curve fitting analysis is done shown in (4.17). It illustrates an inverse correlation, signifying that when the soiling ratio reduces (with more dust collection), the module temperature is increased. The effect is primarily due to decreased light absorption efficiency, resulting in buildup of heat on the module surface when the SR decreases to 83% owing to dust collection, the module temperature may rise to 36.7°C, whereas a clean module (SR = 100%) maintains a

lower temperature of around 25.23°C. This correlation helps in understanding the relation between T_m and SR it is inverse relation which shows that lesser the soling ratio which means more dust, temperature is high.

$$SR = 0.0146 * T_m{}^3 - 1.4196 * T_m{}^2 + 44.2150 * T_m - 346.9506 \tag{4.17}$$

$$P_s = -0.002 * SR^3 + 0.94 * SR^2 - 79 * SR - 0.002 \tag{4.18}$$

(a)　　　　　　　　　　　　　　　(b)
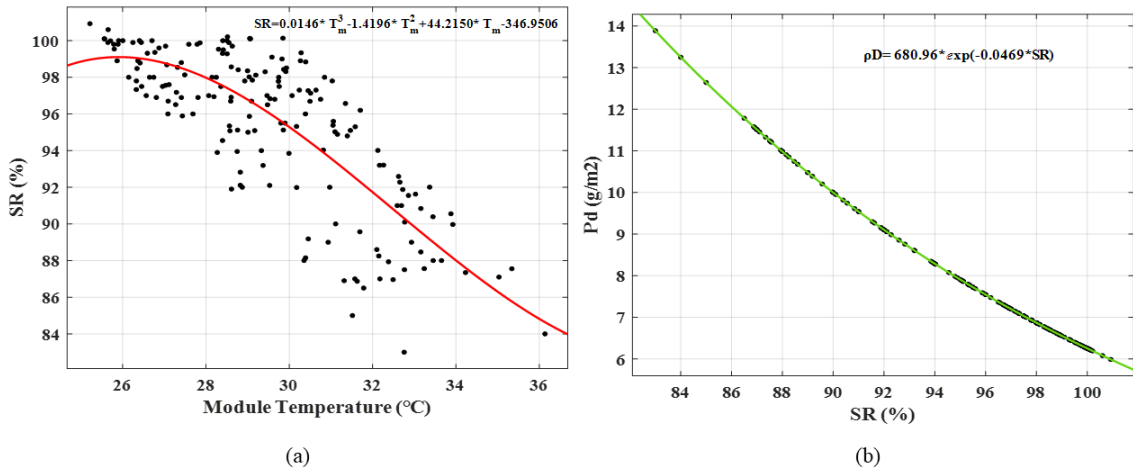
Fig. 4. 3 Correlation plot of Soiling Ratio with (a) Module Temperature (b) Dust Deposition density

The correlation between soiled power and Soiling ratio is shown in (18) which is polynomial type of equation. It measures the direct impact of dust collection on PV module power loss. Power production declines nonlinearly when SR drops because less irradiance is available for power generation. Further corelation between dust deposition and module temperature is shown in Fig. 4.3. This relation shows how the soiling ratio affects the module temperature and further effects the soiled power this soiled power is further forecasted which helps in scheduling cleaning.

The mathematical modelling methodology utilized in this work offers a systematic way for quantifying power losses due by soiling, allowing for a more exact assessment of its influence on PV performance. By combining real-time soiling data, transmission loss measurements, and climatic factors, the model reflects the dynamic link between dust

deposition and power loss. This enables a data-driven knowledge of how varied amounts of soiling affect energy production in various environmental circumstances. The insights acquired from this model help in identifying important thresholds were performance declines dramatically, directing the deployment of optimised cleaning schedules to minimise efficiency loss. Furthermore, the use of deep learning algorithms, namely Stacked LSTM and Bi-LSTM, improves prediction capacities by understanding complicated temporal relationships in soiling patterns and power variations. These models use past power generating data and weather parameters to properly predict dirty power output, allowing a proactive approach to PV system repair.

4.4 RESULT AND DISCUSSION

In this work examination of the effect of soiling ratio, transmission loss on SPV power system performance is analysed. Evaluation of the performance of clean and soiled PV system is done. To evaluate the soiling ratio, a smart explorer Dust IQ soil monitoring system software is used. Further the soiled power is mathematically calculated and Prediction is done in order to forecast the soiled power for further evaluation and cleaning schedule. This section 5 is divided into 2 parts, 1st part shows the effect of modelled soiled power by accumulated dust on SPV module using soil monitoring system based real time data. The 2nd part shows the comparison of predicted soiled PV power using DL models i.e. Bi-LSTM and stacked LSTM.

4.4.1 Performance Analysis of Dust on PV System using Soil Monitoring System

Performance analysis of dust is required to find out the relation between dust and power. The setup is used for capturing the data which collects data for a month for study aspects. The soiling ratio measured by the Dust IQ soil monitoring system for 6 months i.e., March, April, May, June, July and August,2023 is shown in Fig. 4.4 (a). The soiling ratio indicates the amount of dust that has accumulated on the SPV modules. The soiling ratio progressively reduced during the first 12 days in the month of march, suggesting a decrease in PV system performance owing to dust collection. On the twelfth day, the soiling ratio increased rapidly and dramatically, reaching 100%, indicating no soiling loss. This fast rise implies a natural cleaning of the SPV modules, maybe caused by rain. As illustrated in Fig. 4.4 (a) the soiling ratio steadily increase after the natural cleaning event. During the span

of 6 months 6 times natural cleaning occurred, and in the month of July it can be seen that there is maximum accumulation of Dust on PV system when no cleaning action takes place. Fig. 4.4 (b) depicts the transmission loss to further examine the influence of the soiling ratio on SPV power output transmittance loss is less Performance analysis of dust on PV system using soil monitoring system when the modules are cleaned as at day 12 natural cleaning of modules occurs so the loss is zero. Transmission loss is the reduction in the quantity of sunlight travelling through the soiled modules, resulting in lower power production. Relation between the soiling ratio and the resulting drop in power production can be learned by analyzing this plot.

In conclusion, the examination of the soiling ratio and its influence on SPV power output demonstrates that the modules gradually accumulate dust. Periodic natural cleaning events, on the other hand, aid in the general cleanliness of the modules. The decline in the soiling ratio and the resulting transmission loss highlights the need of routine cleaning and maintenance in order to optimise the performance of SPV power systems. (4.3) is used to determine the cleaned output power, which takes temperature, irradiance, and windspeed into consideration. This estimate takes into account the data received by solcast, a platform that delivers solar irradiance and meteorological data.

It is been observed that when there is slight rainfall cleaning of SPV modules are not efficient still there are dust accumulated as it can be seen in Fig. 4.4 on 16 May there is slight rainfall so SR is 98.06 % because of which proper cleaning is not done SPV power output is less on 30 March and May there is a heavy rainfall hence losses are less with heavy rainfall 0 % PV loss and with slight rainfall 1.94 % PV loss occurs.

The information was gathered over the course of 6 months from March 1, 2023 to August 31, 2023. After accounting for -environmental variables such as temperature, irradiance, and windspeed, it estimates the power provided by the SPV modules. It is crucial to remember that dust collection on SPV modules might result in a decrease in output power The Dust IQ system calculates the soiling ratio, which measures the level of dust deposition on the modules. The comparison between Soiling ratio and $\rho_{(d)}$ is represented in Fig. 4.4 (b). Soiled power calculated from (4.12) and mathematically modelled soiled power (4.18) is shown in Fig. 4.5.

Soiled power is calculated with the help of cleaned power and soiling ratio. Fig. 4.6 (a) shows a comparison of the power output of soiled modules and cleaned modules. According to Fig. 4.6 (a), the highest power loss owing to the presence of dust on the modules is 285.35 W in the month of July. This decrease in power output demonstrates the influence that dust collection has on SPV module performance. The soiling ratio, as determined by the Dust IQ method, is critical in calculating power loss due to dust collection.

(a)   (b)
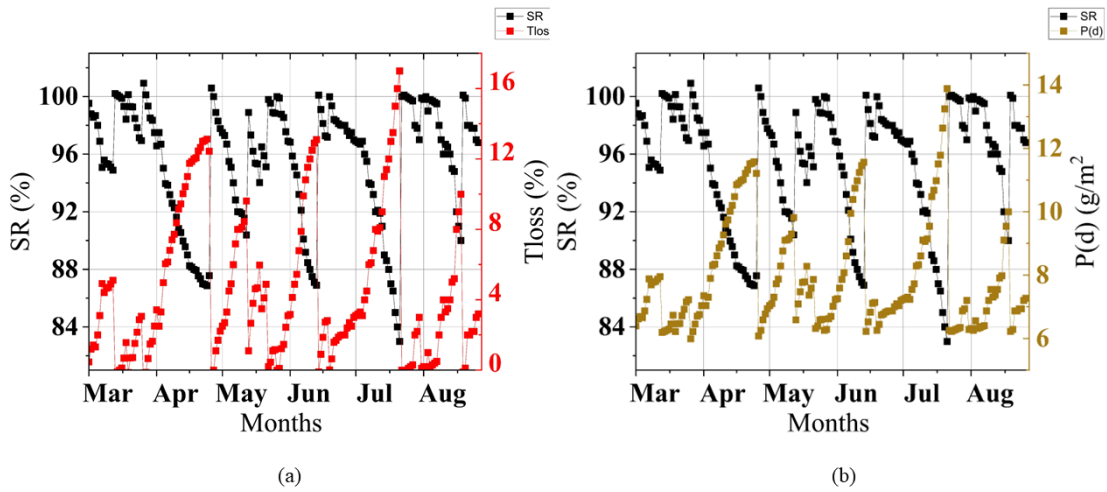
Fig. 4. 4 Comparison plot of (a) Soiling Ratio and SPV loss (b) Soiling Ratio and Dust deposition density

In order to ensure accurate and effective analysis, it is necessary to evaluate the relationship between SR and P_{soiled} in (4.18) and then compared with modelled soiled power (4.12).
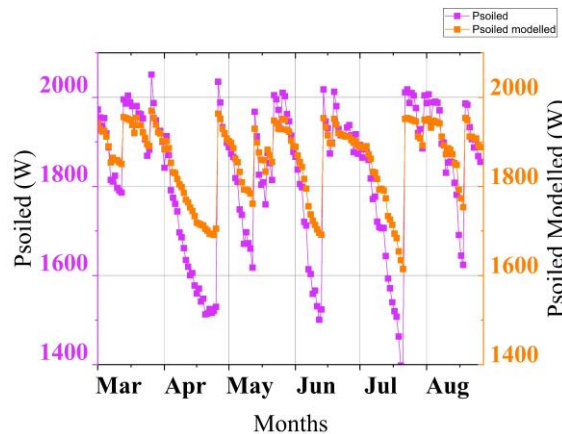
Fig. 4. 5 Comparison of soiled power plotted from (4.15) and (4.18).
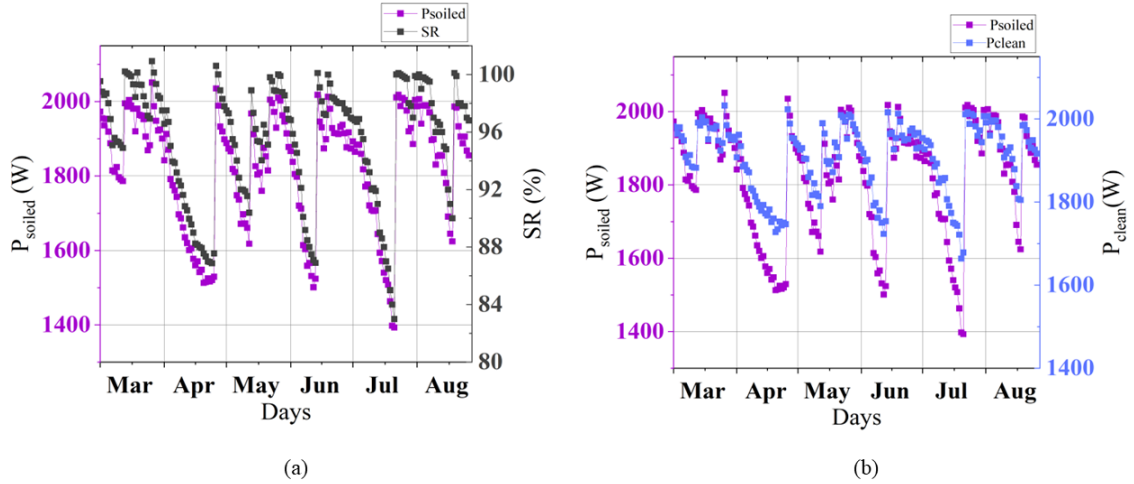
Fig. 4. 6 Comparison plot of (a) clean and dusty modules (b) soiling ratio and PV power.

Comparison of PV power with Soiling ratio is shown in Fig. 4.6 (b) as the dust is accumulated the PV power is reduced when there is natural cleaning the PV power is enhanced. Fig. 4.7 shows the relation of temperature with soiling ratio it can be analyzed that when soiling is more accumulated temperature is increased the maximum temperature is 36.70 º C where SR is 83% and minimum temperature is 25.23 ºC where SR is 100%. Fig. 4. 8 shows the comparison of maximum, minimum and average of soiling ratio, mathematical modelled soiled power and soiled power calculated normally using (4.12) respectively which helps in analyzing the impact of soiling and further shows how natural cleaning effects the PV system performance. SR reaches minimum of 83 % in the month of July among the six months showing transmission loss of 13% from Fig. 4.8 (a). Maximum power is obtained in the month of March which is 2051.06 W and the least power is obtained in the month of July which is 1393.2 W

4.4.2 Sensitivity Analysis

Light rain (<1mm) may not effectively remove dust off SPV modules owing to weak water impact and poor SPV module surface wetting, resulting in partial cleaning or even mud formation. Moderate rain (1-5mm) enhances cleaning efficiency but may still leave residual dust, particularly in areas where fine particulate matter prevails. Heavy rain (>10mm) has been shown to be the most effective in restoring module cleanliness because it causes more surface runoff, effectively removing dust and debris. Correlating these rainfall categories with

soiling ratio improvements allows us to calculate the minimal threshold necessary for successful natural cleaning. The dust deposition mentioned in table 4.3 is been calculated from equation (4.7).
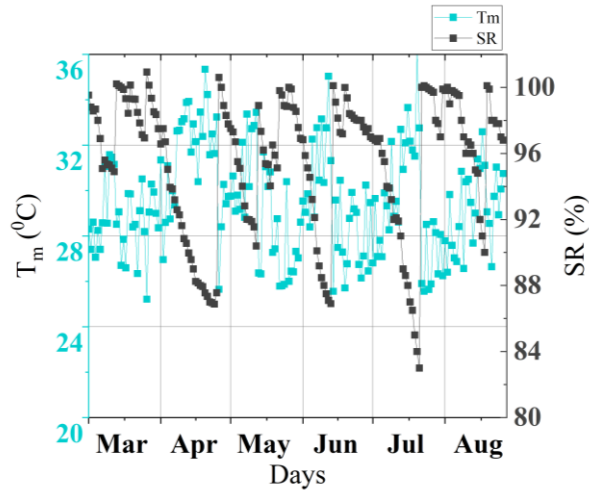
Fig. 4. 7 Comparison Plot of Temperature and Soiling Ratio.

Wind may affect dust re-deposition even after a rainstorm event, lowering the total cleaning impact. Humidity may affect dust adhesion; greater humidity levels may enhance cohesiveness between dust particles, making cleanup more difficult; in dry circumstances, dust may be carried by wind rather than washed away [110]. The results highlight the need for alternate cleaning solutions in areas where light rainfall is common yet inefficient. The SR and dust deposition in Fig. 4.4 (b) are divided in three different cases as shown in table below where it is observed that after light rain, dust is still accumulated there is very less change in dust deposition while in heavy rain the dust is reduced drastically showing maximum cleaning efficiency. There is a moderate change of dust deposition after a moderate rain fall. The table 4. 3 is made with the help of Fig. 4.4 (b).

Table 4. 3 Sensitivity Analysis of Rainfall Intensity on Dust Deposition and SR Recovery

Rainfall Category	Rainfall Amount (mm)	SR Recovery (%)	Dust Deposition density (P(d), g/m²) before cleaning	Dust Deposition density (P(d), g/m²) after cleaning	Remarks
Light Drizzle	<1mm	96 -98	9	8	May form mud layers, leading to re-adhesion of dust.
Moderate Rain	1-5mm	90 – 96	10	7	Efficiency depends on duration and wind conditions.
Heavy Rain	>10mm	85– 90	14	6	Transmission loss reduced to zero, ensuring maximum cleaning efficiency. And SR becomes 100 %

4.4.3   Comparison of Predicted Soiled SPV power

Soiling ratio helps in getting soiled SPV power, soiled power data is modelled for every one hour, this soiled power is the input which is given to the two DL model i.e., Stacked LSTM and Bi LSTM for soiled PV power prediction.
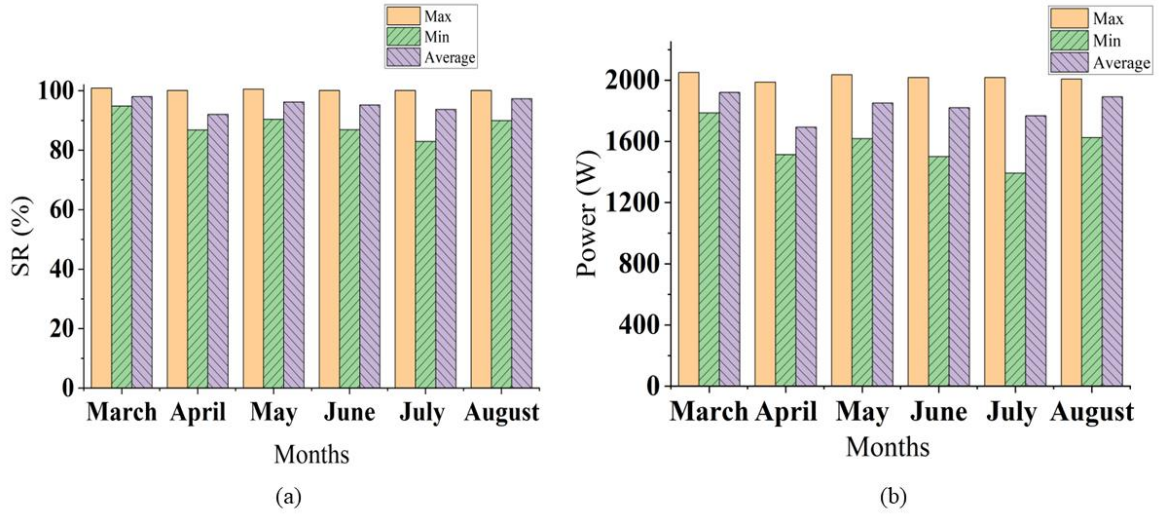
Fig. 4. 8 Performance Analysis of (a) Soiling Ratio (b) Soiled Power Influenced By Dust Accumulation on SPV Modules.

This prediction of soiled power helps in getting us knowledge about the power reduction of SPV module because of dust accumulated on SPV modules the two DL comparison of predicted soil power is shown in Fig. 4.9. This figure is difficult to comprehend; for greater clarity, it is depicted for two different days: first, on July 26th, when maximum dust accumulates and results in a decrease in power output as shown in Fig. 4.10 (a); and second, after cleaning occurs with minimal power losses and a significant increase in power output. The practicality of the two DL models, Stacked LSTM and Bi-LSTM, for accurate predictions in the context of predicting the performance of the models must be evaluated.
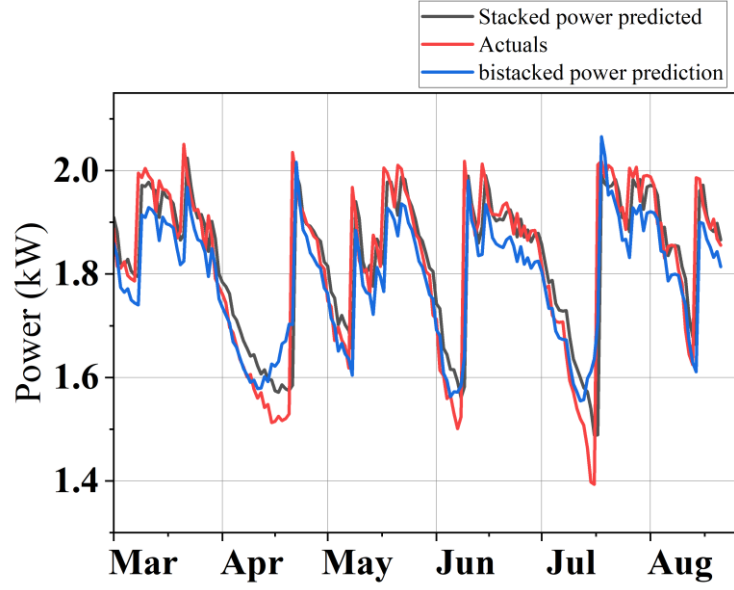
Fig. 4. 9 Soiled SPV Power Comparison Plot of Proposed Forecasting Models i.e.

Stacked LSTM and Bi LSTM.

Performance estimate is an important aspect in establishing a model's forecast accuracy. Variables used in comparison analysis include RMSE, MAE, MSE), and R^2. MAE helps to analyze the prediction model's constant prediction mistakes, RMSE evaluates the model's overall accuracy, and R^2 reflects the strength of the connection between the projected and actual values of the models [111]. Table 4.2 shows the estimation errors for the DL models.

$$MAE = \frac{1}{N}\sum_{i=1}^{N}|A_i - P_i| \tag{4.19}$$

$$MSE = \frac{1}{N}\sum_{i=1}^{N}(A_i - P_i)^2 \tag{4.20}$$

$$RMSE = \sqrt{\frac{1}{N}\sum_{i=1}^{N}(A_i - Pi)^2} \tag{4.21}$$

$$R^2 = 1 - \frac{\Sigma_k(A_i - P_i)^2}{\Sigma_k(A_i - \bar{A})^2} \tag{4.22}$$

Where "N" number of windows, "A_i" actual value, and Pi is the Predicted value. The arithmetic mean of the actual value is $\bar{A}$
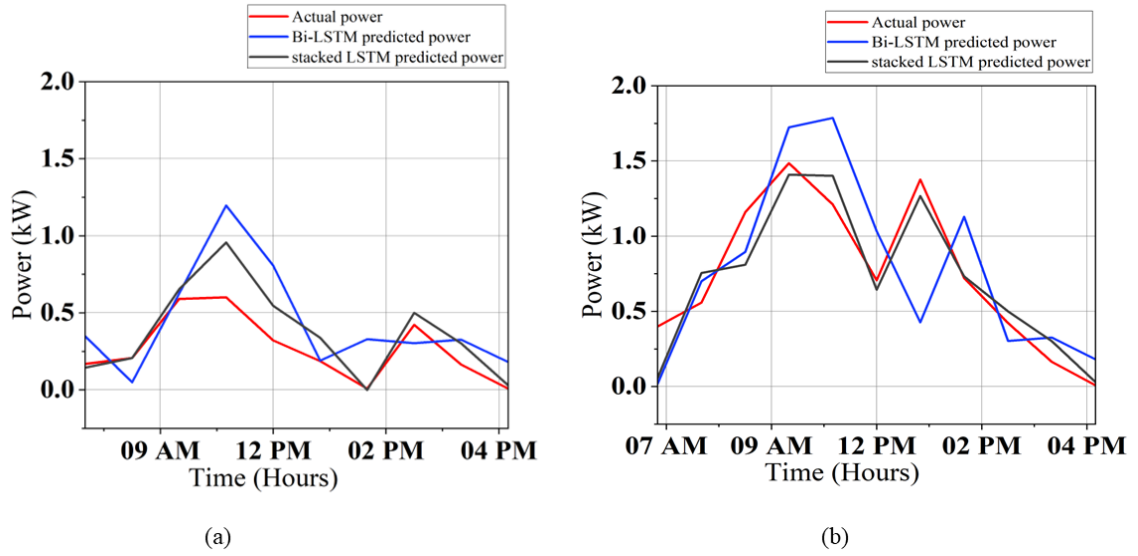
Fig. 4. 10 Soiled SPV Power Comparison Plot of Forecasting Models at Hourly Interval i.e. Stacked LSTM and Bi LSTM for (a) Maximum Soiled (b) After Cleaning.

In deep leaning prediction there is an issue of over fitting but this model is not over fitted. To avoid excessive model complexity, L1/L2 regularization is used in this work to implement weight penalties this helps in ensuring that the models did not overfit the training data. Early stopping was used to stop training whenever the testing loss slowed down, eliminating additional training cycles that might damage generalization. further a dropout layers were utilized to randomly deactivate neurons, forcing the model to learn additional features rather than recalling patterns from the training set.

Fig. 12 shows the comparison of the training and testing loss curves for the Stacked LSTM and Bi-LSTM models the graph shows their learning efficiency across numerous epochs. Both models' loss values steadily decrease throughout training, demonstrating optimization and convergence. No substantial difference between training and testing loss reduction curves shows the models are not overfitting. Additionally, the Stacked LSTM model consistently has a lower total loss than the Bi-LSTM model, indicating better learning efficiency and generalization.
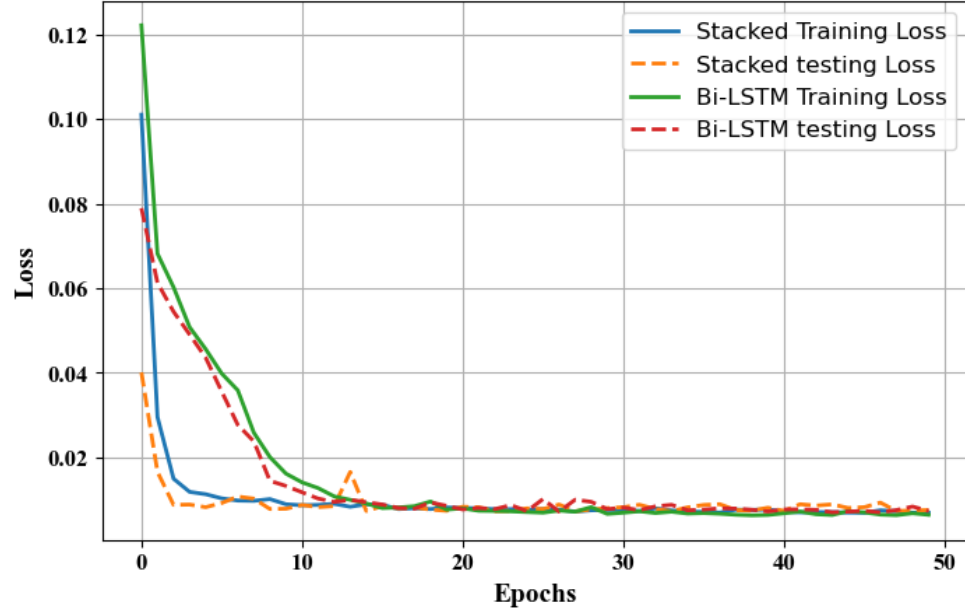
Fig. 4. 11 Comparison of Training and Testing Loss Function Graph for Both Stacked LSTM and Bi- LSTM Models.

Further performance metrics calculated from 19-22 shown in table 4.4, stacked LSTM is the most efficient model according to the obtained result, providing an ideal combination of computational cost and prediction accuracy. While Bi-LSTM improves temporal learning by processing input in both forward and backward directions, it greatly increases computational complexity while providing no significant accuracy benefit. The findings reveal that Stacked LSTM not only trains approximately 3.5 times quicker than Bi-LSTM, but it also has somewhat higher accuracy, making it a more practical option. In real-time applications requiring quick forecasts and frequent model retraining, Stacked LSTM is the recommended model for efficient and dependable forecasting because to its cheap computing cost and good predictive performance. In addition when compared to different studies as: In [105] discusses neural network-based modeling and sensor data to estimate SPV system power output when soiled. The results show that soiled PV modules may be predicted with accuracy of 97%. This study introduces a hybrid AI model combining ResNet-50 CNN for real-time CSP mirror soiling detection and LSTM RNN for predicting future soiling trends using image and meteorological data, achieving 89.5–95.2% accuracy and offering major efficiency improvements for SPV power plant management [112].

Table 4. 4 Estimation Errors for Prediction Model

Models (hourly)	MAE	MSE	RMSE	R2	Training Time(sec)
Stacked LSTM	0.051	0.0078	0.00883	0.9913	17.35
Bi - LSTM	0.0588	0.0082	0.00907	0.9850	61.70

[113] presents a model to correlate soiled SPV module power output, irradiance, and soil particle size composition. Multi linear regression predicts power with 97% accuracy. [34] hybrid clustering for neural network training data preparation. It also uses data division to anticipate soiled SPV module power production with 98% accuracy. The proposed deep learning approach, forecasts soiled power more accurately and effectively.

4.5   CONCLUSION

Power generated by SPV modules is affected by dust and other particulates on their surfaces. These dusts adhere to SPV modules, causing scratches and corrosion and shortening their lifespan. Solar plant design must consider several factors, including local conditions and dust characteristics. In order to develop dust-cleaning methods that are both safe and effective for SPV modules, it is helpful to first investigate the challenges posed by the accumulation of dust on modules, in addition to the negative impacts. In this chapter the real time soiling ratio measured from the soil monitoring system helps in modelling the accurate soiled power which helps in further analysis of loss of power in presence of dust and study the impact of temperature on dust accumulation. The maximum loss achieved is 285.35 W. And it will further degrade if continuous dust accumulation occurs, so cleaning of SPV modules should be at a prior importance to avoid SPV power loss, this chapter further helps in prediction of soiled SPV power using stacked LSTM and Bi-LSTM models and the trained results shows that stacked LSTM performs much better than Bi- LSTM with 99.13%. The model presented in this research not only focuses on predicting power loss due to soiling, but also encompasses broader improvements in the development of future SPV systems.

CHAPTER 5

HOTSPOT FORMATION IN SPV MODULES AND MITIGATION TECHNIQUES USING IMAGE PROCESSING

5.1 INTRODUCTION

Hotspots in SPV modules are localized regions of high temperatures that may result in performance decline, structural damage, and even safety hazards. These hotspots arise from uneven energy distribution, often resulting from shade, dirt buildup, or internal faults. This chapter examines the origins and effects of hotspots, with the use of image processing methods for detection and mitigation tactics aimed at enhancing the efficiency and lifetime of SPV modules.

5.2 CAUSES OF HOTSPOT FORMATION

Hotspots in SPV modules result from several contributing factors: Partial Shading: When certain sections of a panel are obscured by things like trees, buildings, or dust, they produce less current than the unshaded sections. This existing discrepancy compels shaded cells into reverse bias, resulting in the dissipation of surplus energy as heat.

Cell Defects: Manufacturing flaws, micro-cracks, or compromised solder junctions increase local resistance, resulting in localized heating and possible failure. The mismatch in Electrical Attributes: Fluctuations in cell resistance, fill factor, or efficiency result in irregular power distribution, culminating in hotspot development. Dirt and soiling: Accumulated dust, bird waste, and pollutants restrict sunlight absorption, resulting in the overheating of damaged cells.

Aging and Degradation: Prolonged exposure to environmental conditions, including UV radiation and temperature variations, diminishes cell function, hence increasing the probability of hotspots.

5.3 IMPACT OF HOTSPOTS

Because SPV modules are used outside, they are susceptible to environmental factor [114]. Due to the following consequences, the PV module may not function well in these circumstances: Effect of shade: Direct or transient shadows can produce shading. Direct shadows have a negative effect on the SPV module's performance. Shadows that are not permanent are produced by trees, buildings, snow, etc. The shading effect falls into two categories: partially shading and fully shading. While full shade results in output power extraction, shading at least 1/36 of the cell reduces the output power by 75%, Partial shade reduces current, voltage, and output power to half the nominal value. Fig. 5.1. c)

(a) (b) (c)
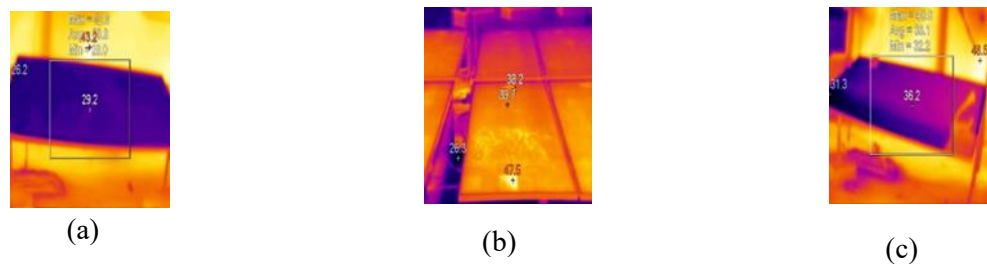
Fig. 5. 1 SPV module thermal images of a) healthy b) Dust c) shadowed

Soiling effect: SPV modules soil when dust particles like sand, cement, dirt, and leaves combine. Various elements that contribute to soiling and power loss include tilt angle, SPV module cleaning solution, and weather. The thermal images captured is shown in Fig. 5.1 b).

5.4 IMAGE PROCESSING TECHNIQUES FOR HOTSPOT DETECTION

Image processing methods provide a non-intrusive and effective approach for identifying hotspots in SPV modules. Several often used strategies encompass: Infrared (IR) Thermography: Employs thermal cameras to detect temperature fluctuations, emphasizing locations of excessive heat inside the module. Edge Detection Algorithms: Techniques such as Canny edge detection facilitate the identification of flaws in photovoltaic cells by examining thermal image gradients. Classification using Machine Learning: Deep learning architectures, particularly Convolutional Neural Networks (CNNs), accurately categorize and identify hotspots. Histogram Equalization: Improves contrast in thermal pictures, making hotspots more

discernible from typical regions.

Fourier Transform Analysis: Examines frequency components in thermal pictures to detect anomalous heating patterns.

5.5 IDENTIFICATION OF ENVIRONMENTAL FAULTS

Thermography: Environmental flaws like SPV module temperature rise and shading effects are invisible. For such instances, thermography can detect the SPV module defect. At temperatures above 0 Kelvin, objects emit infrared radiation proportionate to their inherent temperatures[115][116].A thermal imager detects SPV module infrared radiation and determines module surface temperature when located 1m from the module. An imager turns infrared light into electrical impulses and displays them in different colours at different temperatures [117][118].

Thermal Image Processing: Optimal image processing is a useful tool for enhancing the properties of image data. This study modifies the image processing technique to effectively capture the precise hotspot region of the PV modules and optimize the high level of image contrast for optimal neural network training. Fig.5.1a) shows the healthy modules thermal picture, whereas Fig. 5.1b) and Fig.5.1c) shows the faulty thermal images.

Fault Detection and Identification: SPV modules can have faults that cause them to lose power permanently. However, if there are failure-specific patterns that can be used, a more detailed study may be useful. Because of finding the fault, the efficiency of the solar cells goes up. Hotspots are areas of high temperature that affect a particular portion of a SPV module, reducing the power output and localised efficiency of the SPV modules. Dust accumulation and shadowing on the module are the primary causes of the hot spot phenomena. The early damage to the SPV module can be found via thermal imaging. The hot point on the module is visible in Fig. 5.1 b).

5.6 MITIGATION TECHNIQUES USING TRANSFER LEARNING MODEL

Transfer learning models provide a sophisticated and effective method for reducing hotspots in SPV modules by using pre-trained deep learning architectures. The following procedures are utilized:

Pre-Trained CNN Models: Models like ResNet, VGG, and MobileNet are optimized on thermal imaging datasets of SPV modules to reliably identify hotspot zones. Feature Extraction and Classification: Transfer learning enables pre-trained networks to derive pertinent features from thermal pictures and categorize hotspot severity with reduced data requirements and training duration.

Real-Time Monitoring Utilizing AI: The integration of AI-driven transfer learning models with IoT sensors allows real-time hotspot identification and proactive maintenance. Adaptive Model Training: Continual learning is used for updating the model with new hotspot patterns, hence enhancing detection accuracy progressively. Automated Fault Diagnosis: The transfer learning model can categorize hotspots by severity and recommend mitigation measures, such cleaning, replacing defective cells, or modifying module positioning.

Edge Computing Integration: The implementation of transfer learning models on edge devices enables rapid, on-site hotspot identification, eliminating the need for continuous cloud access and minimizing latency in mitigation efforts.

5.7 DEVELOPMENT OF MITIGATION TECHNIQUES

Transfer learning can significantly enhance SPV module image processing and maintenance by adapting pre-trained models for specific tasks. Here's a brief overview of how it can be applied:

Defect Detection: Pre-trained models like VGG or ResNet can be fine-tuned to detect faults such as cracks, hotspots, and dirt accumulation on SPV modules.

Efficiency Prediction: Transfer learning helps predict module efficiency by analyzing images of solar farms, detecting shading, misalignment, or dirt buildup.

Dirt and Dust Detection: Fine-tuning models to detect dirt accumulation helps optimize cleaning schedules and prevent performance loss.

Infrared Hotspot Detection: Transfer learning is applied to thermal images to detect hotspots indicating faulty modules or connections.

Misalignment or Tracking Issues: Models can be fine-tuned to detect misalignment or malfunctioning tracking systems in solar farms.

Environmental Impact: Transfer learning can help identify cloud coverage, shading, and weather conditions affecting module performance.

Image Enhancement: Transfer learning models improve low-light or low-resolution images for better inspection and defect detection.

Data Augmentation: Transfer learning combined with data augmentation expands small datasets for more robust model training.

Drone Inspection: Aerial and drone images can be analyzed with transfer learning to detect issues like dirt, misalignment, or damage.

Predictive Maintenance: Transfer learning can predict when maintenance is needed by analyzing historical image data, automating maintenance requests.

Transfer learning enables efficient and accurate SPV module monitoring, fault detection, and maintenance, improving performance and reducing costs.

5.7.1 Convolutional Neural Network

DL is a fundamental component of ML that involves the utilization of multiple layers of neurons to perform complex tasks such as abstraction and representation. This enables them to effectively perceive text, sound, and images. A subset DNN, CNNs) are intended to function on visual images [61] [119]. The CNN architecture retrieves and encodes the qualities and attributes of the input images, resulting in a notable reduction in parameters compared to conventional neural networks.

5.7.1.1 Types of CNN

Inception V3- Google developed the Inception-v3 deep convolutional neural network for image recognition. It employs various filter sizes and inception modules to efficiently capture features at various scales. It has influenced the development of subsequent versions such as Inception-v4 and Inception-ResNet by employing techniques such as batch normalization and regularization. These techniques enable it to perform well on image-related tasks and have led to the creation of Inception-v4 and Inception-ResNet.

ResNet-18 – It is a CNN that is a ResNet, which stands for residual network. In the chapter "Deep Residual Learning for Image Recognition" that was published in 2015. The ResNet-18 model is one of the most straightforward ResNet models for the classification of images. Convolutional, batch normalization, ReLU activation functions, totally linked, and softmax

layers are the components that make up ResNet-18's "18" layer combination. Through the utilization of convolutional layers that contain residual connections, ResNet-18 is able to solve the problem of vanishing gradients and train DNN.

Inception-ResNet-v2- This design uses Inception and ResNet ideas to create a deep convolutional neural network structure. The technique was created by Google researchers. This architectural design uses Inception and ResNet to increase Deep Neural Network (DNN) training and efficiency. Inception modules distinguish Google's 2014 Inception architecture. These modules enable the network to extract data at various spatial scales. ResNet is known for its residual connections, which enable deep network training without disappearing gradients. ResNet, developed by Microsoft in 2015, is now generally accepted. Using both architectures' essential features, Inception-ResNet-v2 improves accuracy and processing efficiency. It is suited for computer vision applications, including image classification and object recognition. Inception-ResNet-v2, trained on ImageNet, is utilized as a feature extractor or classifier in various applications. This model was pre-trained using ImageNet. It also underpins transfer learning, which adjusts the pre-trained model on particular datasets for image classification, object recognition, and sem Alex Net

AlexNet's - Deep layers, comprised of 650 thousand neurons and 60 million parameters, allow it to categorise more than 1000 distinct classes. Alexnet consist of 8 layers out of which Five layers are convolutional layers (CLs) and three fully connected layers (FLCs).Input to the First convolution layer is 227 x 227 x 3 to the 1st convolutional layer have 96 filters of size 11 x 11 with sride of 4 pixel after the 1st convolutional layer pooling layer are connected with stride of 2 pixel this pooling layer is sued to reduce the image size then this pooling layer acts as input to the next convolutional layer here there are 256 filters of size 5 x 5 with stride 1 then it is connected to the next pooling layer which will further reduce the size, then all the remaining 3 conventional layers are connected without pooling layer connected in between the conventional layer then 3 fully connected layer are connected where the last layer which uses softmax activation function for output calculation which produces distribution over 1000 class label. The dimension of the 147-input image for the Alex Net needs to be $227 \times 227 \times 3$, and the first CL converts the input image with 96 kernels sized at $11 \times 11 \times 3$ with a stride of four pixels. This image serves as the input to the second layer, and the other details are given in Fig. 5.2.
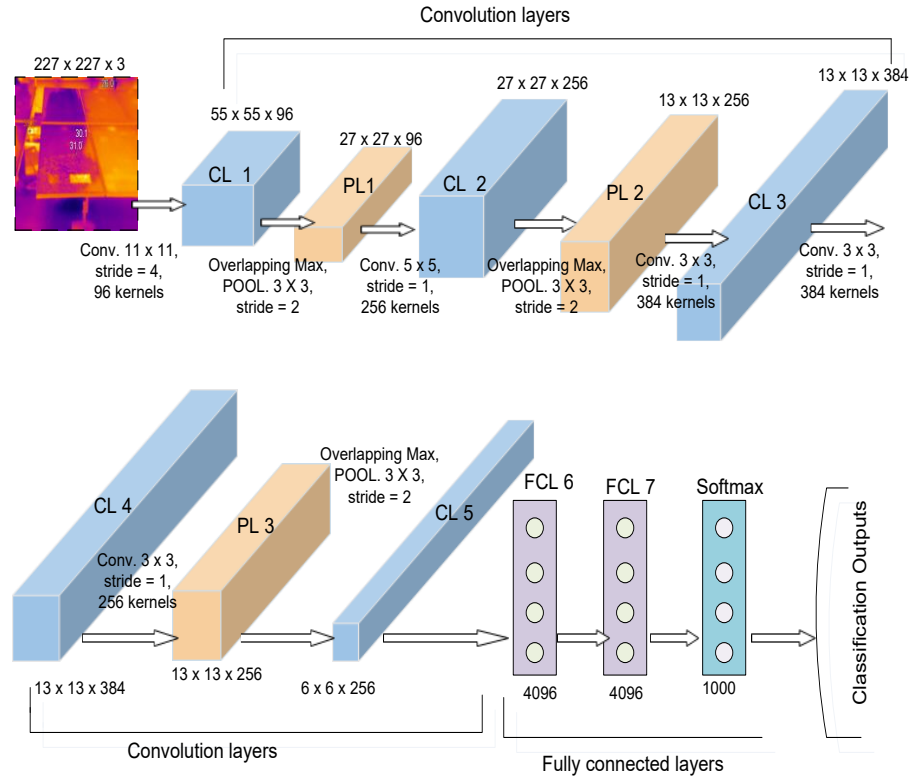
Fig. 5. 2 Structure of AlexNet

Another convolutional neural network (CNN) trained with the Image Net database is Squeeze Net. The Squeeze Net was trained with more than one million photos and had fifty times fewer parameters than the Alex Net. This network is built on a fire module, which is made up of a squeeze layer and a 175 expand layer. The fire module serves as the foundation. The squeeze layer only has 1 x 1 convolution filters, and it feeds into an expand layer that contains 176 a combination of 1 x 1 and 3 x 3 convolution filters Fig.5.3. In order to identify modules as having hotspots or not having hotspots, the pre-trained SqueezeNet model is been used.
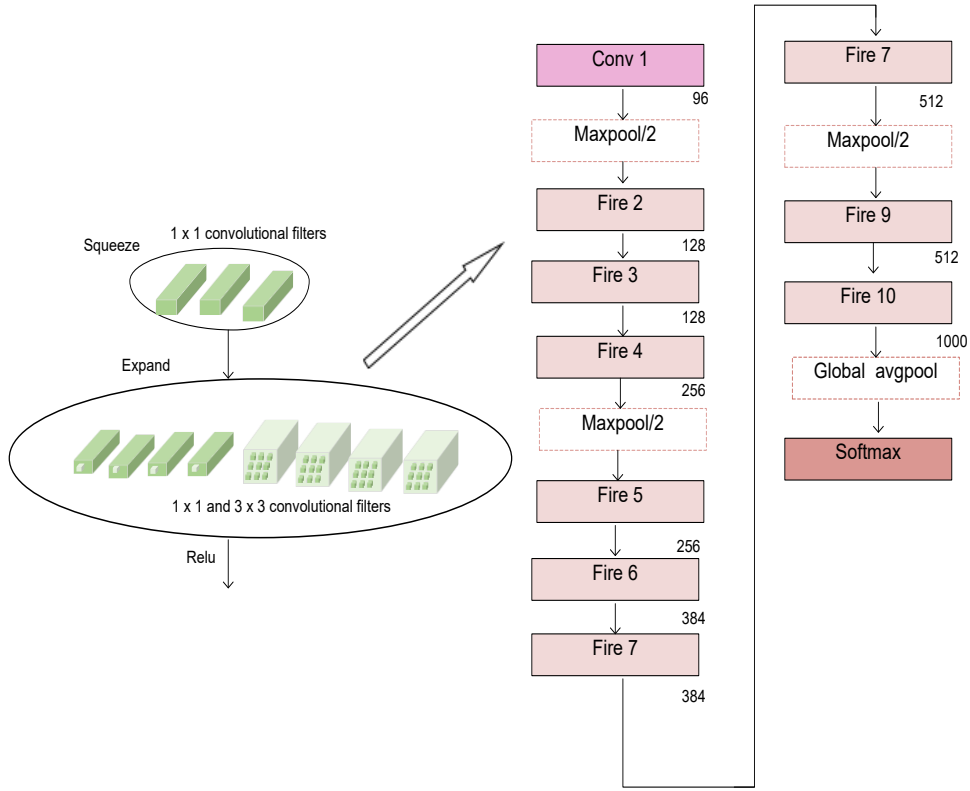
Fig. 5. 3 Structure of squeezeNet.

5.8 DATA ANNOTATION

A thermographic inspection of a SPV Module of 5 kW has been done where dust was manually created on a module which was 240 W_p for studying the hotspots and its effect on the module performances. Further, using a thermal camera image has been captured for hotspot detection and classification. The total number of images captured is 476 of which 251 items is having one Hotspot, 136 items have 3 hotspots, and 89 items have no hotspots i.e., of a healthy module some images from the thermal imager is shown in Fig's below
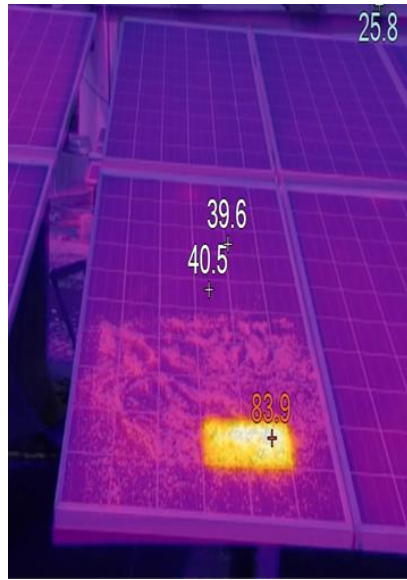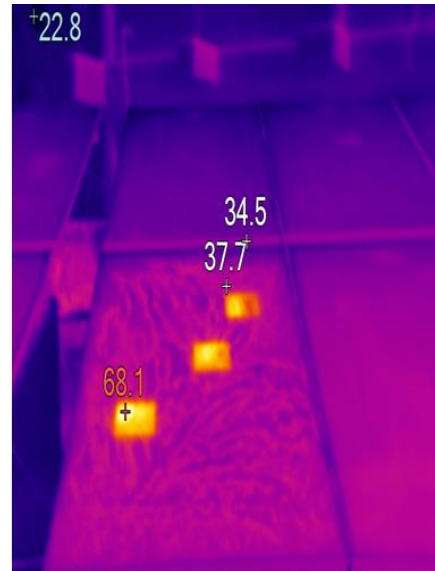
(a)   (b)
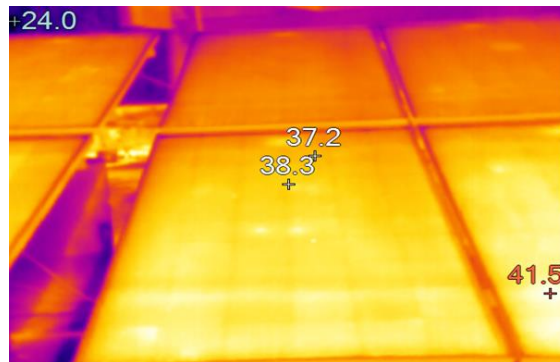
(c)

Fig. 5. 4 Healthy module without hotspot image captured from the thermal imager.

System Implementation Methodology

IR thermography uses midwave (MWIR, 3–5μm) or long-wave (LWIR, 7–14μm) infrared sensors to create thermal images or thermograms of things under inspection. Planck's black body radiation law says all objects produce infrared radiation proportional to their temperatures. IR thermography can measure the surface temperature and temperature trend of a body or SPV module under inspection. The thermal imager used for capturing the images are shown in Fig. 5.5. The hotspot are created by the effect of dust, here dust is spread on a modules in four parts in the first two parts a thin layer of dust is spread over 50% and 100% of a module and in the next parts thick layer of dust is spread over 50 % and 100% of the module and hotspots are formed due to the effect of dust these

Fig. 5. 6 Fluke TiS60 Thermal imager used for capturing images

Fig. 5. 5 Solar system Analyzer 9018BT

hotspot images are captured by the thermal camera and the power drop is recorded by the solar analyzer as shown in Fig. 5.6. Spread. Below are the steps that uses thermal imagers and further obtaining the fault classification.

1. The input for the thermal image comes from the FLIR camera, which uses an already existing data set.

2. The model then locates the spot in the binary mask through image segmentation and identifies the faulty class.

3. Once thermal images are found, the system uses the CNN classifier to determine if a single Hotspot, multiple hotspots, or string features are extracted.

4. Using a fault-classification model that has already been trained.

Pre-processing:

1. The data set is split into two groups: the training group and the validation group.

2. Batch normalisation is used to process colours before they are used.

3. A model based on machine learning and deep learning has been set up to help classify images.

4. Images are put into groups with the help of a 3x3 convolution filter.

5. Faults on the SoftMax layer, which are fully connected, are categorised with 476 images.

5.9   EXPERIMENTAL RESULTS CASE STUDY 1

This part is divided into two sections in the first section, pre-trained Convolutional networks are used to detect the hotspots and classify faulty and healthy modules. These hotspots were created because of the dust accumulation, and in the second section, power losses due to the creation of Hotspot are discussed.

5.9.1   Hotspot Detection Classification

In this work for, hotspot detection classification is done by two methods, Squeeze-Net and Alex-net; these transfer learning is a machine learning technique that uses pre-trained data here total 476 images are used in which 251 items are of 1 hotspot and 136 items are of 3 hotspots and remaining 89 items of healthy modules. All the images are been captured by the thermal imager, here 70% data is been used for training and 30% data is used for testing.

5.9.1.1 Alex-Net Transfer Learning

Alex-Net is CNN's most representative model, with more excellent performance, fewer training parameters, and strong robustness. It is inspired by while simulating dual-channel visual transmission and learning picture attributes via two channels [120]. The pre-trained model is made in MATLAB environment. In Alex-Net, there is an input layer, five convolutional layers, three pooling layers, three fully-connected layers, and an output layer with 3 output class labels. In the full model, two channels are investigated individually in the convolutional layer and only crossed in the third feature extraction layer. The first fully-connected layer cross-mixes the features of two groups. The next fully-connected layer repeats till the last fully-connected layer combines the features of two groups to generate a 4096-dimensional feature vector. This pre-trained model is used for classification, which contains 25 layers, and to image input size is 227 x 227 x 3 for training; 70% of data is used and for testing, 30%. After loading the data training option used here is shown in Table 5.1, and the accuracy and loss plot of Alex-Net transfer learning techniques is shown in Fig. 5.7 and 5.8 respectively. The training accuracy of Alex-net comes out to be 99.7%.
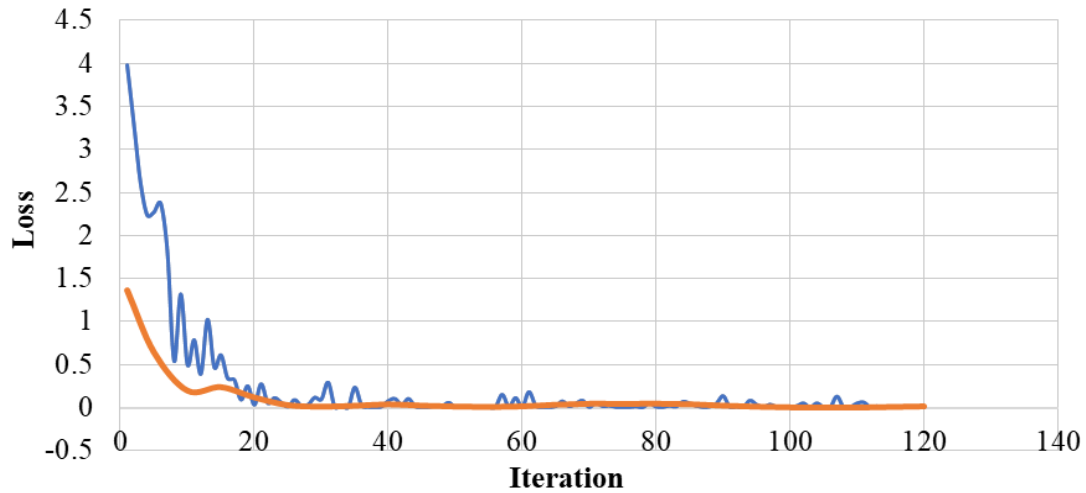
Fig. 5. 7 Accuracy plot for Alex-Net transfer learning method
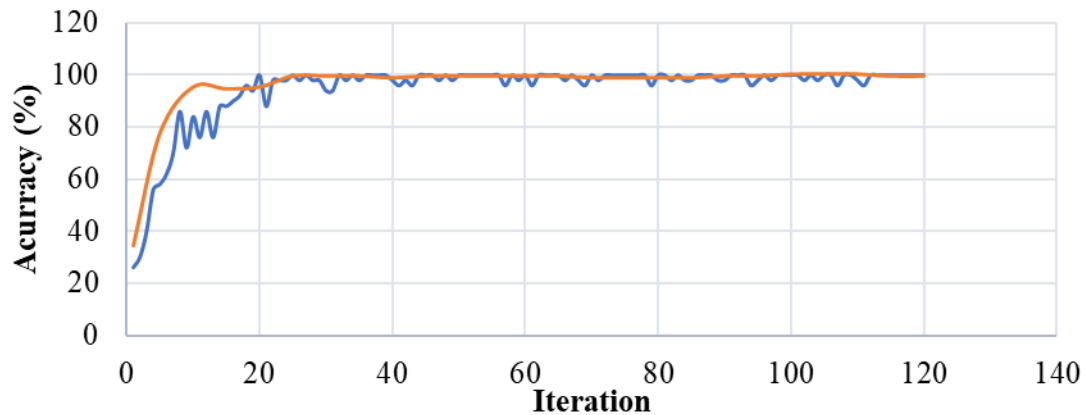
Fig. 5. 8 Loss plot for Alex-Net transfer learning method

5.9.1.2 Squeeze Net Transfer Learning

It uses three ways to improve CNN networks. First, most decreases the number of network weights. It reduces input channels to 3x3 filters. It also reduces network weights. Larger activation maps are down sampled later in the network. It's hypothesized that the size of down sampled activation maps affects categorization accuracy. Removing the fully linked dense layers frequently employed in the network's last layers and replacing them with a convolution layer with the same number of output channels as data classes, dropout layer, and SoftMax activation function decreases the amount of network weights. It contains 68

layers, MATLAB 2021 for squeeze Net transfer learning image classification is used to train the images. Further, the accuracy and loss plot of Squeeze-Net transfer learning techniques is shown in Fig. 5.9 and 5.10, respectively; training options has been considered here as shown in table 5.1. The training accuracy of the squeeze net comes out to be 95.01%.

[121] implemented a Deep learning model AlexNet with normal type of images for training the model and reported accuracy 93.33% . [122] uses VGG 19 model with thermal images for training the model and reported accuracy of 92% and Author in [123] introduces VGG 16 model with thermal images for training the model and reported accuracy of 98% where the proposed work uses Alex-Net and Squeeze-Net model where Alexnet performs best with accuracy of 99.3%.
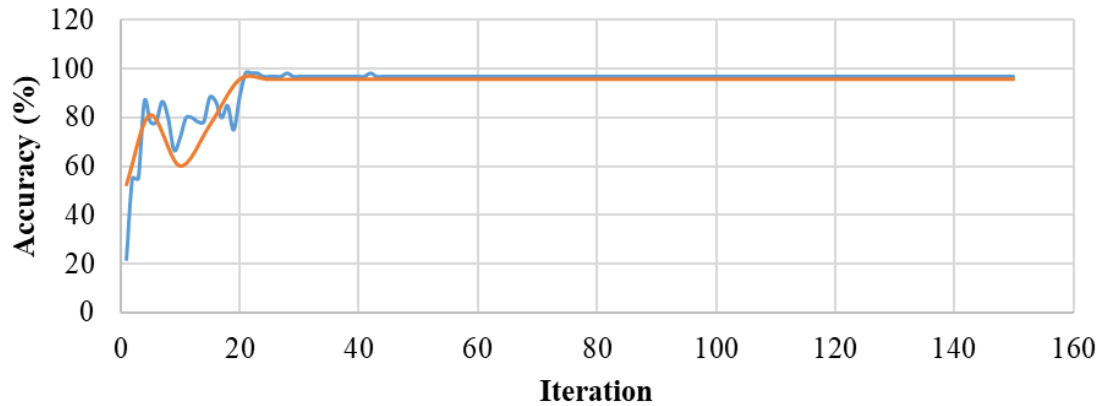
Fig. 5. 9 . Accuracy Plot for Squeeze-Net Transfer Learning Method
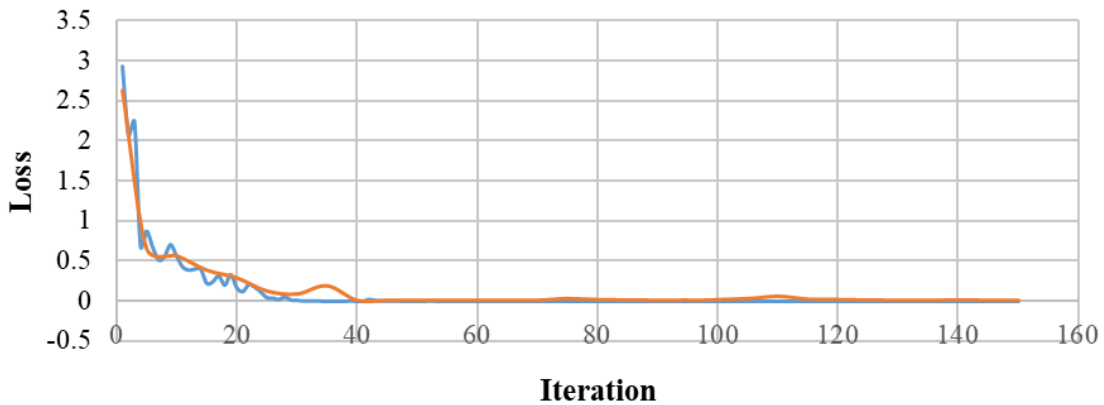
Fig. 5. 10 Loss Plot for Squeeze-Net Transfer Learning Method.

Table 5. 1 Network Parameters and Assigned Values

Training Options	Alex Net	Squeeze net
Learning Rate	0.001	0.001
Mini batch size	50	30
Max Epoch	20	20
Solver	Sgdm	Sgdm

5.9.2   SPV module performance with and without dust accumulation

On the 5 kW SPV module, which is on the rooftop of Delhi Technological University, New Delhi, hotspots are artificially created with the help of dust, for study purpose here only considering five days of data is considered on the first day solar analyser setup was put on peak hrs in which module performs best, the solar analyser for 2 hrs from 11 AM to 1 PM are connected to get the details of modules performance, on the day one the SPV module output performance is shown in Fig. 5.11.
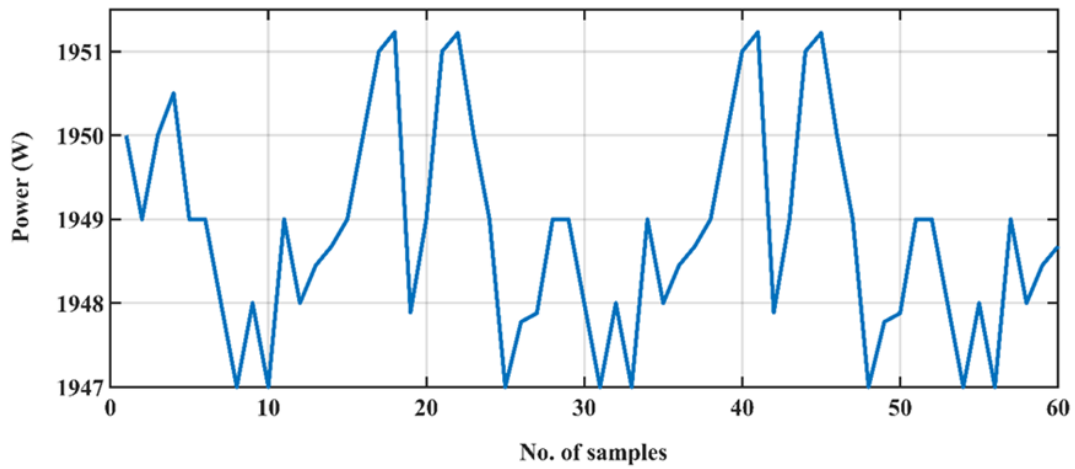
Fig. 5. 11 Day 1 Maximum Power Plot Versus No of Samples Captured from the Solar Analyzer for 2 Hrs.

On the second day to create Hotspot, some dust was intentionally sprinkled on half of the module to see the effect on output power of the SPV modules by the help of solar analyser.
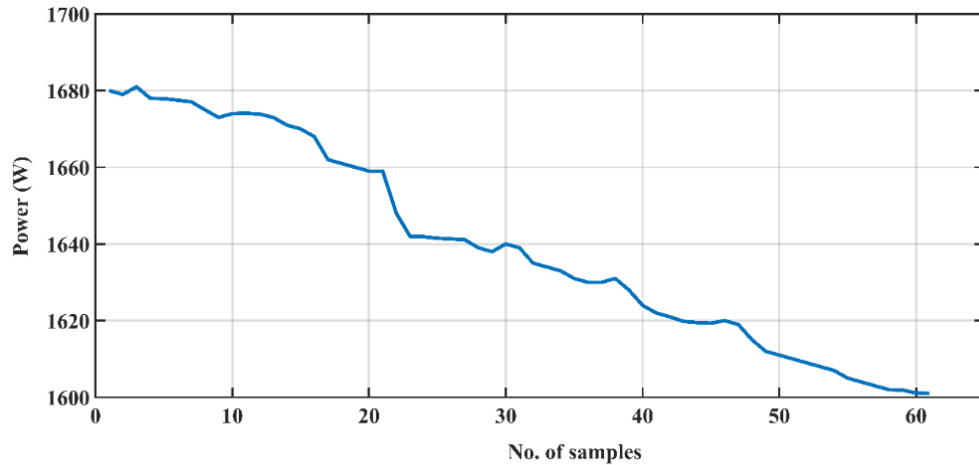
Fig. 5. 12 Day 2 Maximum Power Plot Versus No of Samples Captured from the

Solar Analyser for 2 Hrs

Seeing the Fig.5.12. we can say that power gets reduced as the Hotspot was made from 1680 W to 1601 W, the dust was kept for 2 hrs from 11 AM to 1 PM just for study purpose. The power reduced to 4.7 %. On the third day a thicker layer of dust was sprinkled on half of the SPV module to see the output power of the SPV module. In Fig. 5.13. the power gets reduced as the Hotspot was created from 1688 W to 1587.89, the dust was kept for about 2 hrs from 11AM to 1 PM for study purposes. The power reduced to 5.983 %.
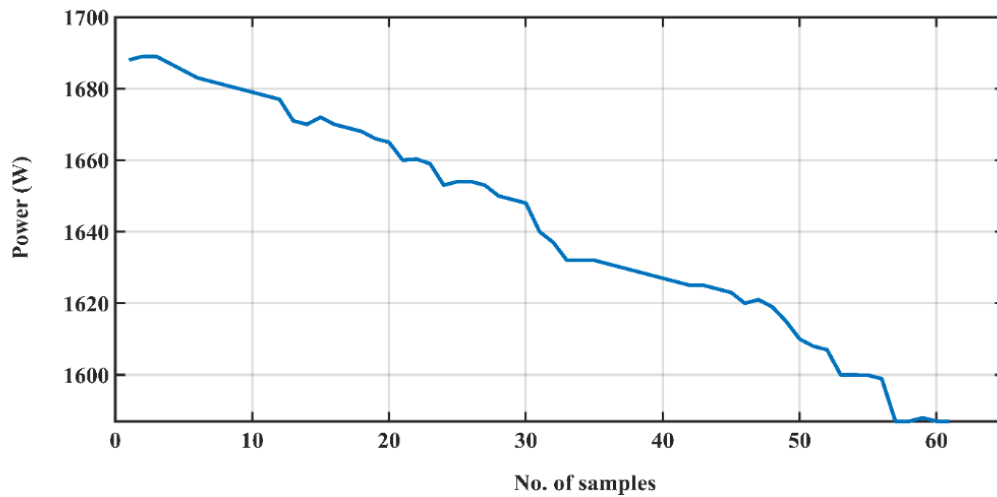
Fig. 5. 13 Day 3 Maximum Power Plot Versus No of Samples Captured from the Solar Analyser For 2 Hr.
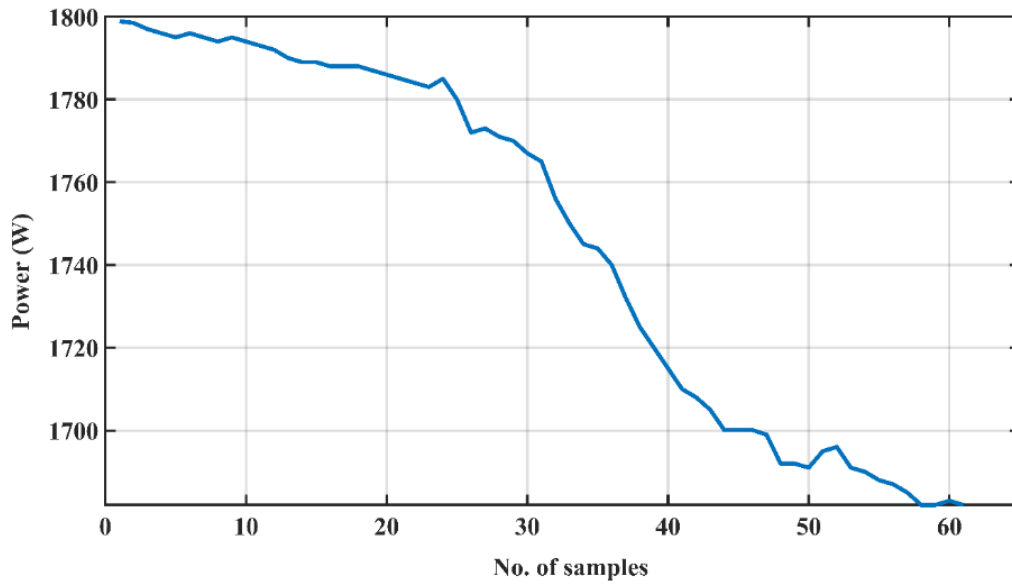
Fig. 5. 14 Day 4 Maximum Power Plot Versus No of Samples Captured from the

Solar Analyser for 2 Hrs.

On fourth day some dust was sprinkled on the complete module to see the output power of the SPV module. In Fig. 5.14 the power gets reduced as the Hotspot was created from 1798.9 W to 1682 W, the dust was kept for about 2 hrs from 11 AM to 1 PM for study purpose. The power was reduced to 6.49 %.
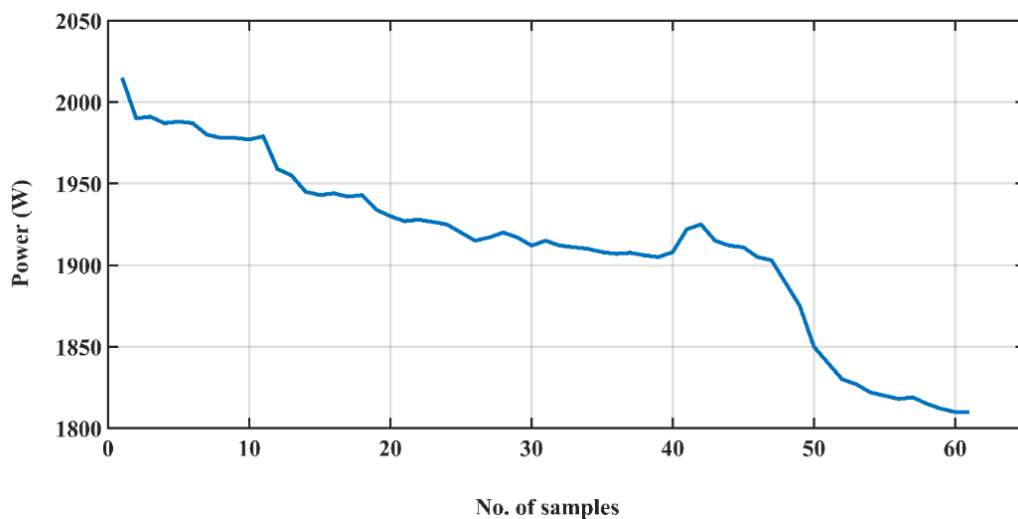
Fig. 5. 15 Day 5 Maximum Power Plot Versus No of Samples Captured from the

Solar Analyser for 2 Hrs.

On Fifth day a thicker layer of dust was sprinkled to see the module performance and create Hotspot from 2015 W to 1810 W while keeping dust on the module for 2 hrs 11 AM. to 1 PM. In Fig. 5.15. It shows that the output power gets reduced after the hotspot creation. The power reduced to 10.17 %.

5.10   EXPERIMENTAL RESULTS CASE STUDY 2

The following case study present a comparison of the fault images that were trained and tested in different neural networks. Additionally, they delve into the process of data collection and clustering of environmental defects in SPV modules. A 335 W SPV module is used to collect thermal images of dusty and shadowed faulty conditions the Fig. 5.16 shows the experimental setup used for collecting thermal images. Fig. 5.17. shows the steps considered in the acquisition of faulty images from SPV modules.

5.10.1 Collection of Dataset and Clustering

No. of images collected is 492 where healthy images are 105 and hotspot created due to dust accumulation mimicked by applying artificial dust is 251 and total shadowed images is 136 which is mimicked by providing obstructions for creating partial shading. The images were subsequently split into 70 and 30 percent ratios for SPV module training and testing.

Fig. 5. 16 Experimental Setup for Collecting Thermal Images by Fluke Thermal Imager
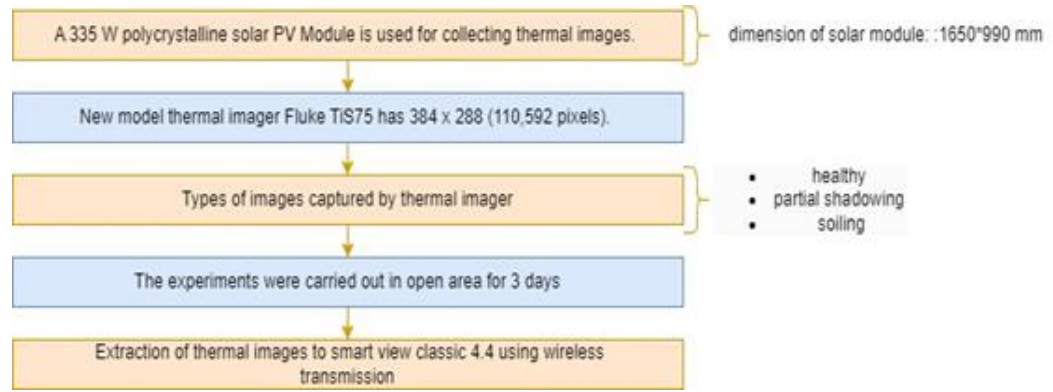
Fig. 5. 16 Methodology for Data Collection and Clustering.

5.10.2 Neural Network Analysis

The MATLAB software's Deep Network Designer tool trains images collected from the thermal imagers to create pretrained neural network such as Resnet-18, Inception V3 and Inception- Resnet -V2. The model is trained as given in Table. 5.1 for best fitting of model.

Table 5. 2 Training Parameters for Different Pretrained Networks

S. NO.	Training options	Value
1.	Solver	SGDM
2.	Maximum epochs	20
3.	Mini batch size	30
4.	Max number of iterations	128
5.	Learning rate	0.0001

In ResNet-18 model 70 % and 30% data are used for training and testing this model is trained with accuracy of 90.18 % and training time for this model is 82 minutes as shown in Table. 5.2

In Inception v3 model 70 % and 30% data are used for training and testing this model is trained with accuracy of   93.34 % % and training time for this model is 97 minutes as shown in Table. 5.2.
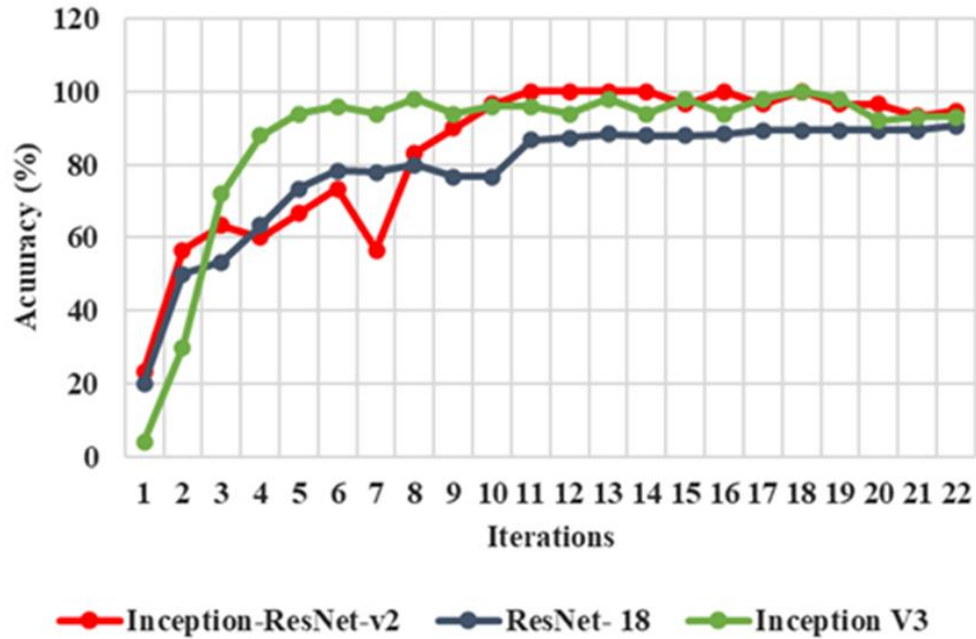
Fig. 5. 17 Accuracy Plot for Different Transfer Learning Model

In Inception ResNet v2 model 70 % and 30% data are used for training and testing this model is trained with accuracy of 94.768 % % and training time for this model is 125 minutes as shown in Table. 5.2
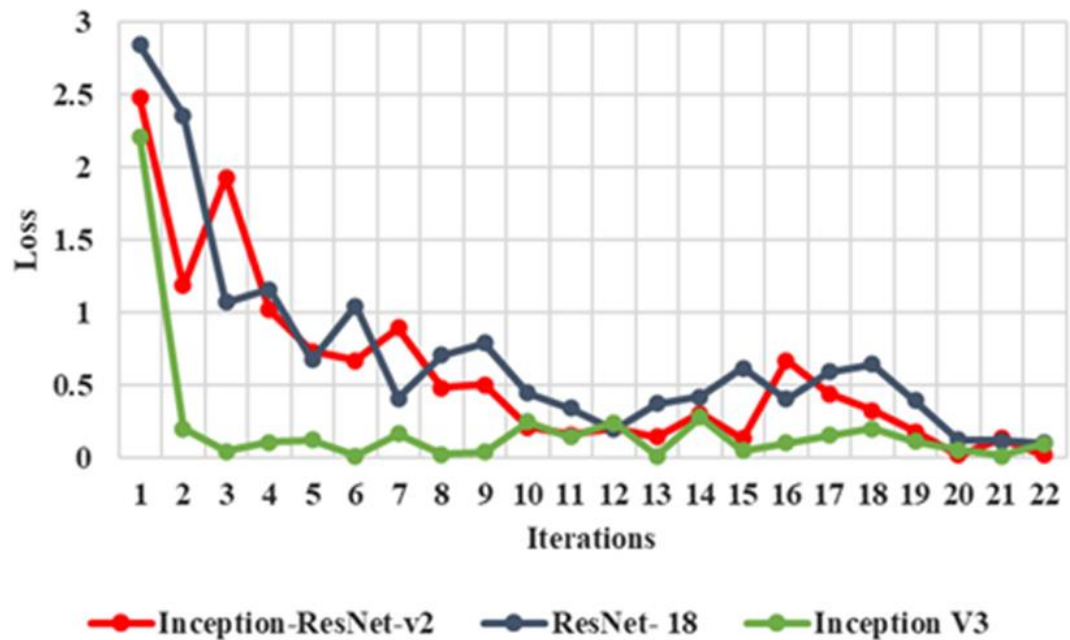
Fig. 5. 18 Accuracy Plot for Different Transfer Learning Models

Comparison plot of performance of different transfer learning methods is displayed in Fig. 5.18. and loss plots are shown in Fig. 5.19.

5.10.3 Performance Evaluation

(i) Accuracy- Model accuracy is an evaluation metric that approximates performance across all classes. To compute, use the following formula:

$$Accuracy = \frac{t_p + t_n}{t_p + t_n + f_n + f_p} \tag{5.1}$$

where tp, tn are the amount of true positives and true negatives, and fp, fn denotes the number of false positives and false negatives.

(ii)   Precision- Precision is a measure that is obtained by dividing the number of true positives by the total number of positives (t_p and f_p). It is determined using the following formula:

$$precision = \frac{t_p}{t_p + f_p} \tag{5.2}$$

(iii) Recall- This measure is the proportion of correctly identified positives (true positives) to total positives (true positives and false negatives). It is determined using the formula given below:

$$Recall = \frac{t_p}{t_p + f_n} \tag{5.3}$$

F-1 score- The F-1 score is calculated as the weighted average of recall and precision.It is calculated as follows:

$$F1 = \frac{2 * precision * Recall}{precision + Recall} \tag{5.4}$$

Table 5. 3 Performance Evaluation of Various Transfer learning Methods

Transfer learning Models	Accuracy	Recall	Precision	F1 score	Computational time
ResNet18	0.901	0.823	0.87	0.84	82 min
Inception V3	0.933	0.88	0.89	0.90	97 min
Inception-ResNet-v2	0.947	0.89	1	0.94	125 min

There are various transfer learning models used for fault classifications. The authors in [61] proposed muti-scale CNN method with accuracy 93.51 %. The author [119] uses Squeeze Net, Google Net, shuffle Net for fault classification with 94.12%, 97.62% and 94.12 % respectively. The proposed work uses much real time captured imaged and trained, where Inception-ResNet -V2 performs best.

5.11   EXPERIMENTAL RESULTS CASE STUDY 3

In this case a meticulous investigation and assessment of different DL architectures is done i.e. ResNet, GoogLeNet, VGG-16, and VGG-19 as proposed in Fig 5.19. By harnessing the power of transfer learning and initializing models with pre-trained weights sourced from extensive datasets. The focal point is the adaptation of pre-existing features to the unique nuances inherent in SPV systems for module condition monitoring. Rigorous evaluation was performed on a dedicated testing set, using comprehensive performance metrics, such as precision, sensitivity, accuracy, specificity, Matthew's correlation coefficient and F1-score.

The results and discussion of this case is parted into two major sections. In the first section, the SPV module condition is analysed using P_{loss}. This loss in power is calculated using the data collected by solar PV analyzer 9018BT. P_{loss} is computed by distinguishing between defective and healthy modules. Additionally, the section divides the data into four classes and constructs an image dataset for the purpose of training the transfer learning model. Where out of 660 images total 251, 136, 168 and 105 images are of hotspot and multi-hotspot, shadowing, cracked and healthy modules respectively. The classes used for classifications is divided in two parts faulty and healthy modules faulty modules are divided in three classes which are hotspot and multi-hotspot, shadowing by nearby objects, cracked modules and healthy modules.
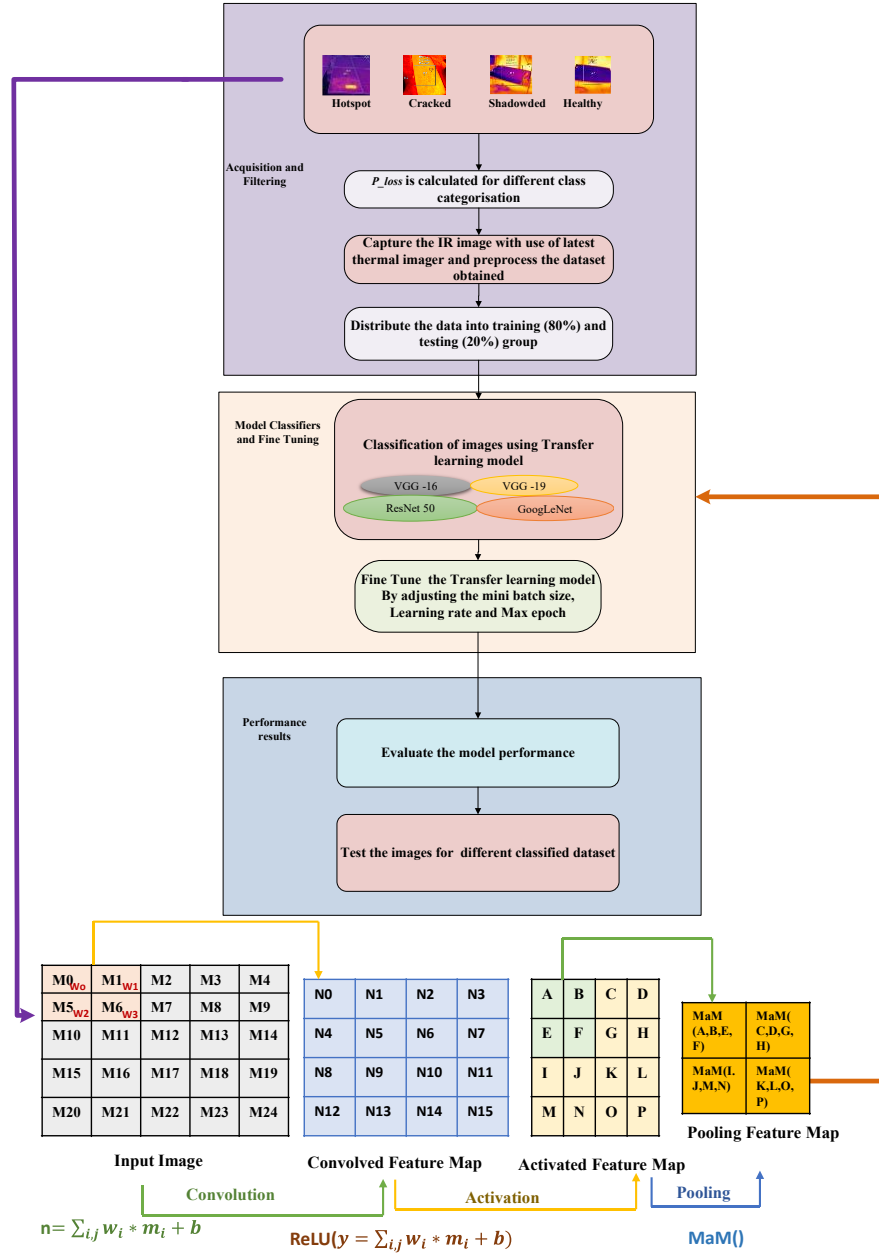
Fig. 5. 19 Proposed framework for PV module condition monitoring.

5.11.1 Comparative Performance for Different Classes on SPV Modules

Different faulty conditions performance is considered, where the power is recorded on 3 different real time PV module Fault scenarios. i.e. Shadowing, Cracked and hotspots which is created by dust and further compared the power recorded against healthy module. The magnitude of the power loss is determined by a variety of parameters, including the severity of the hotspot, the degree of shadowing, and fracture damage.
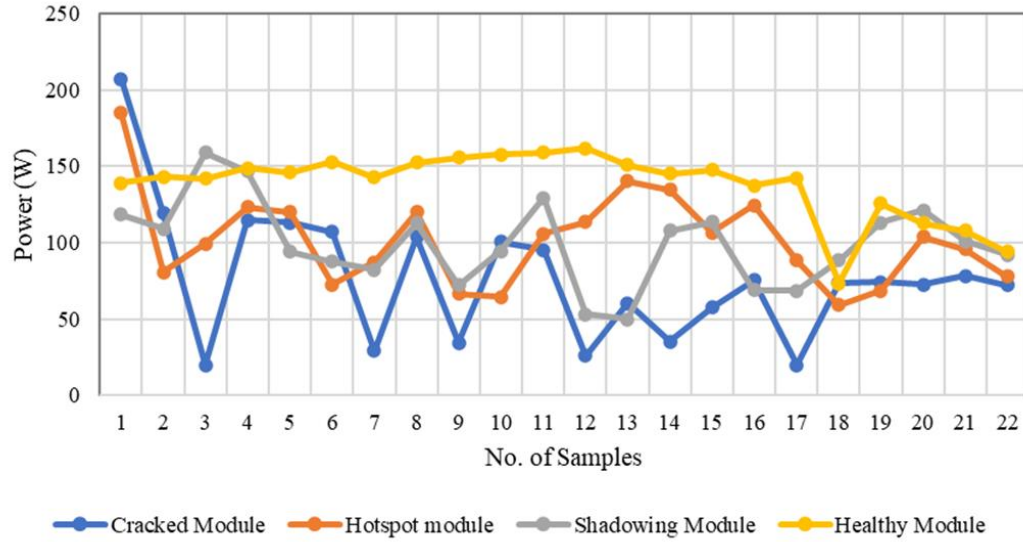
Fig. 5. 20 Comparative Performance of Different Classifications

The power is recorded on a 335 W PV module for 10 minutes interval for different condition by the Solar system analyzer 9018 B for 4 hours. The power recorded is shown in Fig. 5.19 different classes of PV modules are discussed below.

1) Healthy module- The module is cleaned and then power is recorded.
2) Shadowing module – The shadowed condition is been mimicked as short wide (SW) shading condition, discussed in [124] .
3) Cracked module datasets- A same 335 W cracked module is considered to record power, the cracked module considered is having severe cracks.
4) Hotspot modules- Dust was spread for mimicking a real time scenario.

The power loss in different condition is shown in Table 5.4. Where it is observed that the maximum power loss is due to Cracked Module.

Based on this work power loss it can be defined that the solar PV modules as faulty. Here less than 20% power loss is considered to be recoverable and more than 20% power loss the module is stated as cracked and not recoverable and needs replacement. Table III discusses the power loss percentage for different faulty conditions. From Table II different faulty modules can be classified and thermal images are been captured for different stated classes.

Table 5. 4 Power Loss in Different Conditions

Conditions	Healthy Power (W)	Faulty Power (W)	P_{loss} (%)
Hotspots and multi-Hotspots	93.1672 W	77.9319 W	16.35 %
Shadowing	93.1672 W	91.9368 W	2.22 %
Cracked	93.1672 W	72.0247 W	22.69 %

5.11.2 Classification Using Transfer Learning Methods

The captured thermal infrared images are used to train the deep learning CNN transfer learning models GoogLeNet, Resnet- 50, VGG-19 and VGG-16 to classify faulty and healthy solar PV modules. The "GoogLeNet" alters the last three layers of the network these three layers of the network -"loss3-classifier," "prob," and "output"- are replaced with "fully connected," "softmax," and "classification output" layers. Connect the last transferred layer ("pool5-drop_7×7_s1") to the new layers. The data is divided in 8 The fluke thermal imager TiS75+ is used to create hotspots and capture thermal pictures. The photos are acquired over a span of 4 days in order to gather a dataset encompassing 4 distinct classes. The purpose of these photos is to train deep learning CNN transfer learning models, such as GoogLeNet, Resnet-50, VGG-19, and VGG-16, to accurately detect defective and non-defective solar photovoltaic (PV) modules. The last three layers of "GoogLeNet" is modified. The layers of the network, namely "loss3-classifier," "prob," and "output," are substituted by "fully connected," "softmax," and "classification output" layers respectively. Establish a connection between the most recently transferred layer, namely the "pool5-drop_7×7_s1" layer, and the newly introduced layers. The data is partitioned into 80% for training and 20% for validation.

Table 5. 5 Performance Comparison of DNN Architecture During Training Phase

Transfer learning Models	Accuracy	Computational time
ResNet- 50	**83.3 %**	**2 min 19 sec**
Google Net	73.5 %	5 min 17 sec
VGG-19	90.9 %	52 min 12 sec
VGG-16	**95.5 %**	50 min 2 sec

The solver used for transfer learning models are Stochastic gradient descent with momentum (Sgdm). The data is split into training and testing into 80% and 20% respectively

i.e. 528 training images and 132 testing images. The different model training plots of the input images is shown in Fig.5. 20.
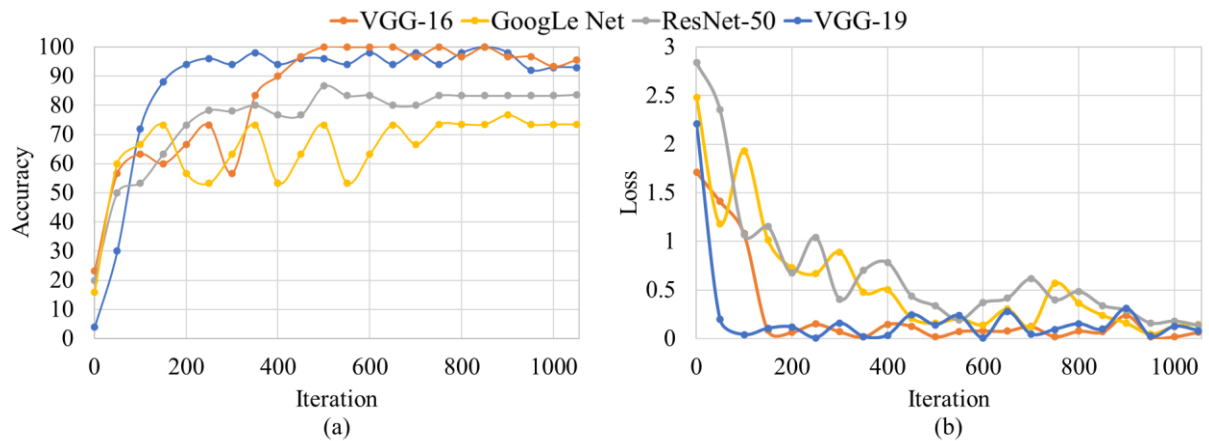
Fig. 5. 21 Comparative performance of various DNN architectures during training phase

(a) Accuracy performance (b) Loss Analysis

The training accuracy and loss plots of different transfer learning model i.e. Resnet-50, GoogLeNet, VGG-16 and VGG-19 is shown in Fig. 5.20 (a) and Fig. 5.20 (b). The models developed is optimized for better results VGG-16 comes out to be 95.5% with highest computational time of approx. 50 minutes and ResNet-50 performs with lowest computational time of 2 min 19 sec with accuracy of 83.3% shown in Table 5.20. From the Fig. 5.21 it is observed that the VGG -16 transfer learning model gives the best performances for classifying the various classes of dataset with highest accuracy.

Table 5. 6 Evaluation Metrices for different Classes of SPV Module Condition

Models-	ResNet-50				GoogLe Net				VGG-19				VGG-16			
Performance metrics	Healthy module	Shadowing module	Cracked module	Hotspot module	Healthy module	Shadowing module	Cracked module	Hotspot module	Healthy module	Shadowing module	Cracked module	Hotspot module	Healthy module	Shadowing module	Cracked module	Hotspot module
A (%)	100	88	90	94	86	77	61	100	100	89	100	94	100	93	100	97
P (%)	100	77	71	88	100	52	35	100	100	78	100	88	100	78	100	100
Sn (%)	100	77	100	88	42	100	67	100	100	78	100	88	100	100	100	89
Sp (%)	100	93	86	96	100	69	59	100	100	93	100	96	100	91	100	100
F1 (%)	100	78	83	88	60	68	46	100	100	78	100	88	100	88	100	94
MCC (%)	100	70	78	84	59	60	23	100	100	70	100	84	100	84	100	93

Performance comparison for complete dataset consisting of different cases is shown in Table 5.6, where 660 images are used to train the transfer learning models. Further after training the entire data set is tested and confusion matrix are made so as to find various performance matrices i.e accuracy, sensitivity, Specificity. The confusion matrix for each of the four DNN architectures for SPV condition monitoring is presented in Fig. 5.21. The four DNN architecture (ResNet-50, GoogLeNet, VGG-19 and VGG-16) symbolizing transfer learning method and their respective confusion matrix to evaluate the performance of each model. The accuracy plot for different classes is showed on the transfer learning models. A systematic approach is necessary to derive accuracy (sensitivity), precision, or specificity values from a confusion matrix. Perform the necessary computations to determine the True Positives (tp), False Positives (fp), True Negatives (tn), and False Negatives (fn) associated with a particular class of interest. As demonstrated by the confusion matrix provided in Fig. 5.21(c), the analysis that is centred on shadowing. tp represents the number of instances that were accurately classified as shadowing, which is 14 in this instance. On the other hand, (fp) represents 13 irrelevant instances that were erroneously classified as shadowing, excluding the first column. This total is calculated by adding the values in the first row. Indicative of correctly identified irrelevant test instances, (tn) is obtained by deducting (fp) from the total number of irrelevant test instances. (tn) is calculated in this context using three irrelevant classes and fourteen test instances per class

as (3*14 -13), which equals 29. In order to identify (fn), which denotes shadowing instances that were incorrectly classified as other

(a)

	Shadowing	cracked Panels	healthy panels	hotspots	
Shadowing	**21** 15.9%	**0** 0.0%	**0** 0.0%	**6** 4.5%	77.8% 22.2%
cracked Panels	**0** 0.0%	**24** 18.2%	**10** 7.6%	**0** 0.0%	70.6% 29.4%
healthy panels	**0** 0.0%	**0** 0.0%	**21** 15.9%	**0** 0.0%	100% 0.0%
hotspots	**6** 4.5%	**0** 0.0%	**0** 0.0%	**44** 33.3%	88.0% 12.0%
	77.8% 22.2%	100% 0.0%	67.7% 32.3%	88.0% 12.0%	**83.3%** **16.7%**

(b)

	Shadowing	cracked Panels	healthy panels	hotspots	
Shadowing	**14** 10.6%	**6** 4.5%	**7** 5.3%	**0** 0.0%	51.9% 48.1%
cracked Panels	**0** 0.0%	**12** 9.1%	**22** 16.7%	**0** 0.0%	35.3% 64.7%
healthy panels	**0** 0.0%	**0** 0.0%	**21** 15.9%	**0** 0.0%	100% 0.0%
hotspots	**0** 0.0%	**0** 0.0%	**0** 0.0%	**50** 37.9%	100% 0.0%
	100% 0.0%	66.7% 33.3%	42.0% 58.0%	100% 0.0%	**73.5%** **26.5%**

(c)

	Shadowing	cracked Panels	healthy panels	hotspots	
Shadowing	**14** 10.6%	**0** 0.0%	**0** 0.0%	**13** 9.8%	51.9% 48.1%
cracked Panels	**0** 0.0%	**34** 25.8%	**0** 0.0%	**0** 0.0%	100% 0.0%
healthy panels	**0** 0.0%	**0** 0.0%	**21** 15.9%	**0** 0.0%	100% 0.0%
hotspots	**0** 0.0%	**0** 0.0%	**0** 0.0%	**50** 37.9%	100% 0.0%
	100% 0.0%	100% 0.0%	100% 0.0%	79.4% 20.6%	**90.2%** **9.8%**

(d)

	Shadowing	cracked Panels	healthy panels	hotspots	
Shadowing	**21** 15.9%	**0** 0.0%	**0** 0.0%	**6** 4.5%	77.8% 22.2%
cracked Panels	**0** 0.0%	**34** 25.8%	**0** 0.0%	**0** 0.0%	100% 0.0%
healthy panels	**0** 0.0%	**0** 0.0%	**21** 15.9%	**0** 0.0%	100% 0.0%
hotspots	**0** 0.0%	**0** 0.0%	**0** 0.0%	**50** 37.9%	100% 0.0%
	100% 0.0%	100% 0.0%	100% 0.0%	89.3% 10.7%	**95.5%** **4.5%**

Fig. 5. 22 Confusion Matrix for Various DNN Architectures (a) ResNet-50 (b) GoogLeNet (c) VGG-19 and (d) VGG-16

defects, the sum of the values in the first column (excluding the first row) yields 0. The sensitivity or accuracy of different classes is represented in the bottom row of the confusion matrix, whereas the precision of different classes is illustrated in the far-right corner. Subsequently, power measurements for both functional and malfunctioning modules are discussed. Thermal images are captured and categorized into four distinct classes, and a

performance analysis is conducted on the aforementioned classes. The performance metrices can be calculated by the confusion matrix w6th the help of fp, fn, tp, tn the testing data set is used to plot the confusion matrix the Fig. 5.21 describes the different classes sensitivity and precision and rest parameters are shown in Table 5.5. This tables concluded that VGG-16 transfer learning models performs best among the other transfer learning models discussed in this chapter.

5.12   CONCLUSION

SPV module hotspots reduce efficiency, performance, and longevity. Dust collection, partial shading, and module faults generate hotspots that impair power output and may cause irreparable damage. Hotspot analysis employing thermal imaging and deep learning-based image processing has been successful in fault identification and classification. Alex Net, Squeeze Net, ResNet-18, Inception v3, Inception-ResNet-v2, ResNet-50, Google Net, VGG-16, and VGG-19 are CNNs and transfer learning models that can accurately identify damaged and healthy modules.

Both studies emphasize the significance of thermal imaging and deep learning in SPV defect detection. Dust collection and shade reduce SPV efficiency by 4.7% to 10.17%, depending on coverage. In case 1 Alex Net detected dust-induced hotspots with 99.3% accuracy, whereas in case 3 Inception-ResNet-v2 classified faults across environmental conditions with 94.8% accuracy, 100% precision, and 94.2% F1-score and in Case 3 VGG-16 model proved to be the best of the assessed models, with classification values 95.5 %. Early hotspot identification is crucial because dust collection and shadowing might cause permanent module deterioration. Various automated detection and maintenance solutions have been investigated to reduce hotspot development and increase SPV system dependability. Image processing methods separate and classify defects, allowing preventive interventions before major power losses. Hotspots may be reduced via module cleaning, anti-soiling coatings, and system optimization. Additionally, AI-driven predictive maintenance may improve SPV system performance and reduce expensive human inspections. Deep learning-based defect detection algorithms are promising, but model overfitting, computational costs, and dataset reliance persist. Future research should build lighter, more efficient models with excellent detection accuracy and minimal

processing power. Infrared thermography with AI-powered automation may increase real-time monitoring and problem mitigation, increasing energy yields, lowering maintenance costs, and improving sustainability.

These studies emphasize the relevance of AI-driven SPV system monitoring, enabling more dependable, cost-effective, and sustainable solar energy generation. Advanced deep learning and image processing may boost SPV module efficiency and lifetime, providing optimum energy production and operational stability. This chapter also focuses on future potential for severity based on fault labelling

CHAPTER 6

DESIGN AND DEVELOPMENT OF MITIGATION TECHNOLOGIES FOR DUST ACCUMULATION ON SPV MODULE

6.1 INTRODUCTION

The collection of dust on SPV modules significantly diminishes their efficiency by obscuring sunlight and reducing power production. Various environmental conditions, including wind, humidity, and precipitation, affect dust deposition rates. Excessive dust collection might result in uneven shading, creating hotspots that diminish the module's longevity and effectiveness. The intensity of the problem varies by geographic location, with dry and semi-arid areas exhibiting the highest levels of dust buildup.

Mitigation techniques are crucial for sustaining optimum performance and guaranteeing long-term dependability. Efficient dust removal techniques save maintenance expenses, enhance energy output, and mitigate environmental effects linked to conventional cleaning practices. This chapter examines current dust mitigation methods, suggests best cleaning methods, and further outlines the design and development process for efficient dust removal systems.

6.2 CLEANING METHODS

Several cleaning methods are developed for SPV module enhancement. There are two types of cleaning methods passive and active cleaning methods. Passive SPV module cleaning options include using rain, tilting modules for natural shedding, hydrophobic coatings, and smooth surfaces. Manual cleaning, automatic cleaning, or self-cleaning modules using robotic arms or water jets are active techniques. Passive methods are cheap but may not work in all situations, while active ones clean better but cost more. Location, weather, budget, and maintenance preferences determine the option.

SPV modules are being cleaned using one of three techniques: mechanical, coating, or electrostatic procedures. Generally speaking, four mechanical methods—air-blowing,

robotic, water-blowing, and ultrasonic vibration—are studied to clean the surface of SPV modules. These techniques require a lot of energy to operate and have moving parts. While consuming a lot of water is a major downside of this method, especially in dry areas, it also saves energy.

Electrostatic cleaning has been the subject of a new design and implementation. Considering the electrode designs, the cleaning performance of this device has been evaluated [83]. The electrostatic dust removal action of transparent conductive films made of carbon nanotubes (CNTs) is the basis for a novel electrostatic adsorption dust removal technique for SPV modules investigated in this work [84]. This study aims to investigate the optimal counteracting force required to eliminate dust particles that have stuck to PV modules. A self-cleaning system that utilizes fluid velocities to lift dust particles stuck to the surface of a SPV module, while minimizing the static charge created, has been developed [85]. In order to clean the SPV module, this work offers the design and experimental analysis of a revolutionary self-powered SPV module cleaning mechanism system. The cleaning method does not require electricity from the SPV module that has to be cleaned because it is powered by two little SPV modules that have rechargeable batteries [86]. This work presents a SPV module cleaning robot that autonomously cleans photovoltaic modules at regular intervals. The robot cleans the surface of the modules by using air blowing, liquid spraying, wiping with a wiper, and drying any moisture on the modules using a cylindrical brush. The suggested robot is operated by IoT from a remote location, thereby minimizing human labor at the solar facility and enabling remote monitoring [87]. SPV modules directly generate electricity from solar radiation. How much light SPV modules use impacts their efficiency. SPV modules use 30%–40% of incident solar radiation. Due to ambient dust and module glass reflection, a lot of incident radiation goes unutilized. To solve these technological challenges, self-cleaning/superhydrophobic antireflection coatings are popular [88]. Superhydrophobic transparent coatings are useful in solar energy for their low cost, self-cleaning, and dust-resistance. Solar energy self-cleaning coatings are complex; therefore, few publications have studied them. Industrial SPV modules need strong coatings owing to demanding environments. Contrasting transparency and roughness cause self-cleaning. Solar superhydrophobic coatings are tricky to study. Transparent and superhydrophobic coating materials, deposition, and

synthesis were rarely covered in literature reviews. Many evaluations highlight superhydrophobic coatings, which segregate water/oil, resist ice, biofouling, and self-clean. However, few studies address solar superhydrophobic coating development. Solar applications require transparency, making this topic difficult. This evaluation covers SPV module dust and efficiency. Self-cleaning, transparent cohabitation, and super hydrophobicity follow [89]. To economically deploy solar in arid places, dust-related power loss in SPV systems must be mitigated. High aerosol concentrations and frequent sand storms cause SPV array dust to accumulate. Dust remains due to occasional light showers. An automated robotic cleaning system was used to test the effectiveness of dry cleaning SPV modules [90].

Therefore, this study employs MICMAC and TOPSIS methodologies in subsequent sections to comprehensively assess and rank available mitigation strategies based on a multi-criteria framework.

6.3 MULTI CRITERIA DECISION MAKING

The MCDM process involves selecting one of two or more solutions based on predetermined criteria and common problems. However, it is important to note that the decision made among the available solutions may not always be correct. MCDM treats a finite set of alternatives that are solved using a mathematical model. MCDM has experienced a substantial surge in usage over the past few decades, resulting in a significant expansion of its application area [125][126][127] MCDM approaches exist, each with conflicting criteria. There are several MCDM techniques with varying criteria. The MCDM technique is often used for both quantitative and qualitative analysis. This method integrates historical data and expert views by quantifying subjective judgment. AHP, PROMETHEE, ELECTRE, TOPSIS, and VIKOR offer several MCDM models. Each technique has its own algorithm, as shown in Fig. 6.1. To find the optimal SPV power plant location, the MCDM model combines DEA, FAHP, and TOPSIS techniques to consider both quantitative and qualitative factors.
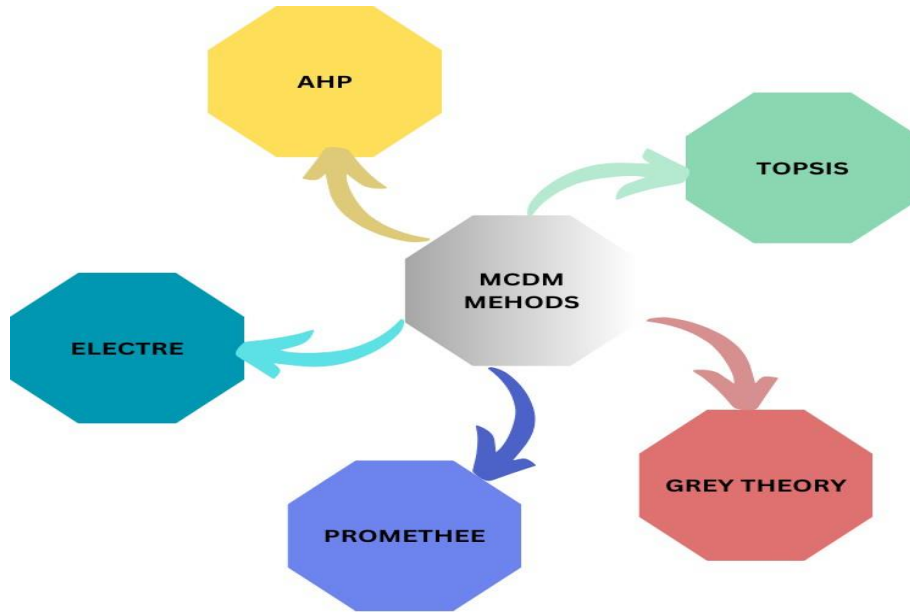
Fig. 6. 1 Different MCDM methods

6.4   PROPOSED METHODOLOGY

This chapter uses MICMAC analysis to find the most suit- able SPV module cleaning parameters. Panel Surface Material (PSM), Location and Environment (LE), Tilt and Orientation (TO), Weather Conditions (WC), Cleaning Frequency (CF), Cleaning Agents (CA), Safety and Accessibility (SA), Cost (C), Panel Efficiency (PE), Manufacturer Recommendations (MR), and Professional Services (PS). are addressed. MIC- MAC analysis identifies the most influential driving and de- pendent factors. Next, TOPSIS-MCDM was used.

6.4.1   MICMAC Analysis

Basically, the MICMAC technique consists of the following steps [128]:

Step 1: Identify the variables. Variables can be determined by a literature research, expert opinion, or brainstorming.

Step 2: Create a structural analysis matrix. The experts supply an integer matrix (M). Each cell a_{ij} in matrix M represents how variable i affects variable j.

• 0 if there is no interaction between i and j.

• 1 if there is little influence between i and j.

• 2 if there is a significant influence between i and j.

- 3 if there is a significant influence between i and j.
- P if there is a possible influence between i and j. All diagonal cells (a_{ij}) are equal to zero.

Step 3: Determine the direct influence. Direct analysis assesses a variable's total influence (DI_i) and dependence (DP_i) on the system using a direct matrix. The formula for calculating influence power (DI_i) and dependence power (DP_i) is in equation 1, 2 respectively. MICMAC classifies in 4 variables i.e. Autonomous variables have limited influence and dependency. Dependent variables, which have high dependency but little effect. linkage Variables with significant influence and high dependency, independent variable have High- influence, low-dependence variables that drive the system.

$$DI_i = \sum_{j=1}^{n} a_{ij} \ (i = 1,2,3, \dots \dots \dots \dots \dots \dots \dots n) \qquad\qquad 6.1$$

$$DP_i = \sum_{j=1}^{n} a_{ji} \ (i = 1,2,3, \dots \dots \dots \dots \dots \dots \dots n) \qquad\qquad 6.2$$

Step 4: Evaluate the indirect influence. Indirect analysis assesses the comprehensive impact and reliance of a variable by considering its relationship with other variables. Indirect classification is achieved by raising the matrix M to higher powers using matrix multiplication ($M^2 = M \times M$, $M^3 = M \times M \times M$, etc.). The algorithms employed in MICMAC examine the propagation of interactions within the system by analyzing the links and feedback loops that link individual components. This enables the prioritization of factors depending on the number of lap settings and the loop length, ranging from 1 to n, for each component. Consequently, the obscure impacts, which provide a challenge for professionals to explicitly ex- plain, become apparent. Typically, the categorization remains consistent after undergoing 3, 4, or 5 rounds of multiplication. Categories of variables in MICMAC include:

6.4.2 TOPSIS Method

TOPSIS evaluates multi-criteria choices. In 1981, Ching-Lai Hwang and Yoon developed it. Yoon improved it in 1987 and Hwang, Lai, and Liu in 1993. It helps rank and choose the best alternative by distance. This research compares TOPSIS MCDM cleaning methods. The main goals are to find the best SPV cleaning process and lessen its

environmental impact. TOPSIS helps decision-makers choose the optimal option. A comprehensive research study shows TOPSIS's advantages, including:

• Easy steps to follow.

• No matter what the options are, the number of steps stays the same.

• Other than when there aren't many factors, it works better than other MCDM methods.

• Able to handle more than one set of factors at the same time.

• It's easy to do calculations and they work well.

• A sensible and easy-to-understand idea to use.

The TOPSIS approach is ideal for dealing with group decision-making issues using precise numbers. The study aimed to include qualitative features into building project performance assessments and convert them into quantitative metrics.

6.4.3 Mathematical Formulation of TOPSIS Method

This section describes the TOPSIS approach and applies it to identify the best SPV panel cleaning procedure. Criterion weights and ratings are used in the traditional TOP- SIS MCDM method. Linguistic variables can indicate criteria and weights. Several academics have utilized grey system theory to broaden the MCDM technique to subjective criteria, interval data, and fuzzy environments. Designing a decision- making matrix is the initial step in solving any multi-criteria problem. The values of alternatives in such matrices can be real, intervals, fuzzy integers, or qualitative labels. Assign variables $C_1, C_2....C_m$ for various alternatives, and variables $V_1, V_2....V_m$ for criteria to judge alternative performance. $X_{ij}{}^{k}$ is the numerical value or interval data decision maker rating of alternative C_i for criterion V_j. Where options are C and V, Table 6.1 displays the multi-criteria problem in matrix form [129]. The proportional relevance of each criterion is defined by a set of weights that have been standardized to add up to 1. We may represent weights as $W^k =$ $[w_1{}^k, w_2{}^k, ..., w_n{}^k]$ where k refers to decision maker. The criterion weights adhere to the constraints $w_1{}^k + w_2{}^k + ... + w_n{}^k = 1$

Table 6. 1 MCDM Criteria and Alternatives in Matrix Form

	V_1	V_2	...	V_n
C_1	x_{11}	x_{12}	...	x_{1n}
C_2	x_{21}	x_{22}	...	x_{2n}
⋮	⋮	⋮	⋱	⋮
C_m	x_{m1}	x_{m2}	...	x_{mn}

Step 1: Create decision matrix for key decision-makers and establish the weights of the criteria. The notation $X^k = (x^k{}_{ij})$ represents a decision matrix for a decision maker or expert.

Step 2: Normalize the decision matrix for each decision maker.

This stage is essential for obtaining numerical and comparable input data, while applying a similar scale and providing a norm or a standard to the input data. In the decision matrix, each criterion has either a monotonically increasing or monotonically decreasing value. Any consequence that is stated in a non-numerical form should be quantified using the appropriate scaling approach. Normalized values are calculated by equation (6.3).

$$r^k{}_{ij} = \frac{r^k{}_{ij}}{\sqrt{\sum_{i=1}^{m} r^k{}_{ij}{}^2}}$$ 6.3

In the subsequent stage, the weights are changed during these computations with the help of equation (6.4) and (6.5).

$$\sigma_j = \sqrt{\frac{1}{m-1}\sum_{i=1}^{m}(x_{ij} - \overline{x_j})^2}$$ 6.4

$$w_j = \frac{\sigma_j}{\sum_{k=1}^{n} \sigma_k}$$ 6.5

Step 3: Determine the positive and negative ideal solutions for each decision maker.

The positive ideal solution C^{+k} for k-decision maker has the following form. C^{+k} is a set that consists of elements $r_1{}^{+k}$, $r_2{}^{+k}$, ..., $r_n{}^{+k}$. These elements are defined as the maximum value of $r_{ij}{}^k$ for all j in set I, and the minimum value of $r_{ij}{}^k$ for all j in set J. The negative ideal solution C^{-k} for a decision maker has the following form: C^{-k} is a set that consists of elements $r_1{}^{-k}$, $r_2{}^{-k}$, ..., $r_n{}^{-k}$. Each element in C^{-k} is determined by taking the minimum value of $r_{ij}{}^k$ for all j in set I, and the maximum value of $r_{ij}{}^k$ for all j in set J.

$$C^{+k} = \{r^{1+k}, r^{2+k}, ..., r_n{}^{+k}\} == \{(\max{(r_{ij}{}^k)} \,|\, j \in I), (\min{(r_{ij}{}^k)} \,|\, j \in J)\}$$ 6.6

$$C^{+k} = \{r^{1+k}, r^{2+k}, ..., r_n{}^{+k}\} == \{(max(r_{ij}{}^k) \,|\, j \in I), (min(r_{ij}{}^k) \,|\, j \in J)\}$$ 6.7

Where I is related with the benefit criterion and J is associated with cost criteria, where cost criteria should be minimized and benefit criteria should be maximized.

Step 4: Calculate the separation measures between the positive ideal solution and the negative ideal solution.

Step 5 involves calculating the separation measures for each individual decision maker. The positive ideal answer $d^+{}_i{}^k$ for each k decision maker is provided as:

$$d^+{}_i{}^k = \sum_{j=1}^{m} w_j{}^k \left((r_{ij}{}^k - r_j{}^{+k})^p \right)^{\frac{1}{p}}, \quad i = 1,2, \dots \dots \dots \dots m \qquad 6.8$$

The negative ideal solution, $d^-{}_i{}^k$ for each decision maker, is provided as follows:

$$d^-{}_i{}^k = \sum_{j=1}^{m} w_j{}^k \left((r_{ij}{}^k - r_j{}^{-k})^p \right)^{\frac{1}{p}}, \quad i = 1,2, \dots \dots \dots \dots m \qquad 6.9$$

Here $p \geq 1$. We use the Euclidean metric for $p = 2$.

Compute the distance metric for the group. The group measure of the positive ideal solution is written as $d^+{}_i$:

$$d^*{}_i{}^+ = \frac{1}{k} \sum_{k=1}^{k} d^+{}_i{}^k \qquad 6.10$$

$$d^*{}_i{}^- = \frac{1}{k} \sum_{k=1}^{k} d^-{}_i{}^k \qquad 6.11$$

Step 6: Calculate the relative proximity to the ideal solution.

The proximity of the alternative C_i to the positive ideal solution is expressed by equation (6.11):

$$R^*{}_i = \frac{d^*{}_i{}^-}{d^*{}_i{}^+ + d^*{}_i{}^-} \qquad 6.12$$

for i=1,2,3,.....m, the assessment of the alternative improves as the index value increases,where,$0 \leq R^*{}_i \leq 1$.

The distances between the positive ideal solution and the negative ideal solution represent the distances of alternatives in matrix form. A ranking of options is created and the most favorable option is offered using the coefficient of relative closeness of each option to the positive ideal solution.

Step7: Prioritize the options or choose the alternative that is most similartothenumber1.

The collection of options may now be ranked using the descending order of the value of R^*_i By following these steps, we can successfully implement the TOPSIS method. The alternatives are rated based on their proximity to the ideal solution R^*_i (the greater the value, the better the option). The option with the greatest value is the optimal choice

6.5   RESULT AND DISCUSSION

This section covers several cleaning methods for SPV modules, including robot water-based, pressure-based, and manual approaches. Cleaning techniques, including nano-coating, are taken into consideration. There are various aspects to consider while choosing the finest cleaning techniques. Factors to consider include panel surface material, location and environment, tilt and orientation, weather conditions, cleaning frequency, cleaning agents, safety and accessibility, cost, panel efficiency, manufacturer recommendations, and professional services. To determine the proper criteria, consider MICMAC analysis is conducted by field specialists based on a survey.

A matrix of direct impact (MDI) and indirect influence (MII) is created, as well as a matrix of possible direct and indirect influence depending on map parameters, for SPV panel cleaning procedures. Fig. 6.2 and 6.3 illustrate direct influence maps and graphs, respectively. The direct influence map displays the direct relationship between components and other variables. Autonomous variables: MR, SA, TO, WC, and PSM.

Dependent Variables: CA Linkage variables: LE, CF, PS, and PE. Independent Variables: C is shown in Fig.6.3a. Fig. 6. 2 and 6. 3b show the matrix of the In-Direct impact map and graph, respectively. The indirect impact map depicts the relationship between the autonomous variables (MR, SA, TO, WC, and PSM) and other variables.

The dependent variables are None, whereas the linkage variables are CA, LE, CF, PS, and PE. The independent variables are displayed in Fig. 6.3b. Fig. 6.2c and 6.3c show the MDPI matrix map and graph, respectively. This extends the Direct Influence Matrix to include both current and projected influences between variables. This improves the understanding of variable interactions. The Potential Direct Influence Map displays the direct relationship between components and other variables. Autonomous Variables: MR, SA, TO, WC and PSM

Table 6. 2 Decision Matrix Considering Major Factors to Build Different SPV Panel Cleaning Methods

Alternatives \ Criteria	Location and Environment	Cleaning Frequency	Cleaning Agent	Cost	Panel Efficiency	Professional services
Robot water-based cleaning technique	3	3	4	2	2	2
Robot pressure-based cleaning technique	3	3	2	3	3	2
Manual cleaning technique	2	2	3	1	2	3
Nano-coating cleaning technique	4	4	2	3	4	1

Fig. 6.2c displays the dependent variables (CA), linkage variables (LE, CF, PS, and PE), and independent variables: C shown in Fig. 6.3b. Matrix of Potential Direct influence (MDPI) map and graph is shown in Fig.6.2c and Fig.6.3c respectively.

Table 6. 3 Normalized Decision Matrix

Alternatives \ Criteria	Location and Environment	Cleaning Frequency	Cleaning Agent	Cost	Panel Efficiency	Professional services
Robot water-based cleaning technique	0.487	0.487	0.645	0.408	0.487	0.408
Robot pressure-based cleaning technique	0.487	0.487	0.484	0.408	0.487	0.612
Manual cleaning technique	0.325	0.325	0.484	0.204	0.325	0.612
Nano-coating cleaning technique	0.649	0.649	0.322	0.612	0.649	0.408

It expands the Direct Influence Matrix (DIM) by including both present and potential impacts between variables. This enhances the under- standing of variable interactions. Potential direct influence map shows the direct relation of the factors with other variables in this Autonomous Variables: MR, SA, TO, WC and PSM. Dependent Variables: CA,

Linkage Variables: LE, CF, PS and PE and Independent Variables: C is shown in Fig. 6.2c. From the MICMAC analysis considerations include location and environment, cleaning frequency, panel efficiency, cost, and cleaning methods.

Table 6. 4 Weighted Normalized Decision Matrix

Alternatives \ Criteria	Location and Environment	Cleaning Frequency	Cleaning Agent	Cost	Panel Efficiency	Professional services
Robot water-based cleaning technique	0.065	0.065	0.091	0.124	0.065	0.041
Robot pressure-based cleaning technique	0.065	0.065	0.068	0.124	0.065	0.061
Manual cleaning technique	0.043	0.043	0.068	0.248	0.043	0.061
Nano-coating cleaning technique	0.086	0.086	0.046	0.083	0.086	0.041

Agents are the most important elements in SPV modules cleaning, according to MICMAC. These elements are strong drivers and moderate to strong dependents. Next, we will rank cleaning techniques by these critical aspects using TOPSIS. Table 6.2 is the decision matrix which is filled by survey and further Table 6.3 is the normalization decision matrix done by TOPSIS using step 2 discussed in section 6.5.3. Weights are calculated by critic method by equation 6.4 and 6.5 as shown in Table 6.5.
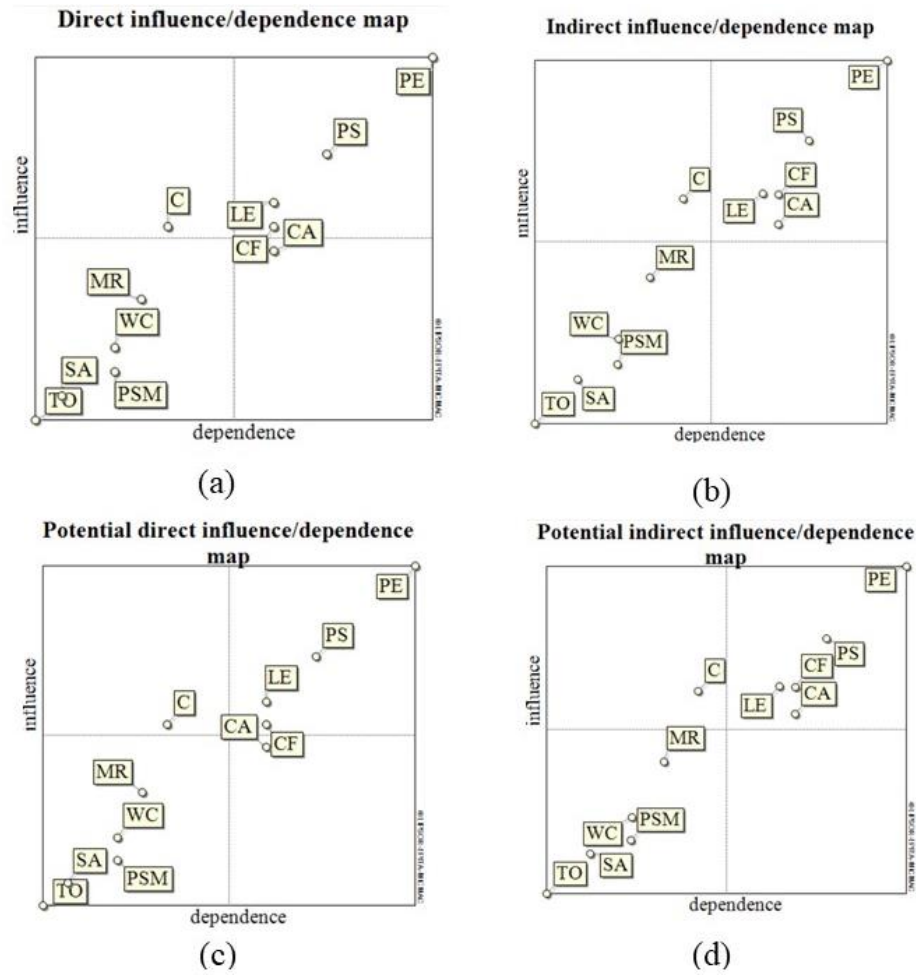
Fig. 6. 2 (a) MDI Direct Map. (b) MII Indirect Map (c) MDPI Potential Direct Map (d) MPII Potential Direct Map

Table 6. 5 Weights for Different Criteria

Criteria	Weight
Location and Environment	0.133
Cleaning Frequency	0.133
Cleaning Agents	0.140
Cost	0.248
Panel Efficiency	0.133
Professional Services	0.104
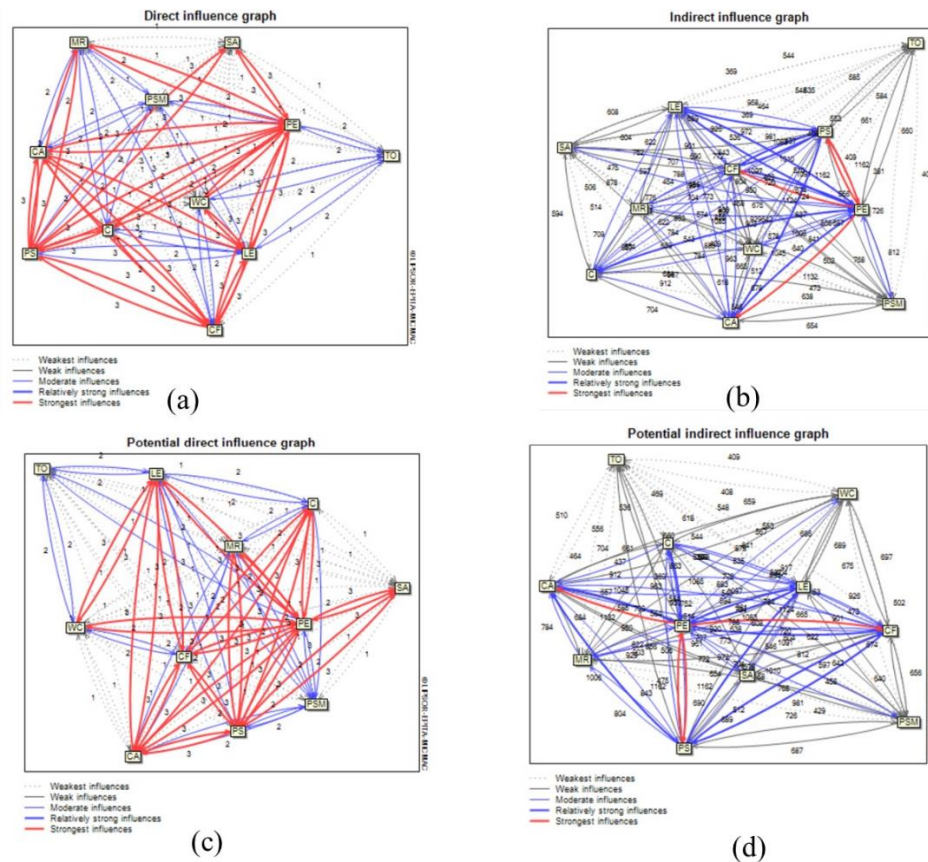
Fig. 6. 3 (a) MDI Direct Graph (b) MII Indirect Graph (c) MDPI Potential Direct Graph (d) MPII Potential Direct Graph

Table 6. 6 Ideal Best and Anti Ideal Solution

Criteria	Ideal Solution	Anti-Ideal Solution
Location and Environment	0.086	0.043
Cleaning Frequency	0.086	0.043
Cleaning Agents	0.091	0.046
Cost	0.083	0.248
Module Efficiency	0.086	0.043
Professional Services	0.061	0.041

Table 6. 7 Relative Closeness to Ideal Solution

Alternative	Relative Closeness
Robot Water-based Cleaning	0.703
Robot Pressure-based Cleaning	0.693
Manual Cleaning	0.142
Nano-Coating Cleaning	0.787

6.6 CONCLUSION

This study presents a systematic and data-driven approach that combines MICMAC with the TOPSIS multi-criteria decision-making method to identify the best SPV module cleaning techniques. The hybrid framework tackles the crucial requirement for proper cleaning in PV systems to improve operating efficiency, durability, and sustainability.

The MICMAC study effectively identified the primary driving and dependant factors that influence SPV module repair choices. The most significant elements were identified as location and environment, cleaning frequency, cleaning agents, safety and accessibility, cost, module efficiency, manufacturer recommendations, and professional services. These elements reflect a complete collection of technical, economic, and operational concerns necessary for long-term SPV module maintenance.

Following that, the TOPSIS approach was used to rank several cleaning options based on their relative proximity to the optimum solution. The investigation found that nano-coating cleaning approaches performed the best overall, followed by robot-based solutions like mechanical and sprinkler systems. Manual cleaning, albeit ubiquitous, was placed last owing to its labour-intensive nature and poor long-term efficiency.

This combined MICMAC-TOPSIS technique not only improves decision-making by providing clarity and impartiality, but it also establishes a solid platform for strategic maintenance planning in solar energy systems. The framework helps to optimize resource use, reduce operational inefficiencies, and promote environmentally friendly energy practices.

In future study, the framework might be expanded to include hybrid MCDM models, real-time sensor data, and environmental simulations. Such developments would allow for more dynamic and context-sensitive decision-making, increasing the feasibility of SPV systems in a variety of geographical and climatic contexts and further the MCDM decision making will help us survey and develop a more novel SPV module cleaning methods which are cheaper and more efficient.

CHAPTER 7

CONCLUSIONS AND FUTURE SCOPE OF WORK

7.1   CONCLUSIONS

Hybrid model significantly improves the precision of short-term photovoltaic power forecasts by effectively collecting both spatial and temporal trends from meteorological data. The model surpassed traditional CNN, LSTM, and MLP models under various weather situations, demonstrating especially excellent accuracy in sunny and cold circumstances. Its robust predictive capabilities enhance the reliability of energy planning and grid integration in SPV power systems.

The effects of dust deposition on photovoltaic performance were comprehensively analysed alongside forecasts. Real-time soiling ratio data enabled precise modeling of dust-induced power loss, with a maximum recorded loss of 285.35 W. A stacked LSTM model had a predictive accuracy of 99.13% for dirty output, exceeding that of the Bi-LSTM. These results underscore the need of astute forecasting amid soiling and advocate for the establishment of automated maintenance processes to guarantee consistent energy output. Thermal imaging integrated with deep learning methodologies shown efficacy in real-time hotspot identification and fault categorization in photovoltaic modules. Models like AlexNet and Inception-ResNet-v2 effectively identified flaws attributed to dust and shading, achieving classification accuracies of up to 99.3%. These methodologies facilitate predictive diagnostics and mitigate the danger of prolonged module deterioration, hence fostering AI-driven, low-maintenance SPV power systems suited for operational stability.

A multi-criteria decision-making framework using MICMAC and TOPSIS was used to assess SPV module cleaning techniques in conjunction with performance optimization. Critical elements like cleaning frequency, safety, environmental conditions, and cost were examined. Nano-coating and robotic methods had the maximum efficacy; however, hand cleaning was the least advantageous owing to its ineffectiveness. The model provides a strategic basis for sustainable cleaning procedures and may be enhanced with real-time sensor data for adaptive maintenance planning.

7.2   FUTURE SCOPE

➤ A potential approach is the merging of hybrid deep learning architectures with real-time environmental data inputs for on-site, edge-based SPV forecasts. Lightweight, adaptable models that function well with constrained computing resources would enhance the scalability and practicality of forecasting tools for distant and decentralized SPV systems.

➤ Future research may investigate the integration of sophisticated atmospheric characteristics, including aerosol optical depth (AOD), air quality indices, and particle composition, especially pertinent in areas with high pollution levels. Incorporating these factors into forecasting and soil models may enhance predictive accuracy and system resilience under swiftly changing environmental circumstances.

➤ In hotspot detection, the integration of drone-assisted thermal imaging with real-time AI-driven fault categorization may be enhanced to provide autonomous problem localization and diagnosis over extensive solar farms. Furthermore, creating small and energy-efficient CNN models for implementation on embedded monitoring devices might provide continuous surveillance with little energy expenditure.

➤ Estimation of soiling loss may be enhanced using physics-informed AI models that account for electrostatic adhesion, dust granulometry, surface energy, and humidity interactions. Such models would more accurately forecast deterioration rates across diverse seasons and regions, facilitating informed cleaning regimens.

➤ There is considerable potential for creating an innovative, AI-enhanced SPV module cleaning method that adapts in real-time according to soiling intensity, environmental factors, and performance criteria. Integrating this with MCDM frameworks such as MICMAC-TOPSIS may improve future cleaning systems for energy recovery, cost-efficiency, resource conservation, and operational practicality in various deployment situations.

7.3   SOCIETAL IMPACT

➢ Enhancing Grid Stability and Energy Security: Grid management is considerably enhanced by precise short-term SPV power forecasts that are generated using hybrid AI models, particularly as solar penetration in global energy mixtures increases.   Reliable forecasts mitigate the risk of power imbalances, reduce dependence on fossil fuel-based reserves, and facilitate the development of smart, resilient energy infrastructures. This is especially important as countries transition to net-zero emission goals.

➢ Improving Operational Efficiency and Sustainability: The deployment of automated, optimized cleaning processes is facilitated by real-time modeling of dust deposition effects and predictive soiling analysis.   This minimizes water wastage, a critical issue in arid and semi-arid regions where solar farms are frequently situated, and diminishes the ecological impact of conventional manual cleansing methods. It promotes the sustainable operation of SPV facilities with minimal environmental impact.

➢ Increasing the Lifespan of Systems and Minimizing E-Waste: AI-powered thermal imaging for early hotspot and defect detection prevents irreversible module degradation, thereby reducing module failure rates and extending the lifecycle of solar assets

➢ Reducing the Cost of Solar Energy for End-Users: The operational and maintenance costs of solar installations are reduced by implementing more accurate forecasting, predictive maintenance, and optimized cleansing strategies.   This promotes equitable energy access by making solar electricity more affordable and accessible to households, industries, and rural communities, as a result of the savings that can be transmitted down the value chain.

➢ Fostering High-Tech Employment and Innovation: The implementation of DL and ML models in solar energy systems fosters innovation in the energy, AI, and smart infrastructure sectors. This promotes the expansion of specialized employment opportunities in the field of AI-based energy analytics, predictive maintenance, and automation, thereby promoting technological leadership and economic development.

- Promoting the Objectives of Climate Change Mitigation: These technologies directly contribute to the reduction of carbon emissions by optimizing solar energy harvest and reducing inefficiencies caused by environmental factors such as thermal defects and pollution. The displacement of fossil fuel generation is expedited by improved solar system reliability, which is consistent with the Paris Agreement and the global Sustainable Development Goals (SDGs).
- Enabling Energy-Aware Societies and Smart Cities: Decentralized energy generation, AI-driven maintenance, and real-time data-driven decision-making will define future urban landscapes, and advanced SPV monitoring and predictive systems are critical enablers for smart city ecosystems. Citizen awareness of energy sustainability is also enhanced by the availability of precise solar generation data to the public.

7.3.1 Linking Research Objectives with SDGs for Societal Impact
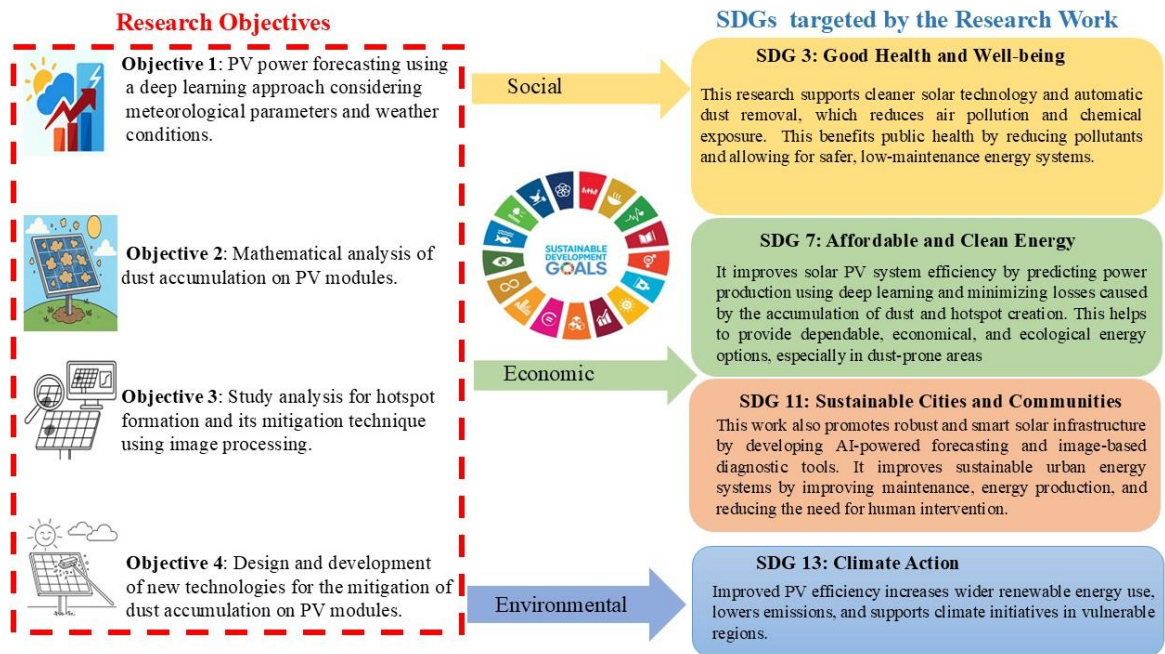
Fig. 7. 1 Integration of Sustainable Development Goals with the thesis objectives

The Fig. 7.1 demonstrates four important research targets in solar PV system development are aligned with three UN Sustainable Development Goals (SDGs). Objective I (PV power forecasting) and Objective II (dust analysis) immediately contribute to SDG 7: Affordable and Clean Energy by increasing efficiency and dependability. Objective III (hotspot identification via image processing) and Objective IV (dust mitigation technology) help to achieve SDGs 7 and 11: Sustainable Cities and Communities by encouraging smarter, cleaner energy infrastructure. Collectively, these aims indirectly improve SDG 3: Good Health and Well-being by promoting cleaner environments and lowering health risks, underlining PV research's larger sustainability advantages.

REFERENCES

[1] IEA, "Total renewable capacity additions by technology, 2019–2024," International Energy Agency, 2025. [Online]. Available: https://www.iea.org/data-and-statistics/charts/total-renewable-capacity-additions-by-technology-2019-2024

[2] Ministry of New and Renewable Energy, "Programme/Scheme wise Cumulative Physical Progress as on March, 2025," Government of India, 2025. [Online]. Available: https://mnre.gov.in/en/physical-progress/. [Accessed: Apr. 24, 2025].

[3] S. Vyas, Y. Goyal, N. Bhatt, S. Bhuwania, H. Patel, S. Mishra, and B. Tripathi, "Forecasting Solar Power Generation on the basis of Predictive and Corrective Maintenance Activities," May 2022, doi: 10.48550/arxiv.2205.08109.

[4] F. Wang, Z. Xuan, Z. Zhen, Y. Li, K. Li, L. Zhao, and M. Shafie-khah., "A minutely solar irradiance forecasting method based on real-time sky image-irradiance mapping model," Elsevier, Accessed: Feb. 24, 2023. [Online].

[5] T. Hussain, F. U. M. Ullah, K. Muhammad, S. Rho, A. Ullah, E. Hwang, J. Moon, and S. W. Baik., "Smart and intelligent energy monitoring systems: A comprehensive literature survey and future research guidelines," Wiley Online Libr., vol. 45, no. 3, pp. 3590–3614, Mar. 2021, doi: 10.1002/er.6093.

[6] M. G. De Giorgi, P. M. Congedo, and M. Malvoni, "Photovoltaic power forecasting using statistical methods: impact of weather data," *IET Sci. Meas. Technol.*, vol. 8, no. 3, pp. 90–97, May 2014, doi: 10.1049/IET-SMT.2013.0135.

[7] Y. K. Wu, C. L. Huang, Q. T. Phan, and Y. Y. Li, "Completed Review of Various Solar Power Forecasting Techniques Considering Different Viewpoints," *Energies 2022, Vol. 15, Page 3320*, vol. 15, no. 9, p. 3320, May 2022, doi: 10.3390/EN15093320.

[8] O. Ait Maatallah, A. Achuthan, K. Janoyan, and P. Marzocca, "Recursive wind speed forecasting based on Hammerstein Auto-Regressive model," *Appl. Energy*, vol. 145, pp. 191–197, May 2015, doi: 10.1016/J.APENERGY.2015.02.032.

[9] K. Khan, R. U. Khan, W. Albattah, D. Nayab, A. M. Qamar, S. Habib, and M. Islam., "Crowd Counting Using End-to-End Semantic Image Segmentation," Electron. 2021, Vol. 10, Page 1293, vol. 10, no. 11, p. 1293, May 2021, doi: 10.3390/ELECTRONICS10111293.

[10] R. C. Deo, X. Wen, and F. Qi, "A wavelet-coupled support vector machine model for forecasting global incident solar radiation using limited meteorological dataset," *Appl. Energy*, vol. 168, pp. 568–593, Apr. 2016, doi: 10.1016/J.APENERGY.2016.01.130.

[11] P. Mandal, S. T. S. Madhira, A. Ul haque, J. Meng, and R. L. Pineda, "Forecasting Power Output of Solar Photovoltaic System Using Wavelet Transform and Artificial Intelligence Techniques," *Procedia Comput. Sci.*, vol. 12, pp. 332–337, Jan. 2012, doi: 10.1016/J.PROCS.2012.09.080.

[12] C. N. Obiora, A. N. Hasan, A. Ali, and N. Alajarmeh, "Forecasting Hourly Solar Radiation Using Artificial Intelligence Techniques," *IEEE Can. J. Electr. Comput. Eng.*, vol. 44, no. 4, pp. 497–508, Sep. 2021, doi: 10.1109/ICJECE.2021.3093369.

[13] M. Abuella and B. Chowdhury, "Random forest ensemble of support vector regression models for solar power forecasting," *2017 IEEE Power Energy Soc. Innov. Smart Grid Technol. Conf. ISGT 2017*, Oct. 2017, doi: 10.1109/ISGT.2017.8086027.

[14] L. Benali, G. Notton, A. Fouilloy, C. Voyant, and R. Dizene, "Solar radiation forecasting using artificial neural network and random forest methods: Application to normal beam, horizontal diffuse and global components," *Renew. Energy*, vol. 132, pp. 871–884, Mar. 2019, doi: 10.1016/J.RENENE.2018.08.044.

[15] S. C. Lim, J. H. Huh, S. H. Hong, C. Y. Park, and J. C. Kim, "Solar Power Forecasting Using CNN-LSTM Hybrid Model," *Energies 2022, Vol. 15, Page 8233*, vol. 15, no. 21, p. 8233, Nov. 2022, doi: 10.3390/EN15218233.

[16] M. Tovar, M. Robles, and F. Rashid, "PV Power Prediction, Using CNN-LSTM Hybrid Neural Network Model. Case of Study: Temixco-Morelos, México,"

Energies, vol. 13, no. 24, p. 6512, Dec. 2020, doi: 10.3390/en13246512.

[17]   C. Chen, S. Duan, T. Cai, and B. Liu, "Online 24-h solar power forecasting based on weather type classification using artificial neural network," *Sol. Energy*, vol. 85, no. 11, pp. 2856–2870, Nov. 2011, doi: 10.1016/j.solener.2011.08.027.

[18]   N. Azizi, M. Yaghoubirad, M. Farajollahi, and A. Ahmadi, "Deep learning based long-term global solar irradiance and temperature forecasting using time series with multi-step multivariate output," *Renew. Energy*, vol. 206, pp. 135–147, Apr. 2023, doi: 10.1016/j.renene.2023.01.102.

[19]   C. Zhu, M. Wang, M. Guo, J. Deng, Q. Du, W. Wei, and Y. Zhang., "Innovative approaches to solar energy forecasting: unveiling the power of hybrid models and machine learning algorithms for photovoltaic power optimization," J. Supercomput., vol. 81, no. 1, p. 20, Jan. 2025, doi: 10.1007/s11227-024-06504-z.

[20]   M. Rizwan, M. Jamil, and D. P. Kothari, "Generalized neural network approach for global solar energy estimation in India," *IEEE Trans. Sustain. Energy*, vol. 3, no. 3, pp. 576–584, 2012, doi: 10.1109/TSTE.2012.2193907.

[21]   M. Rizwan, M. Jamil, S. Kirmani, and D. P. Kothari, "Fuzzy logic based modeling and estimation of global solar energy using meteorological parameters," *Energy*, vol. 70, pp. 685–691, Jun. 2014, doi: 10.1016/J.ENERGY.2014.04.057.

[22]   Y. Gala, Á. Fernández, J. Díaz, and J. R. Dorronsoro, "Hybrid machine learning forecasting of solar radiation values," *Neurocomputing*, vol. 176, pp. 48–59, Feb. 2016, doi: 10.1016/J.NEUCOM.2015.02.078.

[23]   P. Jia, H. Zhang, X. Liu, and X. Gong, "Short-Term Photovoltaic Power Forecasting Based on VMD and ISSA-GRU," *IEEE Access*, vol. 9, pp. 105939–105950, 2021, doi: 10.1109/ACCESS.2021.3099169.

[24]   P. Kumari and D. Toshniwal, "Long short term memory–convolutional neural network based deep hybrid approach for solar irradiance forecasting," *Appl. Energy*, vol. 295, p. 117061, Aug. 2021, doi: 10.1016/J.APENERGY.2021.117061.

[25] D. Lee and K. Kim, "Recurrent Neural Network-Based Hourly Prediction of Photovoltaic Power Output Using Meteorologiac Information," *Energies 2019, Vol. 12, Page 215*, vol. 12, no. 2, p. 215, Jan. 2019, doi: 10.3390/EN12020215.

[26] P. Li, K. Zhou, X. Lu, and S. Yang, "A hybrid deep learning model for short-term PV power forecasting," *Appl. Energy*, vol. 259, p. 114216, Feb. 2020, doi: 10.1016/J.APENERGY.2019.114216.

[27] S. Ghimire, R. C. Deo, N. Raj, and J. Mi, "Deep solar radiation forecasting with convolutional neural network and long short-term memory network algorithms," *Appl. Energy*, vol. 253, p. 113541, Nov. 2019, doi: 10.1016/J.APENERGY.2019.113541.

[28] A. Kumar, M. Alaraj, M. Rizwan, I. Alsaidan, and M. Jamil, "Development of Novel Model for the Assessment of Dust Accumulation on Solar PV Modules," *IEEE J. Photovoltaics*, vol. 13, no. 1, pp. 150–157, Jan. 2023, doi: 10.1109/JPHOTOV.2022.3220923.

[29] H. K. Elminir, A. E. Ghitas, R. H. Hamid, F. El-Hussainy, M. M. Beheary, and K. M. Abdel-Moneim, "Effect of dust on the transparent cover of solar collectors," *Energy Convers. Manag.*, vol. 47, no. 18–19, pp. 3192–3203, Nov. 2006, doi: 10.1016/j.enconman.2006.02.014.

[30] I. Niknia, M. Yaghoubi, and R. Hessami, "A novel experimental method to find dust deposition effect on the performance of parabolic trough solar collectors," *Int. J. Environ. Stud.*, vol. 69, no. 2, pp. 233–252, Apr. 2012, doi: 10.1080/00207233.2012.664810.

[31] S. Biryukov, "An experimental study of the dry deposition mechanism for airborne dust," *J. Aerosol Sci.*, vol. 29, no. 1–2, pp. 129–139, Jan. 1998, doi: 10.1016/S0021-8502(97)00037-2.

[32] J. K. Kaldellis and A. Kokala, "Quantifying the decrease of the photovoltaic panels' energy yield due to phenomena of natural air pollution disposal," *Energy*, vol. 35, no. 12, pp. 4862–4869, Dec. 2010, doi: 10.1016/j.energy.2010.09.002.

[33] L. Micheli and M. Muller, "An investigation of the key parameters for predicting PV soiling losses," *Prog. Photovoltaics Res. Appl.*, vol. 25, no. 4, pp. 291–307, Apr. 2017, doi: 10.1002/pip.2860.

[34] S. Pulipaka and R. Kumar, "Power prediction of soiled PV module with neural networks using hybrid data clustering and division techniques," *Sol. Energy*, vol. 133, pp. 485–500, Aug. 2016, doi: 10.1016/j.solener.2016.04.004.

[35] S. Pulipaka, F. Mani, and R. Kumar, "Modeling of soiled PV module with neural networks and regression using particle size composition," *Sol. Energy*, vol. 123, pp. 116–126, Jan. 2016, doi: 10.1016/j.solener.2015.11.012.

[36] A. Massi Pavan, A. Mellit, D. De Pieri, and S. A. Kalogirou, "A comparison between BNN and regression polynomial methods for the evaluation of the effect of soiling in large scale photovoltaic plants," *Appl. Energy*, vol. 108, pp. 392–401, Aug. 2013, doi: 10.1016/j.apenergy.2013.03.023.

[37] H. A. Kazem, A. H. A. Al-Waeli, M. T. Chaichan, and K. Sopian, "Modeling and experimental validation of dust impact on solar cell performance," *https://doi.org/10.1080/15567036.2021.2024922*, 2022, doi: 10.1080/15567036.2021.2024922.

[38] J. Alonso-Montesinos, J. Barbero, F. J. Batlles, F. Rodríguez-Martínez, G. López, J. Polo, N. Martín-Chivelet, M. Alonso, N. Vela, A. Marzo, and P. Ferrada., "Relevance Analysis of Atmospheric Variables In The Production Of An Experimental Pv Power Plant Considering Dust Deposition In The Mediterranean Coast," 2019, doi: 10.18086/swc.2019.43.01.

[39] U. Pal and S. Chandra, "ANN based performance forecasting for dusty solar panel," *Mater. Today Proc.*, Jun. 2023, doi: 10.1016/j.matpr.2023.05.558.

[40] R. Muhammad Ehsan, S. P. Simon, and P. R. Venkateswaran, "Day-ahead forecasting of solar photovoltaic output power using multilayer perceptron," *Neural Comput. Appl.*, vol. 28, no. 12, pp. 3981–3992, Dec. 2017, doi: 10.1007/s00521-016-2310-z.

[41]   P. Nepal, "Effect of Soiling on the PV Panel kWh Output." 2018. Accessed: May 04, 2023. [Online]. Available: https://repository.tudelft.nl/islandora/object/uuid%3A59b6a100-4db9-4262-bc5e-d0f2e5c6f57a

[42]   S. C. S. Costa, L. L. Kazmerski, and A. S. A. C. Diniz, "Impact of soiling on Si and CdTe PV modules: Case study in different Brazil climate zones," *Energy Convers. Manag. X*, vol. 10, p. 100084, Jun. 2021, doi: 10.1016/j.ecmx.2021.100084.

[43]   A. Sayyah, M. N. Horenstein, and M. K. Mazumder, "Energy yield loss caused by dust deposition on photovoltaic panels," *Sol. Energy*, vol. 107, pp. 576–604, Sep. 2014, doi: 10.1016/J.SOLENER.2014.05.030.

[44]   S. R. Madeti and S. N. Singh, "Monitoring system for photovoltaic plants: A review," *Renew. Sustain. Energy Rev.*, vol. 67, pp. 1180–1207, Jan. 2017, doi: 10.1016/j.rser.2016.09.088.

[45]   A. Kodakkal, R. Veramalla, N. R. Kuthuri, and S. R. Salkuti, "An ALO Optimized Adaline Based Controller for an Isolated Wind Power Harnessing Unit," *Des. 2021, Vol. 5, Page 65*, vol. 5, no. 4, p. 65, Oct. 2021, doi: 10.3390/DESIGNS5040065.

[46]   S. R. Salkuti, "Emerging and Advanced Green Energy Technologies for Sustainable and Resilient Future Grid," *Energies 2022, Vol. 15, Page 6667*, vol. 15, no. 18, p. 6667, Sep. 2022, doi: 10.3390/EN15186667.

[47]   M. Jaszczur, A. Koshti, W. Nawrot, and P. Sędor, "An investigation of the dust accumulation on photovoltaic panels," *Environ. Sci. Pollut. Res.*, vol. 27, no. 2, pp. 2001–2014, Jan. 2020, doi: 10.1007/s11356-019-06742-2.

[48]   J. K. Kaldellis and M. Kapsali, "Simulating the dust effect on the energy performance of photovoltaic generators based on experimental measurements," *Energy*, vol. 36, no. 8, pp. 5154–5161, Aug. 2011, doi: 10.1016/j.energy.2011.06.018.

[49]   S. Mekhilef, R. Saidur, and M. Kamalisarvestani, "Effect of dust, humidity and air velocity on efficiency of photovoltaic cells," *Renew. Sustain. Energy Rev.*, vol. 16, no. 5, pp. 2920–2925, Jun. 2012, doi: 10.1016/j.rser.2012.02.012.

[50] B. R. Paudyal and S. R. Shakya, "Dust accumulation effects on efficiency of solar PV modules for off grid purpose: A case study of Kathmandu," *Sol. Energy*, vol. 135, pp. 103–110, Oct. 2016, doi: 10.1016/j.solener.2016.05.046.

[51] S. A. M. Said, G. Hassan, H. M. Walwil, and N. Al-Aqeeli, "The effect of environmental factors and dust accumulation on photovoltaic modules and dust-accumulation mitigation strategies," *Renew. Sustain. Energy Rev.*, vol. 82, pp. 743–760, Feb. 2018, doi: 10.1016/j.rser.2017.09.042.

[52] S. Fan, Y. Wang, S. Cao, T. Sun, and P. Liu, "A novel method for analyzing the effect of dust accumulation on energy efficiency loss in photovoltaic (PV) system," *Energy*, vol. 234, p. 121112, Nov. 2021, doi: 10.1016/j.energy.2021.121112.

[53] M. J. Adinoyi and S. A. M. Said, "Effect of dust accumulation on the power outputs of solar photovoltaic modules," *Renew. Energy*, vol. 60, pp. 633–636, Dec. 2013, doi: 10.1016/j.renene.2013.06.014.

[54] P. Ray and S. R. Salkuti, "Hybrid Artificial Intelligence Technique Based Fault Location in a Long Transmission Line," *Lect. Notes Electr. Eng.*, vol. 812, pp. 487–505, 2022, doi: 10.1007/978-981-16-6970-5_36.

[55] T. Sinha, P. Ray, and S. R. Salkuti, "Protection Coordination in Microgrid UsingFault Current Limiters," *J. Green Eng.*, vol. 8, no. 2, pp. 125–150, Apr. 2018, doi: 10.13052/JGE1904-4720.822.

[56] Y. HIGUCHI and T. BABASAKI, "Failure detection of solar panels using thermographic images captured by drone," in *2018 7th International Conference on Renewable Energy Research and Applications (ICRERA)*, Oct. 2018, pp. 391–396. doi: 10.1109/ICRERA.2018.8566833.

[57] I. Bodnar and G. Kozsely, "Development of Solar Panel Diagnostic System," in *2022 23rd International Carpathian Control Conference (ICCC)*, May 2022, pp. 221–226. doi: 10.1109/ICCC54292.2022.9805859.

[58] Z. A. Jaffery, A. K. Dubey, Irshad, and A. Haque, "Scheme for predictive fault diagnosis in photo-voltaic modules using thermal imaging," *Infrared Phys. Technol.*, vol. 83, pp. 182–187, Jun. 2017, doi: 10.1016/j.infrared.2017.04.015.

[59] P. Haidari, A. Hajiahmad, A. Jafari, and A. Nasiri, "Deep learning-based model for fault classification in solar modules using infrared images," *Sustain. Energy Technol. Assessments*, vol. 52, p. 102110, Aug. 2022, doi: 10.1016/j.seta.2022.102110.

[60] S. Fan, Y. Wang, S. Cao, B. Zhao, T. Sun, and P. Liu, "A deep residual neural network identification method for uneven dust accumulation on photovoltaic (PV) panels," *Energy*, vol. 239, p. 122302, Jan. 2022, doi: 10.1016/j.energy.2021.122302.

[61] D. Korkmaz and H. Acikgoz, "An efficient fault classification method in solar photovoltaic modules using transfer learning and multi-scale convolutional neural network," *Eng. Appl. Artif. Intell.*, vol. 113, p. 104959, Aug. 2022, doi: 10.1016/j.engappai.2022.104959.

[62] R. A. M. Rudro, K. Nur, M. F. A. Al Sohan, M. F. Mridha, S. Alfarhood, M. Safran, and K. Kanagarathinam, "SPF-Net: Solar panel fault detection using U-Net based deep learning image classification," Energy Reports, vol. 12, pp. 1580–1594, Dec. 2024, doi: 10.1016/j.egyr.2024.07.044.

[63] H. Chen, Y. Pang, Q. Hu, and K. Liu, "Solar cell surface defect inspection based on multispectral convolutional neural network," *J. Intell. Manuf.*, vol. 31, no. 2, pp. 453–468, Feb. 2020, doi: 10.1007/s10845-018-1458-z.

[64] S. A. Anwar and M. Z. Abdullah, "Micro-crack detection of multicrystalline solar cells featuring an improved anisotropic diffusion filter and image segmentation technique," *EURASIP J. Image Video Process.*, vol. 2014, no. 1, p. 15, Dec. 2014, doi: 10.1186/1687-5281-2014-15.

[65] F.-C. Chen and M. R. Jahanshahi, "NB-CNN: Deep Learning-Based Crack Detection Using Convolutional Neural Network and Naïve Bayes Data Fusion," *IEEE Trans. Ind. Electron.*, vol. 65, no. 5, pp. 4392–4400, May 2018, doi: 10.1109/TIE.2017.2764844.

[66] F. Aziz, A. Ul Haq, S. Ahmad, Y. Mahmoud, M. Jalal, and U. Ali, "A Novel Convolutional Neural Network-Based Approach for Fault Classification in Photovoltaic Arrays," *IEEE Access*, vol. 8, pp. 41889–41904, 2020, doi: 10.1109/ACCESS.2020.2977116.

[67] I. Zyout and A. Oatawneh, "Detection of PV Solar Panel Surface Defects using Transfer Learning of the Deep Convolutional Neural Networks," in *2020 Advances in Science and Engineering Technology International Conferences (ASET)*, Feb. 2020, pp. 1–4. doi: 10.1109/ASET48392.2020.9118382.

[68] W. Tang, Q. Yang, K. Xiong, and W. Yan, "Deep learning based automatic defect identification of photovoltaic module using electroluminescence images," *Sol. Energy*, vol. 201, pp. 453–460, May 2020, doi: 10.1016/j.solener.2020.03.049.

[69] Y. Su, F. Tao, J. Jin, and C. Zhang, "Automated Overheated Region Object Detection of Photovoltaic Module With Thermography Image," *IEEE J. Photovoltaics*, vol. 11, no. 2, pp. 535–544, Mar. 2021, doi: 10.1109/JPHOTOV.2020.3045680.

[70] A. Fernández *et al.*, "Robust Detection, Classification and Localization of Defects in Large Photovoltaic Plants Based on Unmanned Aerial Vehicles and Infrared Thermography," *Appl. Sci.*, vol. 10, no. 17, p. 5948, Aug. 2020, doi: 10.3390/app10175948.

[71] Á. Huerta Herraiz, A. Pliego Marugán, and F. P. García Márquez, "Photovoltaic plant condition monitoring using thermal images analysis by convolutional neural network-based structure," *Renew. Energy*, vol. 153, pp. 334–348, Jun. 2020, doi: 10.1016/j.renene.2020.01.148.

[72] D. Manno, G. Cipriani, G. Ciulla, V. Di Dio, S. Guarino, and V. Lo Brano, "Deep learning strategies for automatic fault diagnosis in photovoltaic systems by thermographic images," *Energy Convers. Manag.*, vol. 241, p. 114315, Aug. 2021, doi: 10.1016/j.enconman.2021.114315.

[73] U. Otamendi, I. Martinez, M. Quartulli, I. G. Olaizola, E. Viles, and W. Cambarau, "Segmentation of cell-level anomalies in electroluminescence images of photovoltaic modules," *Sol. Energy*, vol. 220, pp. 914–926, May 2021, doi: 10.1016/j.solener.2021.03.058.

[74] M. Y. Demirci, N. Beşli, and A. Gümüşçü, "Efficient deep feature extraction and classification for identifying defective photovoltaic module cells in Electroluminescence images," *Expert Syst. Appl.*, vol. 175, p. 114810, Aug. 2021, doi: 10.1016/j.eswa.2021.114810.

[75] Y. Lebrini, A. Boudhar, R. Hadria, H. Lionboui, L. Elmansouri, R. Arrach, P. Ceccato & T. Benabdelouahab, "Identifying Agricultural Systems Using SVM Classification Approach Based on Phenological Metrics in a Semi-arid Region of Morocco," *Earth Syst. Environ.*, vol. 3, no. 2, pp. 277–288, Aug. 2019, doi: 10.1007/S41748-019-00106-Z/METRICS.

[76] G. Cipriani, A. D'Amico, S. Guarino, D. Manno, M. Traverso, and V. Di Dio, "Convolutional Neural Network for Dust and Hotspot Classification in PV Modules," *Energies*, vol. 13, no. 23, p. 6357, Dec. 2020, doi: 10.3390/en13236357.

[77] F. Aziz, A. Ul Haq, S. Ahmad, Y. Mahmoud, M. Jalal, and U. Ali, "A Novel Convolutional Neural Network-Based Approach for Fault Classification in Photovoltaic Arrays," *IEEE Access*, vol. 8, pp. 41889–41904, 2020, doi: 10.1109/ACCESS.2020.2977116.

[78] K. Dhibi, R. Fezai, M. Mansouri, M. Trabelsi, A. Kouadri, and K. Bouzara., "Reduced Kernel Random Forest Technique for Fault Detection and Classification in Grid-Tied PV Systems," *IEEE J. Photovoltaics*, vol. 10, no. 6, pp. 1864–1871, Nov. 2020, doi: 10.1109/JPHOTOV.2020.3011068.

[79] S. P. Pathak, D. S. Patil, and S. Patel, "Solar panel hotspot localization and fault classification using deep learning approach," *Procedia Comput. Sci.*, vol. 204, pp. 698–705, 2022, doi: 10.1016/j.procs.2022.08.084.

[80] M. Jemmali, A. K. Bashir, W. Boulila, L. K. B. Melhim, R. H. Jhaveri, and J. Ahmad, "An Efficient Optimization of Battery-Drone-Based Transportation Systems for Monitoring Solar Power Plant," *IEEE Trans. Intell. Transp. Syst.*, vol. 24, no. 12, pp. 15633–15641, 2023, doi: 10.1109/TITS.2022.3219568.

[81] S. Sengupta, S. Sengupta, and H. Saha, "Comprehensive Modeling of Dust Accumulation on PV Modules through Dry Deposition Processes," *IEEE J. Photovoltaics*, vol. 10, no. 4, pp. 1148–1157, 2020, doi: 10.1109/JPHOTOV.2020.2992352.

[82] F. A. Mejia and J. Kleissl, "Soiling losses for solar photovoltaic systems in California," *Sol. Energy*, vol. 95, pp. 357–363, Sep. 2013, doi: 10.1016/j.solener.2013.06.028.

[83] M. Altıntaş and S. Arslan, "The Study of Dust Removal Using Electrostatic Cleaning System for Solar Panels," *Sustainability*, vol. 13, no. 16, p. 9454, Aug. 2021, doi: 10.3390/su13169454.

[84] Y. Liu, H. Li, L. Li, X. Yin, X. Wu, Z. Su, F. Gao, Y. Liu, L. Tang, S. Zhou, and L. Yang., "A new electrostatic dust removal method using carbon nanotubes transparent conductive film for sustainable operation of solar photovoltaic panels," Energy Convers. Manag., vol. 300, p. 117923, Jan. 2024, doi: 10.1016/j.enconman.2023.117923.

[85] M. P. Ndeto, F. Njoka, D. W. Wekesa, and R. Kinyua, "Mechanisms and economics of a self-powered, automated, scalable solar PV surface cleaning system," *Renew. Energy*, vol. 226, p. 120477, May 2024, doi: 10.1016/j.renene.2024.120477.

[86] M. K. Swain, M. Mishra, R. C. Bansal, and S. Hasan, "A Self-Powered Solar Panel Automated Cleaning System: Design and Testing Analysis," *Electr. Power Components Syst.*, vol. 49, no. 3, pp. 308–320, Feb. 2021, doi: 10.1080/15325008.2021.1937400.

[87] S. Santosh Kumar, S. Shankar, and K. Murthy, "Solar Powered PV Panel Cleaning Robot," in *2020 International Conference on Recent Trends on Electronics, Information, Communication & Technology (RTEICT)*, Nov. 2020, pp. 169–172. doi: 10.1109/RTEICT49044.2020.9315548.

[88]   D. Amjad, A. Khan, R. Nazar, Y. Q. Gill, A. N. A. Farhad, A. Ishfaq, M. H. Iqbal, and U. Mehmood., "Smart polymer-based self-cleaning coatings for commercial solar cells and solar panels," in Polymer Nanocomposite Films and Coatings, Elsevier, 2024, pp. 409–435. doi: 10.1016/B978-0-443-19139-8.00018-8.

[89]   B. Nomeir, S. Lakhouil, S. Boukheir, M. A. Ali, and S. Naamane, "Recent progress on transparent and self-cleaning surfaces by superhydrophobic coatings deposition to optimize the cleaning process of solar panels," *Sol. Energy Mater. Sol. Cells*, vol. 257, p. 112347, Aug. 2023, doi: 10.1016/j.solmat.2023.112347.

[90]   B. Parrott, P. Carrasco Zanini, A. Shehri, K. Kotsovos, and I. Gereige, "Automated, robotic dry-cleaning of solar panels in Thuwal, Saudi Arabia using a silicone rubber brush," *Sol. Energy*, vol. 171, pp. 526–533, Sep. 2018, doi: 10.1016/j.solener.2018.06.104.

[91]   A. Agga, A. Abbou, M. Labbadi, Y. El Houm, and I. H. Ou Ali, "CNN-LSTM: An efficient hybrid deep learning architecture for predicting short-term photovoltaic power production," *Electr. Power Syst. Res.*, vol. 208, p. 107908, Jul. 2022, doi: 10.1016/J.EPSR.2022.107908.

[92]   H. Zang, L. Liu, L. Sun, L. Cheng, Z. Wei, and G. Sun, "Short-term global horizontal irradiance forecasting based on a hybrid CNN-LSTM model with spatiotemporal correlations," *Renew. Energy*, vol. 160, pp. 26–41, Nov. 2020, doi: 10.1016/j.renene.2020.05.150.

[93]   M. Elsaraiti and A. Merabet, "Solar Power Forecasting Using Deep Learning Techniques," *IEEE Access*, vol. 10, pp. 31692–31698, 2022, doi: 10.1109/ACCESS.2022.3160484.

[94]   J. Qu, Z. Qian, and Y. Pei, "Day-ahead hourly photovoltaic power forecasting using attention-based CNN-LSTM neural network embedded with multiple relevant and target variables prediction pattern," *Energy*, vol. 232, p. 120996, Oct. 2021, doi: 10.1016/J.ENERGY.2021.120996.

[95] M. Alaraj, A. Kumar, I. Alsaidan, M. Rizwan, and M. Jamil, "Energy Production Forecasting from Solar Photovoltaic Plants Based on Meteorological Parameters for Qassim Region, Saudi Arabia," *IEEE Access*, vol. 9, pp. 83241–83251, 2021, doi: 10.1109/ACCESS.2021.3087345.

[96] F. H. Gandoman, S. H. E. Abdel Aleem, N. Omar, A. Ahmadi, and F. Q. Alenezi, "Short-term solar power forecasting considering cloud coverage and ambient temperature variation effects," *Renew. Energy*, vol. 123, pp. 793–805, Aug. 2018, doi: 10.1016/J.RENENE.2018.02.102.

[97] M. S. Ahamed, H. Guo, and K. Tanino, "Cloud cover-based models for estimation of global solar radiation: A review and case study," *https://doi.org/10.1080/15435075.2021.1941043*, vol. 19, no. 2, pp. 175–189, 2021, doi: 10.1080/15435075.2021.1941043.

[98] M. N. I. Sarkar, "Estimation of solar radiation from cloud cover data of Bangladesh," *Renewables Wind. Water, Sol.*, vol. 3, no. 1, p. 11, Dec. 2016, doi: 10.1186/s40807-016-0031-7.

[99] W. Zhang, X. Chen, K. He, L. Chen, L. Xu, X. Wang, and S. Yang., "Semi-asynchronous personalized federated learning for short-term photovoltaic power forecasting," Digit. Commun. Networks, Mar. 2022, doi: 10.1016/J.DCAN.2022.03.022.

[100] A. Mellit, A. M. Pavan, and V. Lughi, "Deep learning neural networks for short-term photovoltaic power forecasting," *Renew. Energy*, vol. 172, pp. 276–288, Jul. 2021, doi: 10.1016/J.RENENE.2021.02.166.

[101] Mustaqeem, M. Ishaq, and S. Kwon, "A CNN-Assisted deep echo state network using multiple Time-Scale dynamic learning reservoirs for generating Short-Term solar energy forecasting," *Sustain. Energy Technol. Assessments*, vol. 52, p. 102275, Aug. 2022, doi: 10.1016/J.SETA.2022.102275.

[102] K. Wang, X. Qi, and H. Liu, "Photovoltaic power forecasting based LSTM-Convolutional Network," *Energy*, vol. 189, p. 116225, Dec. 2019, doi: 10.1016/j.energy.2019.116225.

[103] N. Sharma *et al.*, "A sequential ensemble model for photovoltaic power forecasting," *Comput. Electr. Eng.*, vol. 96, p. 107484, Dec. 2021, doi: 10.1016/j.compeleceng.2021.107484.

[104] Solcast, "Historical Time Series Request," [Online]. Available: https://toolkit.solcast.com.au/historical/timeseries/request. [Accessed: Apr. 28, 2025].

[105] S. Shapsough, R. Dhaouadi, and I. Zualkernan, "Using Linear Regression and Back Propagation Neural Networks to Predict Performance of Soiled PV Modules," *Procedia Comput. Sci.*, vol. 155, pp. 463–470, 2019, doi: 10.1016/j.procs.2019.08.065.

[106] P. Singla, M. Duhan, and S. Saroha, "A Hybrid Solar Irradiance Forecasting Using Full Wavelet Packet Decomposition and Bi-Directional Long Short-Term Memory (BiLSTM)," *Arab. J. Sci. Eng.*, vol. 47, no. 11, pp. 14185–14211, Nov. 2022, doi: 10.1007/s13369-022-06655-2.

[107] P. Nepal, M. Korevaar, H. Ziar, O. Isabella, and M. Zeman, "Accurate Soiling Ratio Determination With Incident Angle Modifier for PV Modules," *IEEE J. Photovoltaics*, vol. 9, no. 1, pp. 295–301, Jan. 2019, doi: 10.1109/JPHOTOV.2018.2882468.

[108] M. Alaraj, A. Kumar, I. Alsaidan, M. Rizwan, and M. Jamil, "Energy Production Forecasting From Solar Photovoltaic Plants Based on Meteorological Parameters for Qassim Region, Saudi Arabia," *IEEE Access*, vol. 9, pp. 83241–83251, 2021, doi: 10.1109/ACCESS.2021.3087345.

[109] A. Kumar, M. Rizwan, and U. Nangia, "A Hybrid Intelligent Approach for Solar Photovoltaic Power Forecasting: Impact of Aerosol Data," *Arab. J. Sci. Eng.*, vol. 45, no. 3, pp. 1715–1732, Mar. 2020, doi: 10.1007/s13369-019-04183-0.

[110] O. Bamisile, C. Acen, D. Cai, Q. Huang, and I. Staffell, "The environmental factors affecting solar photovoltaic output," *Renew. Sustain. Energy Rev.*, vol. 208, p. 115073, Feb. 2025, doi: 10.1016/j.rser.2024.115073.

[111] T. Rajasundrapandiyanleebanon, K. Kumaresan, S. Murugan, M. S. P. Subathra, and M. Sivakumar, "Solar Energy Forecasting Using Machine Learning and Deep Learning Techniques," *Arch. Comput. Methods Eng.*, vol. 30, no. 5, pp. 3059–3079, Jun. 2023, doi: 10.1007/s11831-023-09893-1.

[112] A. Oufadel, M. El Ydrissi, I. Taabane, A. Azouzoute, A. H. Aicha, and H. Ghennioui, "Soft sensors for dust estimation with high accuracy: AI-driven approach for CSP solar mirror soiling classification," *Int. J. Sustain. Energy*, vol. 44, no. 1, Dec. 2025, doi: 10.1080/14786451.2025.2475305.

[113] F. Mani, S. Pulipaka, and R. Kumar, "Characterization of power losses of a soiled PV panel in Shekhawati region of India," *Sol. Energy*, vol. 131, pp. 96–106, Jun. 2016, doi: 10.1016/j.solener.2016.02.033.

[114] M. K. Alam, F. Khan, J. Johnson, and J. Flicker, "A Comprehensive Review of Catastrophic Faults in PV Arrays: Types, Detection, and Mitigation Techniques," *IEEE J. Photovoltaics*, vol. 5, no. 3, pp. 982–997, May 2015, doi: 10.1109/JPHOTOV.2015.2397599.

[115] W. Yongqing, G. Zongqing, W. Shuonan, and H. Ping, "The temperature measurement technology of infrared thermal imaging and its applications review," in *2017 13th IEEE International Conference on Electronic Measurement & Instruments (ICEMI)*, Oct. 2017, pp. 401–406. doi: 10.1109/ICEMI.2017.8265833.

[116] F. fang Song, X. He, P. Lai, and R. Wang, "The Study of infrared radiation thermal imaging technology for temperature testing," in *2012 13th International Conference on Electronic Packaging Technology & High Density Packaging*, Aug. 2012, pp. 1336–1339. doi: 10.1109/ICEPT-HDP.2012.6474853.

[117] J. A. Tsanakas, L. Ha, and C. Buerhop, "Faults and infrared thermographic diagnosis in operating c-Si photovoltaic modules: A review of research and future challenges," *Renew. Sustain. Energy Rev.*, vol. 62, pp. 695–709, Sep. 2016, doi: 10.1016/j.rser.2016.04.079.

[118] T. Takashima, J. Yamaguchi, K. Otani, T. Oozeki, K. Kato, and M. Ishida, "Experimental studies of fault location in PV module strings," *Sol. Energy Mater. Sol. Cells*, vol. 93, no. 6–7, pp. 1079–1082, Jun. 2009, doi: 10.1016/j.solmat.2008.11.060.

[119] W. Ahmed, A. Hanif, K. D. Kallu, A. Z. Kouzani, M. U. Ali, and A. Zafar, "Photovoltaic Panels Classification Using Isolated and Transfer Learned Deep Neural Models Using Infrared Thermographic Images," *Sensors*, vol. 21, no. 16, p. 5668, Aug. 2021, doi: 10.3390/s21165668.

[120] M. Pa and A. Kazemi, "A Fault Detection Scheme Utilizing Convolutional Neural Network for PV Solar Panels with High Accuracy," Oct. 2022, doi: 10.48550/arxiv.2210.09226.

[121] I. Zyout and A. Oatawneh, "Detection of PV Solar Panel Surface Defects using Transfer Learning of the Deep Convolutional Neural Networks," pp. 1–4, Jun. 2020, doi: 10.1109/ASET48392.2020.9118384.

[122] A. Raorane, D. Magare, and Y. Mistry, "Performance of fault classification on Photovoltaic modules using Thermographic images," *ITM Web Conf.*, vol. 44, p. 03065, 2022, doi: 10.1051/ITMCONF/20224403065.

[123] I. Zyout and A. Oatawneh, "Detection of PV Solar Panel Surface Defects using Transfer Learning of the Deep Convolutional Neural Networks," in *2020 Advances in Science and Engineering Technology International Conferences (ASET)*, Feb. 2020, pp. 1–4. doi: 10.1109/ASET48392.2020.9118384.

[124] A. Kumar, M. Rizwan, U. Nangia, and M. Alaraj, "Grey Wolf Optimizer-Based Array Reconfiguration to Enhance Power Production from Solar Photovoltaic Plants under Different Scenarios," *Sustainability*, vol. 13, no. 24, p. 13627, Dec. 2021, doi: 10.3390/su132413627.

[125] A. Ishizaka and S. Siraj, "Are multi-criteria decision-making tools useful? An experimental comparative study of three methods," *Eur. J. Oper. Res.*, vol. 264, no. 2, pp. 462–471, Jan. 2018, doi: 10.1016/j.ejor.2017.05.041.

[126] E. Triantaphyllou, "Multi-Criteria Decision Making Methods," 2000, pp. 5–21. doi: 10.1007/978-1-4757-3157-6_2.

[127] C.-N. Wang, V. T. Nguyen, H. T. N. Thai, and D. H. Duong, "Multi-Criteria Decision Making (MCDM) Approaches for Solar Power Plant Location Selection in Viet Nam," *Energies*, vol. 11, no. 6, p. 1504, Jun. 2018, doi: 10.3390/en11061504.

[128] R. K. Singh and A. Gupta, "Framework for sustainable maintenance system: ISM– fuzzy MICMAC and TOPSIS approach," *Ann. Oper. Res.*, vol. 290, no. 1–2, pp. 643–676, Jul. 2020, doi: 10.1007/s10479-019-03162-w.

[129] J. Więckowski and W. Sałabun, "MakeDecision: Online system for the graphical design of decision-making models in crisp and fuzzy environments," *SoftwareX*, vol. 26, p. 101658, May 2024, doi: 10.1016/j.softx.2024.101658.

LIST OF PUBLICATION

• **List of papers (s) published in Peer Reviewed Referred International Journals**

1. R. Aman, M. Rizwan and A. Kumar, "A novel deep learning framework for PV module thermal condition monitoring". Electrical Engineering, 2024 1-17. Impact factor 1.6 (SCIE Journal).

2. R. Aman, M. Rizwan and A. Kumar, "Fault classification using deep learning-based model and impact of dust accumulation on solar photovoltaic modules." Energy Sources, Part A: Recovery, Utilization, and Environmental Effects, Vol. 45, Issue 2, pp. 4633-4651, 2023, ISSN: 4633-4651. Impact factor 2.3 (SCIE Journal).

3. R. Aman, M. Rizwan and A. Kumar, "A novel hybrid intelligent approach for solar photovoltaic power prediction considering UV index and cloud cover". Electrical Engineering 107, 1203–1224, 2025, Impact factor 1.6 (SCIE Journal).

4. R. Aman, M. Rizwan and A. Kumar, "Novel Deep Learning Assisted Framework for the Assessment of Real Time Dust Accumulation Data on Solar PV Modules, AJSE, Impact factor: 2.5 (SCIE Journal)

• **List of Paper(s) Published in Peer Reviewed International Conference**

1. R. Aman, M. Rizwan and A. Kumar, "Comparative Analysis of Transfer Learning Techniques for Enhanced Fault Detection in Solar Photovoltaic Modules." 2024 IEEE 4th International Conference on Sustainable Energy and Future Electric Transportation (SEFET), 31st July – 3rd August, 2024, Hyderabad, India. [Scopus Indexed Conference].

2. R. Aman, A. Abdul, D. Kumar, A. Kumar, and M. Rizwan, "An IoT integrated novel self-cleaning strategy for enhancing efficiency of solar photovoltaic modules," IEEE Trans. Ind. Inform., [Under Review].

3. M. Rizwan, R. Aman, and A. Kumar, "An optimized deep learning framework for solar PV power forecasting using advanced hyperparameter tuning technique," in Proc. 2nd Int. Conf. Sustainable Power and Energy Research (ICSPER 2025), [Accepted].

4. R. Aman, M. Rizwan and A. Kumar, "Investigating the Effect of Dust on the Performance of Rooftop Solar Photovoltaic System," 2023 International Conference

on Modelling, Simulation & Intelligent Computing (MoSICom), Dubai, United Arab Emirates, 2023, pp. 99-104, [Scopus Indexed Conference].

5. R. Aman and M. Rizwan, "Power Enhancement and Hotspot Reduction of a Rooftop Solar PV Array Using MOSFETs", 2022 International Conference on Electrical, Computer, Communications and Mechatronics Engineering (ICECCME 2022), Maldives, pp. 1-6, [Scopus Indexed Conference]

6. R. Aman and M. Rizwan, "A Modified Shade Dispersion Technique to Enhance the Performance of Photovoltaic System Under Various Shading Conditions," 2022 IEEE Delhi Section Conference (DELCON), New Delhi, India, 2022, pp. 1-7, doi: 10.1109/DELCON54057.2022.9753011. [Scopus Indexed Conference].

List of other publications

1. R. Aman, M. Aminovich, Z. Ulmas, A. Kumar, and M. Rizwan, "A Novel Hybrid GWO-Bi-LSTM Based Metaheuristic Framework for Short Term Solar Photovoltaic Power Forecasting", JRSE [Revision].

2. R. Aman, A. Abdul, D. Kumar, A. Kumar, and M. Rizwan, "An IoT integrated novel self-cleaning strategy for enhancing efficiency of solar photovoltaic modules," IEEE Trans. Ind. Inform., [Under Review].

3. M. Rizwan, R. Aman, and A. Kumar, "An optimized deep learning framework for solar PV power forecasting using advanced hyperparameter tuning technique," in Proc. 2nd Int. Conf. Sustainable Power and Energy Research (ICSPER 2025), [Accepted].

4. R. Aman, M. Rizwan and A. Kumar "Novel Hybrid MICMAC-TOPSIS based Framework for Solar Photovoltaic Module Cleaning", 5th IEEE International Conference on Sustainable Energy and Future Electric Transportation (IEEE SeFet 2025) (Accepted)

5. A. Gupta, A. Jangra, A. Goyal, M. Rizwan, R. Aman, and A. Azeem "Novel Autonomous SPV Module Cleaning Using Shape Memory Alloy And Internet of Things for Enhanced Energy Efficiency", 5th IEEE International Conference on Sustainable Energy and Future Electric Transportation (IEEE SeFet 2025) (Accepted)

Final Thesis@RAHMA_30.04.2025_new1.pdf

Delhi Technological University

Document Details

Submission ID

trn:oid:::27535:93810460

Submission Date

May 1, 2025, 12:39 PM GMT+5:30

Download Date

Jun 16, 2025, 11:41 AM GMT+5:30

File Name

Final Thesis@RAHMA_30.04.2025_new1.pdf

File Size

5.7 MB

163 Pages

39,355 Words

221,175 Characters

6% Overall Similarity

The combined total of all matches, including overlapping sources, for each database.

Filtered from the Report

- Bibliography
- Quoted Text
- Cited Text
- Small Matches (less than 14 words)

Exclusions

- 5 Excluded Sources

Match Groups

91 Not Cited or Quoted 6%
Matches with neither in-text citation nor quotation marks

0 Missing Quotations 0%
Matches that are still very similar to source material

0 Missing Citation 0%
Matches that have quotation marks, but no in-text citation

0 Cited and Quoted 0%
Matches with in-text citation present, but no quotation marks

Top Sources

5% 🌐 Internet sources

4% 📖 Publications

2% 👤 Submitted works (Student Papers)

Integrity Flags

0 Integrity Flags for Review

No suspicious text manipulations found.

Our system's algorithms look deeply at a document for any inconsistencies that would set it apart from a normal submission. If we notice something strange, we flag it for you to review.

A Flag is not necessarily an indicator of a problem. However, we'd recommend you focus your attention there for further review.

CURRICULUM VITAE

Name- Rahma Aman
Date of Birth: 18/09/1996 | Nationality: Indian | Sex- Female
E-mail: rahmaaman96@gmail.com
Mob: 8173870496

ABOUT ME

To succeed in an environment of growth and excellence and earn a job which provides me satisfaction and self-development and help me to achieve organizational goal.

PERSONAL QUALITIES

- ❖ Disciplined, Punctual, Obedient, Responsible, Sincere in work. Positive Attitude, Good listener, leadership skills, curiosity to know things.
- ❖ Can be a part of an organization in the best and positive way.
- ❖ Having cooperative and friendly nature that helps me to interact with people

EDUCATION

Qualification	College/Institutes	Board/ University	Year	Aggregate
PhD	Delhi Technological University	Delhi Technological university	2025	
M. Tech	Jamia Milia Islamia	Jamia Milia Islamia	2021	91%
B. Tech Electrical Engineering	United Institute of Engineering& Research Allahabad	AKTU	2018	82.3%
Intermediate	St Mary's Convent	ISC	2014	82%
High School	St Mary's Convent	ICSE	2012	87%

PROFESSIONAL SKILLS

- ❖ Deep learning
- ❖ MATLAB simulation
- ❖ SCADA Systems (Supervisory Control and Data Acquisition)
- ❖ AutoCAD
- ❖ Good Interpersonal skills
- ❖ Good Communication skills
- ❖ Coding in python/ MATLAB

EDUCATIONAL TRAINING

| S. No | Organization | Period | | Details of Training/ Project undertaken |
		From	To	
1	Industrial training in northern central railways	05.06.2017	05.07.2017	Traction Distribution Including power supply & SCADA
2	IEEE Uttar Pradesh, India	21.06.2016	16.07.2016	Summer Internship in electrical engineering and done a MATLAB project (SOLAR WIND HYBRID SYSTEM Based on MATLAB SIMULINK

• List of papers (s) published in Peer Reviewed Referred International Journals

1. R. Aman, M. Rizwan and A. Kumar, "A novel deep learning framework for PV module thermal condition monitoring". Electrical Engineering, 2024 1-17. Impact factor 1.6 (SCIE Journal).

2. R. Aman, M. Rizwan and A. Kumar, "Fault classification using deep learning- based model and impact of dust accumulation on solar photovoltaic modules." Energy Sources, Part A: Recovery, Utilization, and Environmental Effects, Vol. 45, Issue 2, pp. 4633-4651, 2023, ISSN: 4633-4651. Impact factor 2.3 (SCIE Journal).

3. R. Aman, M. Rizwan and A. Kumar, "A novel hybrid intelligent approach for solar photovoltaic power prediction considering UV index and cloud cover". Electrical Engineering 107, 1203–1224, 2025, Impact factor 1.6 (SCIE Journal).

4. R. Aman, M. Rizwan and A. Kumar, "Novel Deep Learning Assisted Framework for the Assessment of Real Time Dust Accumulation Data on Solar PV Modules, AJSE, Impact factor: 2.5 (SCIE Journal)

• List of Paper(s) Published in Peer Reviewed International Conference

1. R. Aman, M. Rizwan and A. Kumar, "Comparative Analysis of Transfer Learning Techniques for Enhanced Fault Detection in Solar Photovoltaic Modules." 2024 IEEE 4th International Conference on Sustainable Energy and Future Electric Transportation (SEFET), 31st July – 3rd August, 2024, Hyderabad, India. [Scopus Indexed Conference].

2. R. Aman, M. Rizwan and A. Kumar "Short-Term Solar Power Forecasting Based on Deep Learning Approach.", 2024 IEEE Third International Conference on Power Electronics, Intelligent Control and Energy Systems (ICPEICES), New Delhi, India,26th April – 28th April, 2024. [Scopus Indexed Conference].

3. R. Aman, M. Rizwan and A. Kumar, "Investigating the Effect of Dust on the Performance of Rooftop Solar Photovoltaic System," 2023 International Conference on Modeling, Simulation & Intelligent Computing (MoSICom), Dubai, United Arab Emirates, 2023, pp. 99-104, [Scopus Indexed Conference].

4. R. Aman and M. Rizwan, "Power Enhancement and Hotspot Reduction of a Rooftop Solar PV Array Using MOSFETs", 2022 International Conference on Electrical, Computer, Communications and Mechatronics Engineering (ICECCME 2022), Maldives, pp. 1-6, [Scopus Indexed Conference]

5. R. Aman and M. Rizwan, "A Modified Shade Dispersion Technique to Enhance the Performance of Photovoltaic System Under Various Shading Conditions," 2022 IEEE Delhi Section Conference (DELCON), New Delhi, India, 2022, pp. 1-7, doi: 10.1109/DELCON54057.2022.9753011. [Scopus Indexed Conference].

List of other publications

1. R. Aman, M. Aminovich, Z. Ulmas, A. Kumar, and M. Rizwan, "A Novel Hybrid GWO-Bi-LSTM Based Metaheuristic Framework for Short Term Solar Photovoltaic Power Forecasting", JRSE [Revision].

2. M. Rizwan, R. Aman, and A. Kumar, "An optimized deep learning framework for solar PV power forecasting using advanced hyperparameter tuning technique," in Proc. 2nd Int. Conf. Sustainable Power and Energy Research (ICSPER 2025), [Accepted]

3. R. Aman, M. Rizwan and A. Kumar "Novel Hybrid MICMAC-TOPSIS based Framework for Solar Photovoltaic Module Cleaning", 5th IEEE International Conference on Sustainable Energy and Future Electric Transportation (IEEE SeFet 2025) (Accepted)

4. A. Gupta, A. Jangra, A. Goyal, M. Rizwan, R. Aman, and A. Azeem "Novel Autonomous SPV Module Cleaning Using Shape Memory Alloy And Internet of Things for Enhanced Energy Efficiency", 5th IEEE International Conference on Sustainable Energy and Future Electric Transportation (IEEE SeFet 2025) (Accepted)

EXPERTISE

I have expertise in solar photovoltaic power enhancement using a deep learning approach, and several optimization techniques, proficient in MATLAB/SIMULINK software.

My B. tech project was Simulation of Solar Charge Controller Using Maximum Power Point Tracking Technique in MATLAB and my MTech project were Modelling And Performance Analysis of PV System Under Mismatch Scenarios and also done its hardware and pursuing Ph.D. on, **"*Deep Learning based Approach to Maximize PV power production"*.**

Declaration: I hereby declare that the above-mentioned information is correct up to my knowledge and I bear the responsibility for the correctness of the above-mentioned particulars.

Rahma Aman